Doctoral Dissertation (Shinshu University)

Development of electrospun functional nanofibers for antibacterial and coloration performances

（エレクトロスピニングによる抗菌性・着色性機能ナノファイバーの開発に関する研究）

March, 2019

JATOI ABDUL WAHAB

Dedicated to

Memona, Mehak and

Abdul Sami

ACKNOWLEDGEMENTS

I pay my utmost gratitude to Almighty ALLAH, The most merciful and beneficent, and bow my head in front of His supremacy for His support and help at every stage of my life.

I pay special thanks to Engr. Nakamura Miho and Engr. Ayako Nishida for kind support in equipment operations.

I am profoundly gratified to my parents whose support and encouragements have helped me at every stage of my life particular during my hard times at Shinshu University, Ueda, Japan.

CONTENTS

CHAPTER 11
Ultrasonic Energy Assisted Dyeing of Nylon-6 Nanofibers

CHAPTER 12
Conclusions

List of Figures

List of Tables

List of Schemes

Abbreviations

AgNP	Silver Nanoparticles
ASTM	American Society for Testing and Materials
BE	Binding Energy
CA	Cellulose Acetate
CI	Color Index
CN	Cellulose Nanofibers
CNT	Carbon Nanotube
DMF	N, N-Dimethylformamide
DNA	Deoxyribonucleic Acid
DOPA	3, 4-Dihydroxyphenylalanine
ECM	Extra Cellular Matrix
EDX	Energy Dispersive X-ray
ES	Electrospinning
EtOH	Ethanol
FCC	Face Centred Cubic
FESEM	Field Emission Scanning Electron Microscopy
FTC	Federal Trade Commission
FTIR	Fourier Transform Infra-red Spectroscopy
FWHM	Full Width at Half Maximum
HCl	Hydrochloric Acid
MPTMS	3-mercaptapropyl Trimethoxy Silane
MRSA	Methicillin Resistant Staphylococcus Aureus
MWCNT	Multiwall Carbon Nanotube
NaOH	Sodium Hydroxide
NBRC	NITE Biological Resource Center
NF	Nanofibers
NITE	National Institute of Technology and Evolution
NM	Nanometer
OD	Optical Density
PAN	Polyacrylonitrile
pDOPA	Polydopamine
PHMBs	Polyhexamethylene Biguanides
PVA	Polyvinyl Alcohol
PVP	Poly (vinylpyrrolidone)
PU	Polyurethane
ROS	Reactive Oxygen Species
SEM	Scanning Electron Microscopy
SMP	Shape Memory Polyurethane
SWCNT	Single Wall Carbon Nanotube
TCD	Needle-tip to Collector Distance
TEM	Transmission Electron Microscopy
TEOS	Tetra Ethyl Ortho Silicate
Tg	Glass Transition Temperature

US	Ultrasonic
UV	Ultra Violet
XPS	X-ray Photoelectron Spectroscopy
XRD	X-ray Diffraction
ZnO	Zinc Oxide

Abstract

In this research polymer/silver nanoparticle composite nanofibers and ultrasonic dyeing have been investigated for antibacterial properties and functional colored applications of electrospun nanofibers. For antibacterial activities cellulose acetate (CA) and polyvinyl alcohol (PVA) based AgNP composite nanofibers were fabricated. The CA/AgNP composite nanofibers were successfully prepared by dopamine process, heat treatment and DMF assisted process for generation of AgNPs on deacetylated electrospun CA nanofibers. The dopamine method is an environmentally green process for synthesis of AgNPs while the heat treatment and DMF methods were effective and efficient in generating well dispersed fine sized (<10nm) AgNPs having higher contents and good spatial distribution on CA surfaces. Although CA/AgNP composite nanofibers have been excellent in antibacterial activities due to surface functionalized AgNPs, however, AgNPs on the surface may induce detrimental side-effect such as *carcinoma*, *argeria*, *argyrosis* and *allergies* due to prolonged exposure and excess release of silver ions. At the same time produce comparatively limited time antibacterial activities due to rapid depletion of silver. Thus to avoid these detrimental side-effects and achieve extended time antibacterial performances research was extended to synthesize AgNPs immobilized TiO_2, multiwall carbon nanotubes (CNTs), silica nanoparticles and ZnO nanoparticles to fabricate CA/TiO_2/AgNP, CA/CNT/AgNP, PVA/silica/AgNP and CA/ZnO/AgNP composite nanofibers for biologically safer and extended time antibacterial applications. The antibacterial assays were conducted against *E. coli* and *S. aureus* bacterial strains. All the composite nanofibers demonstrated adequately higher antibacterial properties (*halo width* measured via Kirby-Bauer disk diffusion test method) and long time liquid medium bacterial growth inhibition properties for the tested times. The CA/TiO_2/AgNP composites were successful in antibacterial activities for upto 72 hours. The CA/CNT/AgNP was investigated for upto 48hours and found effective against both the strains. Thus the CA/TiO_2/AgNP, CA/CNT/AgNP and PVA/silica/AgNP composite nanofibers could be used for safer and extended time antibacterial applications.

The ultrasonic dyeing method for coloration of electrospun nanofibers have been used for dying of polyurethane (PU), polyacrylonitrile (PAN) and Nylon-6 nanofibers. Generally coloration of nanofibers has been challenging in achieving higher color strengths due to scattering of high proportion of light from nanofiber surfaces owing to their very high surface to volume ratio and nano scale diameters. The ultrasonic energy helps in ensuring higher dye-uptakes may be due to breaking of dye aggregates and high mass transfer from dye solution to into the nanofibers due to the effect of ultrasonic cavitations. Process parameters such as dyeing time, dyeing temperature and dye concentrations were optimized for PU, PAN and Nylon-6 nanofibers. The optimal process

time and temperature for ultrasonic dyeing of PU were 40 minutes and 70^0C. For ultrasonic dyeing of PAN, the optimized process time and temperatures were 80^0C and one hour. While for Nylon-6 the optimized time and temperatures were 30minutes and 80^0C. Furthermore, for all the three studied nanofibers, ultrasonic dyeing did not significantly affect morphology, chemical structure and crystallinity of the nanofibers. Mechanical strength of all the three nanofibers was increased by ultrasonic dyeing method. Thus due to improved dye up-take, dyed PU, PAN and Nylon-6 nanofibers could be utilized in functional colored applications.

CHAPTER 1

Introduction

1.1 Introduction

This chapter presents basic theoretical information about the materials and methods utilized in the research. The electrospinning has been discussed at the beginning. Basic theoretical discussion about the polymers used, antibacterial activities, antibacterial agents and template nanoparticles for immobilization of AgNPs has been provided. At the end of chapter, dyeing and dyeing methods are discussed.

1.2 Nanofibers

Technically the nanofibers are the fibers having their diameters within 100nm. However, in literature the fibers with their diameters around upto 500nm are considered as nanofibers. Owing to such a small fiber diameters, higher surface area, larger surface to volume ration, high porosity, small pore sizes, breathability and sufficient mechanical properties, the nanofibers have been extensively used in numerous applications such as biomedical, energy, catalysis, environment science and antibacterial materials. The three-dimensional structure of nanofiber webs have certain resemblance with extra cellular matrix (ECM) which along with porosity, breathability and adequate mechanical strength are highly desirable for varying biomedical applications[1].

1.3 Electrospinning

It is commonly accepted that the first electrospinning system was developed by Anton Formhals 1930s[2], however, the term 'electrospnning' was first used by Reneker in early 1990s. Although the nanofibers can be prepared by a number of alternate processes such as phase separation, drawing, self assembly and template-synthesis, however, the electrospinning technique still remains extensively used in fabrication of nanofibers due its simplicity, operational flexibility and cost-effectiveness.

Basic set-up of an electrospinning unit consists of a syringe which holds the spinning solution, electric power supply for producing electric voltage to generate the nanofiber strings and a grounded collector for collection of the produced nanofibers. In the basic principle of operations, electrospinning polymer solution is filled in the syringe which is loaded on a syringe pump for controlling solution feed-rate (flow rate).

A needle on the syringe is connected to the positive electrode of electric power supply while the negative electrode is connected with the collector which either is a rotating cylinder (rotary collectors) or metallic plate (plate-type collectors) or rods (rod-type collectors). When the applied electric voltage exceeds the surface tension of the polymer solution, fine charged strings of fibers emerge from the needle tip and travel in whipping motion towards the collector.

Electrostatic interactions in the charged fluid jets produce jet instabilities that dictate final fiber architecture. These instabilities cause the polymer jets to form Taylor cone at the needle-tip. As the jet emerge attenuation begins, the solvent evaporates leaving behind polymer fibers which are deposited on a grounded collector. The jet instabilities that result from the rheological behavior of the polymer fluid are crucial for fiber formation. Most instabilities cause breakage and prevent the formation of continuous fibers. However, the bending stability is crucial to nanofiber formation; the nanofibers are formed when the charged polymer jet bends in expanding loops and then collected on a substrate[3].

Certain parameters need careful consideration for producing nanofibers having controlled and desired characteristics. These parameters mainly belong to three groups such as polymer solution parameters (i.e. viscosity, surface tension, conductivity and molecular weight of the polymer), process parameters (such as electric voltage, needle tip to grounded collector distance and solution flow rate) and environmental parameters (i.e. temperature and relative humidity). Adequately optimized parameters produce nanofibers with desirable properties and higher reproducibility.

1.4 Polymers

Electrospinning as a fabrication technique is highly flexible in polymer selection. Almost all the polymers dissolved in a suitable solvent system can be electrospun to fabricate their nanofiberous webs. However the polymer used in the research are briefly described below.

1.4.1 Cellulose acetate

The cellulose acetate (CA) is a carbohydrate polymer obtained by acetylation of cellulose by using acetic acid. The CA polymer is composed of acetylated glucose units joined together by glycosidic linkages. Contrary to cellulose which contains three hydroxyl groups (OH) on each glucose unit, the number of OH groups on each glucose unit in CA depend on type of CA and hence on the degree of acetylation. In the *di-acetates*, 74-92 % of the OH groups are acetylated while in a *tri-acetate* over 92% (>92%) of the OH groups have been acetylated.

The CA is biocompatible and biodegradable biopolymer having very good to excellent hydrophilicity and moisture management properties. It can be easily electrospun into nanofiber webs using various solvent systems, however a DMF/acetone (1:2) solvent system has been a common and more suitable solvent system for production of smooth and regular CA nanofibers.

1.4.2 Polyvinyl alcohol

Polyvinyl alcohol (PVA) is a synthetic polymer prepared by reaction of acetic acid with acetylene or ethylene in the presence of catalyst i.e. zinc acetate. It is soluble in water and has excellent film-forming properties. Due to OH groups PVA polymer can be easily functionalized and cross-linked by a suitable mechanism. It is a biodegradable and biocompatible polymer having excellent properties suitable for biomedical applications such as antibacterial products. The PVA can be easily electrospun into nanofibers by using water as a solvent.

1.4.3 Polyurethane

Polyurethane (PU) is a polymer in which organic units are joined together by urethane bond (HNCOO). It is formed by reacting a di-isocyanate with a diol such as 4,4'-diisocyanato-diphenylmethane with ethylene glycol in the presence of a catalyst. The PU polymer has repeating segmented structure with a hard segment and a soft segment which ensures and controls its self-healing properties. The PU polymer can be electrospun into nanofibers using DMF and/or DMF/THF (tetrahydrofuran) as solvent system.

1.4.4 Polyacrylonitrile

Polyacrylonitrile(PAN) is a synthetic polymer composed of acrylonitrile [$CH_2CH(CN)$] repeating units. The Federal Trade Commission defines acrylic fibers as "a manufactured fiber in which the fiber forming substance is any long-chain synthetic polymer composed of at least 85% by weight of acrylonitrile units ($-CH_2-CH[CN]-)_x$". The PAN can be easily electrospun into nanofibers by using DMF as a solvent.

1.4.5 Nylon

Nylon is a synthetic polymer in which repeating units are joined together by amide linkages (-OC-NH). The FTC defines nylon as "a manufactured fiber in which the fiber forming substance is a long-chain synthetic polyamide in which at least 85% of the amide-linkages (-CO-NH-) are attached directly to two aliphatic groups". Two common variants of nylon are nylon-6 and nylon-66. The nylon-6 are prepared from caprolactam while the nylon-66 from adipic acid and hexamethylene

diamine monomers. The nylon-6 can be easily electrospun into nanofibers by using formic acid as a solvent.

1.5 Antibacterial activities

All of the microorganisms are not harmful to human health and ecosystem. Majority of the microbes are vital for balance of ecosystem and survival of human civilization. However, related to harmful microorganism (pathogenic) such as certain bacteria, viruses and fungus, microbial protection becomes seriously important for healthy life. Some of these species could be extremely dangerous and may induce severe infections and diseases. Particularly wounds, cuts, burn and exposed organs need intense care and due protections against harmful microorganisms not only for healing but also for protection from infections.

Additionally, textile substrates and human skin provides suitable environment for growth of microorganisms. Human sweat and perspiration contain nutrients for bacterial growth and the textile materials support bacteria colonization. Thus bacterial protection is needed not only in wound healing and protection from infections but also for inhibition of bacteria colorizations.

1.5.1 Antibacterial agents

Numerous antibacterial agents can be used for wound healing, infection protections and inhibition of bacteria colonization. These antibacterial agents can be classified into two groups namely *bactericidal* and *bacteriostatic*. The *bacteriostatic* bacteria can only inhibit bacterial growth by stopping their reproduction but cannot kill them. However, the *bactericidal* bacteria can harm and kill the bacteria[4]. Many antibacterial agents have so far been used for protection from pathogenic bacterial species. For examples metals and metal ions, quaternary ammonium compounds, chitosan polyhexamethylene biguanides (PHMBs), triclosans and N-halamines. Among these antibacterial agents, metals and metal ions such as AgNPs have been highly effective in bacterial protection.

1.5.2 Silver nanoparticles (AgNPs)

AgNPs are highly effective antimicrobial agents against wider bacterial species. History of using silver in protection from bacteria, viruses, fungus and in healing of wounds, cuts and burns is very old. The AgNPs have attained greater interest since they are effective against antibiotic resistant bacteria species i.e. methicillin resistant *Staphylococcus aureus*, as well. Although, due to structural differences between prokaryotic cells and eukaryotic cells, silver has been reported as safe for human cells, however, excess exposure to silver and excess release of silver are prone to induce detrimental side effects. The reported detrimental side effects of silver are *carcinoma*, *argyria*,

argyrosis and *allergies* [5]. In a textile structure, AgNPs on surface such as on the surface of nanofibers can produce efficient antibacterial properties. However, this AgNP/nanofiber architecture may induce detrimental side effects owing to possibility of AgNP's exposure to the human cells and/or excess release of silver ions. Release of silver ions in excess from a substrate may also yield limited time antibacterial performances due to silver depletion.

A proposed approach to ensure prolonged antibacterial properties accompanying protection from the mentioned detrimental side effects is anchoring of the AgNPs on certain organic or inorganic nanomaterial then embedding the AgNP anchored composite nanoparticle into polymer matrix such as into nanofibers has been suggested. This polymer/nanomaterial/AgNP composite architecture could ensure prolonged antibacterial performances while being biologically safe. However, antibacterial properties of this three phase architecture should not be compromised. In the present research CA/AgNP composite having AgNPs on nanofiber surfaces were synthesized by dopamine process, thermal procedure and DMF assisted procedures, which were found to be efficient against *E. coli* and *S. aureus* strains. Then the CA/TiO_2/AgNP, CA/CNT/AgNP, PVA/silica/AgNP and CA/ZnO/AgNP nanofibers, incorporated with TiO_2/AgNP, CNT/AgNP, silica/AgNP and ZnO/AgNP hybrid nanoparticles, were fabricated and investigated for their antibacterial performances. Effective antibacterial performances on agar plates, excellent bactericidal activities (relative cell viabilities) and prolonged bacterial growth inhibition in liquid medium (LB medium) by these composite nanofibers were confirmed.

1.5.3 Multiwall carbon nanotubes

The carbon nanotubes were first revealed by Iijima in 1990[6]. These carbon nanotubes are cylindrical tubular sp^2 hybridized six-membered cyclic carbon rings. The single wall carbon nanotubes (SWCNT) are composed of a single member of such structure while multiwall carbon nanotubes (MWCNT, designated in this research as CNTs) may consist of 6 to 25 tubes. Diameters of CNTs may be up to 30nm depending on number of the nanotubes. The CNTs may be a desirable substrate to immobilize AgNPS due to their excellent thermal, electrical, mechanical, electronic properties. They possess chemical and mechanical stability and have been reported to possess a degree of antibacterial properties as well.

1.5.4 Titanium dioxide

Titanium di oxide (TiO_2) is a semiconducting material which possesses catalysis, optical, electronic and physical properties. The TiO_2 nanoparticles are available in three phases namely anatase, rutile and brookite. The TiO_2 may produce ultraviolet (UV) light induced photocatalytic and antibacterial

properties. Under UV light, the TiO_2 produces reactive oxygen species, superoxide and hydroxide radicals which disrupt the bacterial cell walls and block their respiratory system.

1.5.5 Zinc Oxide

Zinc oxide is a metal oxide which possesses antibacterial, anticancer, antifungal and catalytic properties thus has been extensively used in such applications. It has been suggested that mechanism of antimicrobial activities of ZnO is based on generation of reactive oxygen species (ROS), release of Zn^+ ions and contact killing owing to their larger surface area.

1.6 Dyeing

Dyeing is a process of applying colorants such as dyes and pigments onto various substrates such as nanofibers in order to produce colored materials either for aesthetic or for functional purposes. Dyeing can be carried out in various forms such as in fibers, yarns, fabrics and garments etc. Dyeing methods for coloration are classified as continuous method, semi-continuous and batch-wise dyeing methods.

1.6.1 Ultrasonic dyeing

The ultrasonic dyeing methods are generally batch-wise dyeing processes augmented with ultrasonic energy. The ultrasonic energy has been proposed for higher mass transfer into the fibers. The ultrasonic cavitations in the bulk media break-up the dye aggregates, transient cavitations promote dye sorption and open-up polymer chains for dye diffusions inside the polymer chains[7].

1.6.2 Dyes

Dyes are organic compounds which produce color on the material on which they are applied. The dye molecules can have selective absorption and reflection of light in the visible region and can ensure adequate attachment with fibers either by chemical bond (i.e. reactive dyes) or by physical attachments. The dye molecules contain *chromophores* and *auxochromes* in their structure. The *chromophores* ensure selected absorption and reflection of light while the *auxochromes* intensify and deepen the color and promote dye solubility. The dyes have been classified as reactive, direct, acidic and vat dyes based on the method of application.

1.6.3 Disperse dyes

The name disperse dyes has been taken from the dyeing method used for these dyes. These dyes have lower solubility in water thus are applied via aqueous dispersion. These dyes are more suitable for polyester, polyamide and can be used for other synthetic polymers. The dyeing processes for

these dyes are either carried out at elevated temperature or need some carrier agent. In the former case, the dyeing process is termed as *high temperature dyeing* while in later case called *carrier dyeing*.

1.7 Aims and objectives

Advents of nanotechnology have outperformed in many application domains. Designing novel nano architectures, manipulation and control of properties at nano-level have solved many problems and substantially improved human life. Varying 1D, 2D and 3D nanostructures opened new doors and challenges for researchers and investigators. Synthesis and innovations in nanoparticles, quantum dots, nanotubes, graphene and nanofibers developed novel structures and produced outstanding properties. Combining these nanomaterials into their composites yielded extended, hybrid and tunable characteristics. Biomedical, energy, environment, robotics and textiles are among the most benefited domains. Apart from the milestones achieved by nanomaterials there exists huge room to further improve performance, resolve demerits/drawbacks and overcome the challenges in exploiting these novel structures in existing/new functional and conventional application areas.

Among these nanostructures nanoparticles and nanofibers are being extensively investigated and used owing to their distinctive properties. The very small size/diameters and very high surface areas of these nanomaterials bestow them structural benefits over conventional micro and macro structured architects.

The present research targeted two important areas namely antibacterial nanomaterials and coloration of nanofibers. Related to antibacterial nanomaterials domain huge work has already been done in synthesis of state of the art nanoparticles, functionalized and inherent antibacterial polymer nanofibers and their composites to achieve desired functionalities. For antibacterial applications silver nanoparticles (AgNPs) has always been a best choice owing to their excellent bacteriostatic and bactericidal properties. The AgNPs have been studied and used as nanoparticles and AgNP/polymer composites in such applications. Although, the AgNPs and AgNP/polymer composites (particularly AgNPs/nanofibers) retained their excellence in antibacterial material domain, however, several researches reported their detrimental side-effects to human health. It has been reported that excess contact/release of AgNPs can cause *carcinoma*, *argyria*, *argyrosis* and *allergies*. They may result in accumulation of the nanoparticles in human organs, be allergic and a more severe case may be *carcinoma* (a type of cancer in skin cells, liver and kidneys).

Thus the present research targeted to design an strategy/structure to achieve protection from the detrimental side effects of excess contact with AgNPs maintaining the extraordinary potential of

these nanoparticles in antibacterial domain. The, AgNPs were immobilized on several substrates such as silica, TiO_2, multiwall carbon nanotubes (MWCNT) and ZnO nanoparticles to synthesize hybrid nanoparticles. These composite nanoparticles were then incorporated into cellulose acetate (CA) and polyvinyl alcohol (PVA) nanofibers. It has suggested that anchoring of AgNPs on these substrate and their embedding in a polymer matrix should reduce excess AgNP contact/release thus would avoid the reported harmful side effects. Furthermore, it has been suggested that mechanism of antibacterial activities be generation of reactive oxygen species (ROS) thus these composite nanofiber structures would be ideal nanomaterials for sustained excellent antibacterial applications. The objectives of the research related antibacterial area are given below:

- Designing of strategies to avoid detrimental side effect of excess contact/release of AgNPs maintaining their excellent antibacterial properties
- Synthesis of AgNP, their hybrid nanoparticles and composite nanofibers to avoid AgNP's harmful side-effects such as *carcinoma*, *argyria*, *argyrosis*, *allergy* and accumulation on the human organs.
- Synthesis of AgNP based composite nanofibers for sustained and long-term excellent antibacterial applications.

The second area present research aimed at was investigating strategies to improve coloration performance of polymer nanofiber for their uses in aesthetic applications. Though several researchers reported varying strategies for coloration of nanofibers, however, a higher color yield still remains a challenge due to distinctive properties of nanofibers. Due to very small diameters of the nanofibers, these fiber reflect higher proportion of incident light from their surfaces thus result in lower coloration performance. To solve this problem, present research suggests ultrasonic dyeing methods to increase mass transfer of dyes into the nanofibers in order to improve color build-up on nanofibers. Use of ultrasonic energy generates ultrasonic cavitations in the bulk media which break the dye aggregates and promote exhaustion of the dye molecules on to nanofibers. Transient cavitations near the nanofiber surfaces improve sorption of these dye molecules and control their mobility. As a combined effect of sonication and dyeing temperature, polymer chains open-up at greater extent to create larger space for penetration of the dye molecules into polymer chains. By this way, ultrasonic energy assisted coloration of polymer nanofibers ensure higher color build-up on the nanofibers. For ultrasonic dyeing Nylon-6, polyurethane (PU) and polyacrylonitrile (PAN) nanofibers were selected and investigated in detail.

1.8 Thesis composition

Based on the research, the thesis can be divided into four parts. First part (Chapter 1 and Chapter 2) presents basic insight into theoretical background and experimental details such as materials, procedures and characterization techniques employed in the experiments. In the second part (Chapter 3 and Chapter 4) synthesis and characterization of CA/AgNP composite nanofibers by dopamine, heat treatment and DMF process are reported. These composite nanofibers were characterized for antibacterial applications. The AgNPs were generated on nanofiber surface after electrospinning. In the third part (Chapter 5 to Chapter 8) synthesis and characterization of AgNPs anchored on several substrates/nanoparticles (i.e. silica, TiO_2, MWCNTs and ZnO) and fabrication of their composite nanofibers are given. This part proposes composite nanofibers for increased biological safety and sustained antibacterial properties where the AgNPs have been anchored and embedded into the nanofibers. The fourth part (Chapter 9 to Chapter 11) presents research on ultrasonic dyeing of polymeric nanofibers (Nylon-6, PU and PAN nanofibers). The thesis comprises of twelve (12) chapters. In the final chapter (Chapter 12) conclusions and future suggestions are given.

References

[1] J.A. Wahab, G. Xu, H. Lee, P.D. Nam, K. Wei, S.H. Kim, I.S. Kim, Fabrication of silk fibroin/eggshell nanofiber membranes for facemasks, Fibers and Polymers 17(11) (2016) 1776-1781.

[2] F. Anton, Artificial thread and method of producing same, Google Patents, 1940.

[3] D.H. Reneker, A.L. Yarin, H. Fong, S. Koombhongse, Bending instability of electrically charged liquid jets of polymer solutions in electrospinning, Journal of Applied physics 87(9) (2000) 4531-4547.

[4] S. Bernatová, O. Samek, Z. Pilát, M. Šerý, J. Ježek, P. Jákl, M. Šiler, V. Krzyžánek, P. Zemánek, V. Holá, Following the mechanisms of bacteriostatic versus bactericidal action using Raman spectroscopy, Molecules 18(11) (2013) 13188-13199.

[5] A.W. Jatoi, Y.K. Jo, H. Lee, S.G. Oh, D.S. Hwang, Z. Khatri, H.J. Cha, I.S. Kim, Antibacterial efficacy of poly (vinyl alcohol) composite nanofibers embedded with silver-anchored silica nanoparticles, Journal of Biomedical Materials Research Part B: Applied Biomaterials 106(3) (2018) 1121-1128.

[6] Y.-H. Li, J. Ding, Z. Luan, Z. Di, Y. Zhu, C. Xu, D. Wu, B. Wei, Competitive adsorption of Pb2+, Cu2+ and Cd2+ ions from aqueous solutions by multiwalled carbon nanotubes, Carbon 41(14) (2003) 2787-2792.

[7] A.W. Jatoi, I.S. Kim, Q.-Q. Ni, Ultrasonic energy-assisted coloration of polyurethane nanofibers, Applied Nanoscience (2018) 1-10.

CHAPTER 2

Experimental Details

2.1 Introduction

This chapter provides details about the experimental procedures used in the research. Details of the materials used, characterization techniques and research methodologies are concisely reported.

2.2 Materials

Cellulose acetate (Mw: 30kDa) was purchased from Sigma Aldrich, Japan. The silver nitrate ($AgNO_3$), 3, 4-dihydroxyphenethylaine hydrochloride (Dopa), sodium hydroxide (NaOH), N, N-dimethylformamide (DMF), acetone and acetic acid were purchased from Wako Pure Chemicals, Japan. 1M TRIS HCl buffer (pH 8.5) was purchased from Nippon Gene Co, Ltd, Japan. The bacteria strains, gram-negative strains *Escherichia coli* (*E coli:* NBRC 3301) and gram-positive strain *Staphylococcus aureus* (*S aureus*: NBRC 12732), were purchased from NITE Biological Resource Center (NBRC), Japan. Miller's Luria-Bertani broth (LB broth) and agar powder were obtained from Sigma Aldrich, Japan. Titanium dioxide (TiO_2: rutile phase) was purchased from Sigma Aldrich, Japan. Glutaraldehyde solution (25%) and ethanol (99.5%) were purchased from Wako Pure chemicals, Japan. Multiwall carbon nanotubes (CNT: 40-70nm), nitric acid (HNO_3: 69-70%), sulfuric acid (H_2SO_4: 95%) were purchased from Wako Pure Chemicals, Japan.

The ammonia solution (NH_4OH; 25%) was purchased from Wako Pure Chemicals, Japan. The HPLC grade ethanol (99.9%) was obtained from Duksan Pure Chemical Company, Korea. Tetraethyl orthosilicate (TEOS: 98%), 3-mercaptopropyltrimethoxysilane (MPTMS: 97%), PVA (87-89% hydrolyzed, M_n: 85000-124000 g/mol), glutaraldehyde solution (Grade-1, 50%; used as cross-linking agent in PVA nanofibers) and hydrochloric acid (HCl: ≥37% for fuming) were purchased from Sigma Aldrich, Japan. Poly(vinylpyrolidone) (PVP K-15; M_w: 10,000 g/mol) was obtained from Junsei Chemical Company, Japan. The Milli-Q de-ionized water by Millipore, France, was used in the synthesis of silica/AgNP core-shell nanoparticles. The zinc oxide (ZnO, 20nm) were obtained from Wako Pure Chemicals, Japan.

Polyurethane pellets (MM, 9020) were purchased from SMP Technologies, Tokyo, Japan. The CI Disperse Blue 56 (CIB, anthraquinone dye) and CI Disperse Red 167:1 (CIR, azoic dye) colorants were supplied by Sumitomo Chemical Co., Ltd., Japan. Polyacrylonitrile (Mw= 150kDa) was purchased from Sigma Aldrich, Japan. Nylon-6 (pellets 3 mm) was purchased from Sigma Aldrich, Japan. Formic

acid (98%) was obtained from Wako Pure Chemical Industries, Japan. De-ionized (DI) water was obtained from Wako Pure Chemicals, Japan.

2.3 Electrospinning of cellulose acetate

The cellulose acetate (CA) nanofibers were fabricated using DMF and acetone (1:2) solvents. A 17 % (wt %) of CA powder was dissolved in the solvent system and was continuously stirred for 24 hours on a magnetic stirrer. Electrospinning equipment, Katotech Electrospinning Unit, Katotech Co, Japan was used to fabricate the nanofiber mats. The electric voltage and needle tip to collector distance were 15kV and 15cm respectively. The CA nanofibers were fabricated at 25^0C temperature and 40% relative humidity.

2.4 Deacetylation of cellulose acetate nanofibers

The CA nanofibers were surface modified by a deacetylation process with sodium hydroxide in order to remove acetyl groups and produce hydroxyl groups to increase the adsorption of silver ions. Typically, the CA samples were treated in a 0.01M NaOH solution for 48 hours. At the end of deacetylation process samples were repeatedly washed to remove remaining alkali.

2.5 Characterizations

Morphology of the nanofiber samples were observed using scanning electron microscope (SEM), Hitachi VP-SEM SU1510, Hitachi High Technologies, America. All the nanofiber samples were sputtered with Pt for 160s at 20mA to form 8nm conductive coating on the samples prior to SEM observations. The Fourier transform infrared spectroscopy (FTIR), IR Prestige-21, Shimadzu, Japan, was used to study chemical structures of the samples. For crystallographic analysis of the samples, X-ray diffraction equipment (XRD), Rigaku MiniFlex300, Rigaku Co, Japan, was utilized. The elemental compositions and mappings were obtained using SEM, Hitachi, S-3000N, installed with energy dispersive X-ray (EDX) analyzer, Horiba, EX 200. The chemical states of the samples were studied using X-ray photoelectron spectrometer (XPS), AXIS-ULTRA DLD, Kratos Analytical, Shimadzu Corporation, Japan. Transmission electron microscopy (TEM) images were obtained using TEM, JEM-2100, Jeol, USA. Field emission scanning electron microscope (FESEM), Hitachi S-5000, Hitachi High Technologies, was utilized for high resolution and high magnification morphological analysis. Diameters of the nanofibers and sizes of the nanoparticles were measured using imageJ software. The differential thermogravimetric analysis (DTA) studies were carried out using Thermo plus, TG 8120, Rigaku Corp., Japan. For DTA thermograms, samples were heated from 0-600^0C at 10^0C/min. using air.

The Bio-Shaker BR-300LF was used for incubation of the samples to control and maintain the standard environment required for strain cultivation. The absorbance (OD_{590nm}) values were recorded using microplate reader, ImmunoMiniNJ-2300, Biotec, Tokyo, Japan.

The mechanical properties were studied using Tensilon Universal Testing Machine, RTC1250A, A & D Company Ltd., Japan. The tensile properties were determined following standard test method ASTM D-638 using 10N load and at cross-head speed of 5mm/minute. Five samples from each group were measured in tensile strength tests.

2.6 Sizes of nanoparticles

Average sizes of the AgNPs were calculated using Debye-Sherrer method (equation 1)

$$A = {K\lambda}/{\beta cos\theta} \qquad \text{(eq. 1)}$$

Where A= average crystallite sizes (nm), K= shape factor (0.9), λ= incident X-ray wavelength (1.54 Å), β= FWHM (radians) and θ= Bragg's angle.

2.7 Specific surface area of the nanoparticles

Specific surface area (S) of the AgNPs was calculated using equation 2.

$$S = 6 * 1000/Dp * \rho \qquad (\text{eq. } 2)$$

Where, S= specific surface area, Dp= size of the nanoparticles and ρ = density. For silver ρ = 10.5 g/cm^3 (1.05 $x10^{21}$ nm^3).

2.8 Cross-linking density

The poly(vinyl alcohol) (PVA) nanofibers were cross-linked using glutaraldehyde as crosslinking agent and HCl was used as catalyst. The cross-linking density (n) was calculated using Flory-Rehner equation 3 [1].

$$\mathrm{n} = \frac{-[\ln(1-Vr)+Vr+\chi Vr^2}{\mathrm{V}\,(\mathrm{Vr}^{\frac{1}{3}}-\frac{\mathrm{Vr}}{2})} \qquad \text{(eq. 3)}$$

Where, n= crosslinking density (mol/cm^3), V = molar volume of H_2O, V_r =volume fraction of PVA in the swollen samples and χ= interaction constant of PVA/water system [2]. The value of Flory interaction constant χ used in this research was 0.494 [2].

2.9 Swollen ratio

Crosslinking of the PVA was further studied by swollen ratio measurements. The swollen ration (Δm) of PVA in H_2O was calculated using equation 4.

$$\Delta m(\%) = \frac{(W_s - W_o)x100}{W_o} \quad \text{(eq. 4)}$$

Where, W_s = swollen sample weight and W_o =initial sample weight.

2.10 Average molecular weight between cross-links

Average molecular weight between the cross-links (M_c) was calculated using equation 5[3].

$$M_c = \frac{1}{2n} \quad \text{(eq. 5)}$$

Where, Mc= average molecular weight between the cross-links and n=crosslinking density (eq. 3).

2.11 Residual acetyl contents

Surface modification of CA (deacetylation) was confirmed by calculating residual acetyl contents (%) using FTIR results of CA, deacetylated CA and partially deacetylated CA (Chapter 4, section 4.4.4; CA/AgNP-P sample). The residual acetyl contents were calculated by ration of absorbance at 1740 cm^{-1} (A1740) to absorbance at 1030 cm^{-1} (A1030) as given in equation 6.

$$\text{Residual acetyl contents } (\%) = \left(\frac{A1740}{A1030}\right)x100 \quad (eq.\ 6)$$

2.12 Antibacterial assays

Detailed procedures of antibacterial tests performed are briefly described below. For antibacterial tests *E. coli* (gram-negative bacteria) and *S. aureus* (gram-positive bacteria) strains were used.

2.12.1 Disc diffusion method

To investigate growth inhibition (halo width) of the strains on agar plates Kirby Bauer disc diffusion antibacterial assay was performed. To prepare agar plates, 2g/100mL of agar powder and 2.5g/100mL of LB broth were well mixed, autoclaved at 120^0C for 20 minutes and spread on the plastic dishes (20mL of the LB agar solution for each plate). Then, the overnight cultured bacterial strains, *E coli* and *S aureus* were spread on the agar plates using glass rods. The nanofiber samples (10-11mm diameter) were incubated overnight on the prepared agar plates at 37^0C. At the end of test, the hollow widths in mm were recorded using imageJ software.

2.12.2 Bacterial growth curves

To observe growth inhibition of the strains by samples in liquid medium (LB medium) bacterial growth curves were obtained. For this purpose 1:100 dilutions of the overnight cultured strains were used. A 50 µL of each culture were added in 450 µL of LB medium solution (10g/L of Millers LB broth). The nanofiber samples were added and incubated at 37^0C using 48 well cell culture plates using shaking incubator (Bio-Shaker BR-300LF) at 140rpm. The absorbance (OD_{590nm}) values were recorded at defined intervals using ImmunoMiniNJ-2300 microplate reader.

2.12.3 Relative cell viability (%)

The bactericidal performances of the samples were measured via relative cell viability test. The relative cell viability (%) was measured using 10^8 serial dilutions of overnight cultured strains which yielded 10^{11} colony forming units per mL (CFU/mL) of both the *E. coli* and *S. aureus*. The samples were incubated for 24 hours in 500µL of the culture medium using 48-well cell culture plates. Afterwards, 100µL of the culture medium were taken and spread on the agar plates which were then incubated at 37^0C for 24 hours. Colony forming units were counted in the end and relative bacterial cell viability (%) was calculated using equation 7.

$$\text{Relative Cell Viability } (\%) = \left(\frac{\text{CFU NF}}{\text{CFU control}}\right) \text{x}100 \qquad \text{(eq. 7)}$$

Where, $CFU_{control}$ = colony forming units without nanofiber samples and CFU_{NF} = colony forming units with respective nanofiber samples.

2.12.4 SEM observations of incubated nanofibers

For physical observation of the bacterial cell morphology of the bacteria cells exposed to and without exposure to the antibacterial sample SEM analysis was conducted. After 24 hours incubation in the cultured medium (500µL of culture medium as reported in section 2.11.3), the nanofiber samples were taken out. To fix the test strain, the samples were soaked in glutaraldehyde (2% solution) followed by dehydration with ethanol for five minutes.

2.13 Color measurements

2.13.1 K/S values

Konica Minolta spectrophotometer, CM3600d, was used for color measurements. The measurements were performed using standard illuminant D65 using SCE mode (specular component excluded). The color yield, measured as K/S values were obtained using equation 8.

$$\frac{K}{S} = \frac{(1-R)^2}{2R} \quad \text{(eq. 8)}$$

Where, K= absorption co-efficient; S=scattering co-efficient and R is decimal fraction of reflection.

2.13.2 Dye fixation

The dye fixation (F, %), uptake of the dye by nanofibers, was calculated using equation 9.

$$F(\%) = \frac{(K/S)a}{(K/S)b} \times 100 \quad \text{(eq. 9)}$$

Where, F= dye fixation (%), $(K/S)_a$= K/S values after washing-off process and $(K/S)_b$ = K/S values before washing-off process[4].

Except for dye fixation calculations, the K/S values were measured after final washing-off process. While for calculation of dye fixation, the K/S values were measured before and after washing-off process.

2.14 Color fastness tests

The color fastness tests measure the color bleeding resistance of the samples after exposure to respective agent (i.e. washing, light and hot-pressing etc. termed as washing fastness, light fastness and hot-pressing fastness respectively) at standardized conditions following set standards. Related to dyed textile applications, adequate washing fastness, light fastness and hot pressing fastness are common end-use requirements. Thus, washing fastness (shade change and staining on multi-fibers), light fastness and hot-pressing fastness tests were conducted. Washing fastness tests were conducted on Gyrowash, James H. Heal Co., UK, following ISO 105-C10 standard test method. Following ISO 105 BO2 standard test method, light fastness tests were carried out on Appollo, light fastness tester, James H. Heal Co., UK. For hot pressing fastness tests, standard test method ISO 105 X11 was followed.

References

[1] M. Smith, S. Berlioz, J. Chailan, Radiochemical ageing of butyl rubbers for space applications, Polymer Degradation and Stability 98(2) (2013) 682-690.

[2] N.A. Peppas, E.W. Merrill, Determination of interaction parameter χ1, for poly (vinyl alcohol) and water in gels crosslinked from solutions, Journal of Polymer Science: Polymer Chemistry Edition 14(2) (1976) 459-464.

[3] L.F. Gudeman, N.A. Peppas, Preparation and characterization of pH-sensitive, interpenetrating networks of poly (vinyl alcohol) and poly (acrylic acid), Journal of applied polymer science 55(6) (1995) 919-928.
[4] A.W. Jatoi, P.K. Gianchandani, I.S. Kim, Q.-Q. Ni, Sonication induced effective approach for coloration of compact polyacrylonitrile (PAN) nanofibers, Ultrasonics sonochemistry (2018).

CHAPTER 3

Cellulose Acetate/AgNP Composite Nanofibers By Dopamine Process

3.1 Introduction

This chapter reports synthesis and characterization of cellulose acetate (CA) based silver nanoparticles (CA/AgNP) composite nanofibers prepared by an environmentally benign process using dopamine hydrochloride (Dopa) as adhesive film forming and reducing agent for antibacterial applications. The AgNPs were generated on CA nanofiber surfaces. The CA nanofibers were prepared by electrospinning and surface modified via an alkaline deacetylation process to replace acetyl groups of CA with hydroxyl groups for better dopamine coating and subsequently for improved adsorption of silver ions (Ag^{+}). The dopamine is a biopolymer capable of forming a polydopamine coating (pDopa) and reducing the metal ions into nanoparticles. The dopamine coated, de-acetylated CA samples were treated with silver nitrate solutions. The SEM, XRD, FESEM, EDX, XPS, TEM, FTIR analysis and antibacterial assays were used for characterization and performance evaluations of the CA/AgNP composite nanofibers. Sizes of the AgNPs were calculated by Debye-Scherrer method and from TEM images.

3.2 Research background

Polymer/AgNP composites have been extensively researched and used in diverse fields such as in biomedical, conductive, catalysis and optical applications. Final performance of the composite depend on the polymer used, AgNPs and structural characteristics (i.e. nanofibers). The CA is a biocompatible and biodegradable biopolymer having good hydrophilicity and moisture management properties which are extensively needed in antibacterial uses[1]. However, acetyl groups of CA limit higher adsorption of silver ions. Thus a deacetylation process, such as with sodium hydroxide, would ensure surface modification of CA and replace acetyl groups with hydroxyl groups which infact converts CA into cellulose[2].

The excellence bactericidal, electrical, thermal, optical and catalytic properties of silver have been extensively studied and used in numerous applications. As an antimicrobial agent and disinfectant, silver has a long history of use in purification of water, treatments of wounds, cuts and burns. Structural difference in prokaryotic and eukaryotic cells enables silver to be non-toxic to human cells (in low concentrations) while being extremely toxic to bacteria, virus and fungus. Silver is toxic to and efficient against antibiotic resistant microorganisms such as methicillin resistant *Staphylococcus aureus* (MRSA) as well and has been effective against cancer cells. AgNPs in comparison to ionic silver due to their larger surface area and gradual release of silver ions produce better antibacterial

properties. The AgNPs rupture cell wall of bacteria, block their respiratory systems and denature DNA leading to bacteria death.

The nanofiber structures due to nano-scale diameter and very high surface to volume ratio of the nanofibers, high porosity and breathability, mechanical strength and resemblance with human extra cellular matrix (ECM) have shown extended performances in many applications such as in biomedical, catalysis, energy, filtration, sensors, environmental, textiles and protective fields[3].

The 3,4-dihydroxyphenylalanine (Dopa) is a biomaterial and a key constituent of mussel adhesive proteins (maps). It possesses extremely large adhesive, cohesive and mechanical properties. It has been used as neurotransmitter in the treatments of Parkinson disease in human as well. The catechol and amine groups possess capability of reducing metal ions into nanoparticles and can react with various functional groups including amine, quinone, hydroxyl and thiol groups via Michael addition and Schiff-base reaction. At alkaline pH (8.5), Dopa self polymerizes to form adhesive polydopamine coating (pDOPA) over numerous organic and inorganic material surfaces[4]. During oxidation catechol groups of Dopa lose their electrons to metal ions thereby generate metal nanoparticles. The hydroxyl groups of catechol reduce silver ions into AgNPs and amine groups promote stabilization of AgNPs and inhibit their aggregation [5-6].

Although Dopa has been extensively studied in many applications, however, to the best of our knowledge it has not yet been reported in generation of AgNPs on CA for antibacterial applications. Thus, present study was first time conducted to prepare CA/AgNP by exploiting metal reducing properties of Dopa. A systematic research was conducted for generating AgNPs by a facile dipping method. No other stabilizing agent or any co-reducing mechanism was used. The proposed method is effective and environmental friendly procedure for synthesis of AgNPs on surface modified CA nanofibers. Antibacterial test results confirmed very good antibacterial activities of the CA/AgNP composites. Thus, CA/AgNP nanofibers produced by a facile and green procedure could be used as an effective antimicrobial nano biocomposite.

3.3 Dopamine method for generation of AgNPs

The silver nanoparticles (AgNPs) were generated on modified CA surfaces by exploiting adhesive and metal ion reducing properties of dopamine hydrochloride (Dopa). The samples were treated in a Dopa solution to form a polydopamine coating (pDopa) on the nanofibers. The Dopa coated samples were immersed in a silver nitrate solution for adsorption of silver ions and their subsequent reduction into AgNPs. Typically, 2mg of Dopa per mL of 1M Tris HCl buffer was prepared and samples were immersed into it. The samples were kept under slow stirring on the magnetic stirrer for eighteen hours. The stirrer speed (rpm) was adjusted to avoid damage to the nanofiber samples. The samples were repeatedly washed with DI water in order to remove excess Dopa. Afterwards, a

150mM $AgNO_3$ solution was prepared and the Dopa coated samples were treated in it for eighteen hours while keeping under slow stirring. The stirrer speed was adjusted to minimum in order to avoid damage to nanofiber samples. The experiments were conducted at room temperature. At the end, the samples were washed in DI to remove unfixed AgNPs and dried at 40^0C in a drying oven.

3.4 Results and discussions

3.4.1 SEM observations

The SEM images of the samples depicted in Figure 3.1 show smooth, regular and bead free CA, modified CA and CA/AgNP nanofibers. The alkaline deacetylation of CA nanofibers did not show a significant change in the morphology and diameters of the nanofibers. The average size of CA, modified CA and CA/AgNP nanofibers were found to be 293nm, 291nm and 331nm respectively. Increase in the average diameters of the CA/AgNP nanofibers may be the result of dopa coating (pDopa) on nanofiber surfaces. Inset in the SEM image of CA/AgNP (Figure 1C) is a high magnification FESEM image of the CA/AgNP nanofibers exhibiting distribution of the AgNPs.

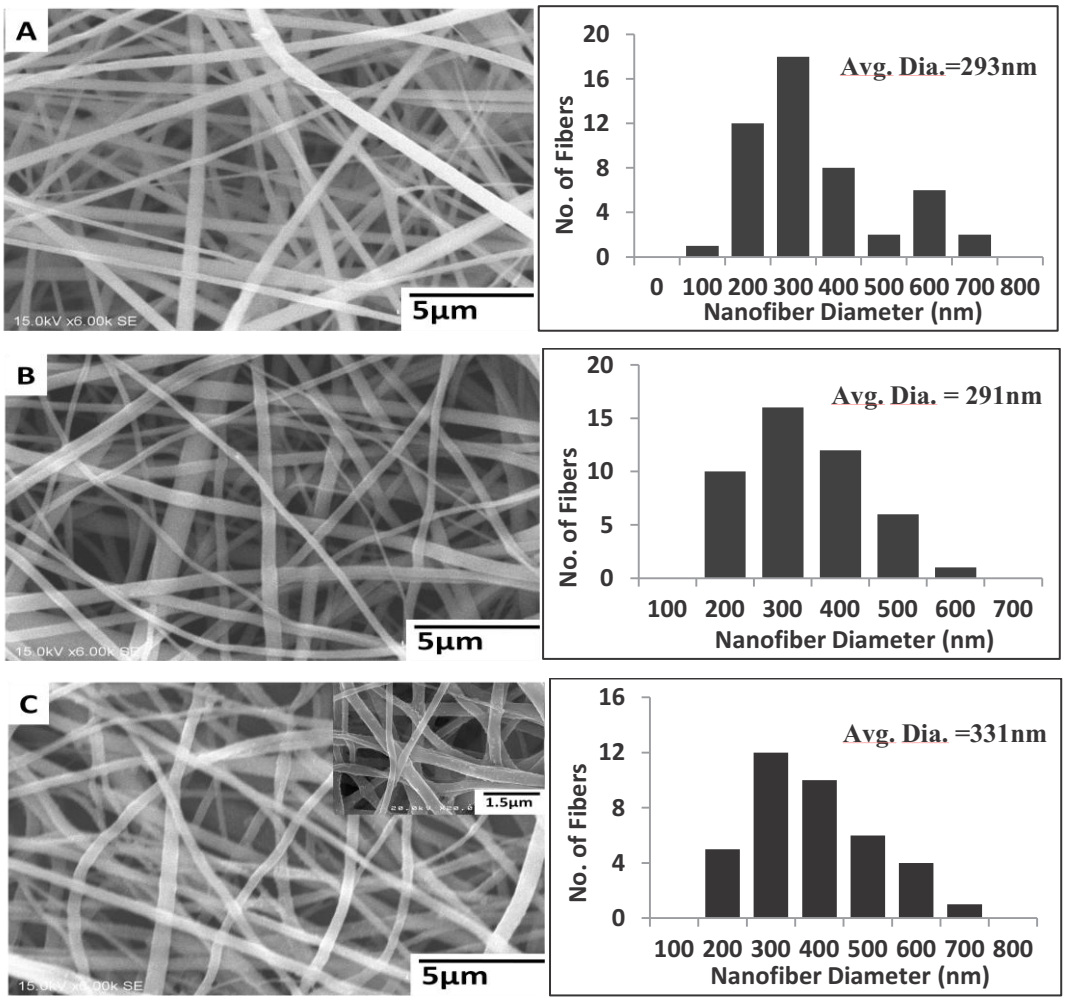

Figure 3.1 SEM images of (a) CA (b) modified CA(c) CA/AgNP

3.4.2 X-ray diffraction studies of the CA/AgNP

Synthesis of the AgNPs on CA nanofiber surfaces by dopamine (Dopa) were primarily studied with X-ray diffraction analysis. The XRD patterns of CA/AgNP nanofibers (Figure 3.2) confirmed formation of metallic AgNPs. The diffraction angles (2θ values) at 38.2^0, 44.4^0, 64.45^0 and 77.4^0 are indexed as (111), (200), (220) and (311) planes of metallic silver having face centered cubic (FCC) structure; thus confirm purity and crystallinity of the AgNPs. The DOPA forms an adhesive coating on the surface of CA nanofibers which possess higher potential to reduce metal ions. The adhesive coating improves adsorption of silver ions and subsequently reduces these ions into nanoparticles during oxidation. The Dopa molecule is composed of catechol and amine groups. The two hydroxyl groups in catechol lose their electron to silver ions during oxidation into quinone and form silver nanoparticles. Furthermore, the amine groups can serve the function of stabilizing agents and help in avoiding aggregation of the AgNP. The crystallite sizes of the formed AgNPs calculated by Debye-Sherrer equation were 20nm. These small sized AgNPs, owing to their larger surface areas, more effectively inhibit growth of bacteria and kill the bacterial species.

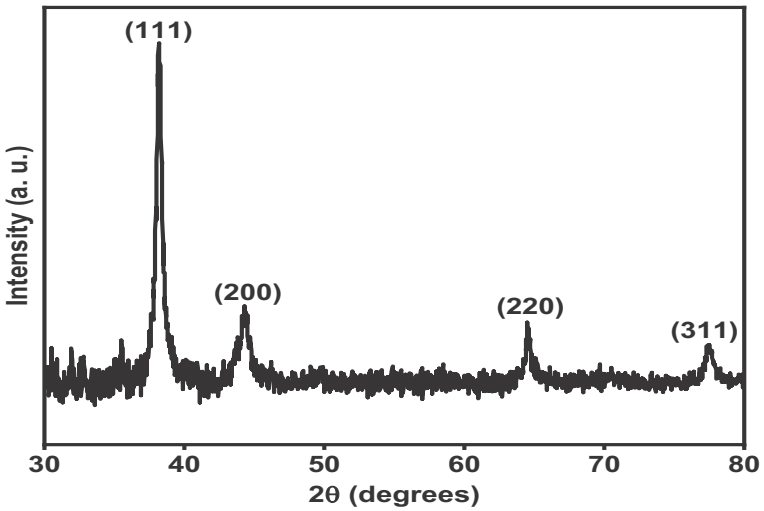

Figure 3.2 XRD pattern of the CA/AgNP nanofibers

3.4.3 EDX analysis

Figure 3.3 and Table 3.1 show EDX spectrum, elemental maps and elemental compositions of CA/AgNP respectively. The EDX spectrum clearly depicts AgNP peaks at 3.01keV and 3.2keV. A nitrogen peak at 0.4 keV was due to pDopa (amine groups). The elemental composition results of CA/AgNPs (Table 3.1) show 14.98 wt.% and 20.49wt.% of silver and nitrogen contents respectively. Elemental maps (Figure 3.3B) depict CA nanofibers densely coated with uniformly distributed AgNPs.

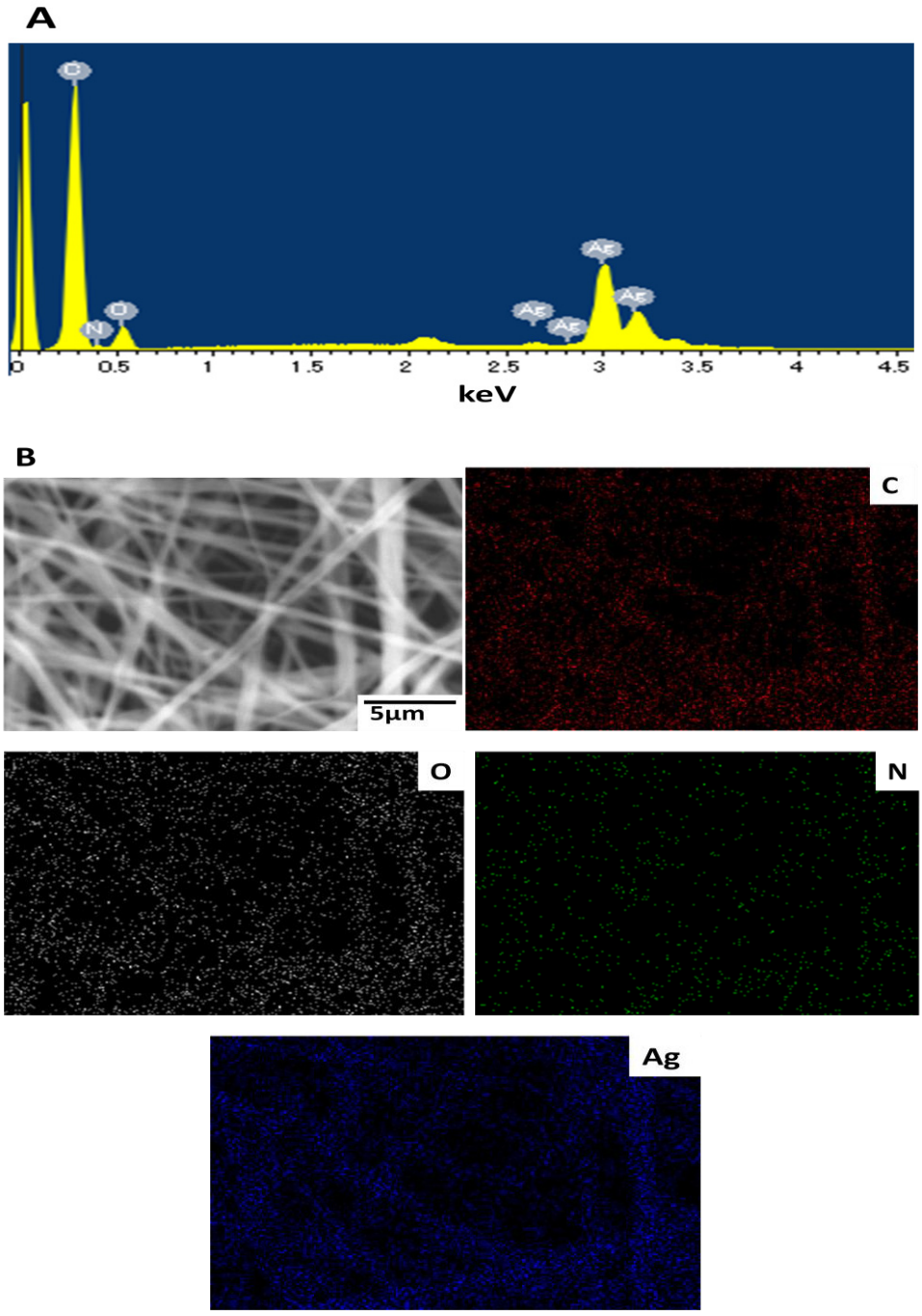

Figure 3.3 EDX results of CA/AgNP (A) EDX spectrum (B) Elemental maps

Table 3.1 Elemental compositions of CA/AgNP

Elements	Mass Percentage (%)	Atomic Percentage (%)
CK	50.69	63.11
NK	20.49	21.87
OK	13.85	12.94
AgL	14.98	2.08
Total	100	100

3.4.4 XPS studies

Chemical states of the samples were studied with XPS (Figure 3.4). The CA structure can be validated from C1s and O1s peaks in the XPS spectra at binding energy (B. E.) of 283.9 eV and 530.5eV respectively. The N1s peak at B. E. 397.03eV belongs to pDOPA (Wang, Huang, & Jiang, 2017). The C 1s narrow spectrum shows three peaks at 282.7eV, 284.3eV and 285.7eV representing C-C, C-OH of deacetylated CA (Gopiraman et al., 2016) and C-N groups of pDOPA (Liebscher et al., 2013) respectively. Formation of pDOPA was further evidenced from N 1s narrow spectrum. The three peaks in N 1s narrow spectrum at B. E. 397.5eV, 399eV and 401eV correspond to C_2NH, =N- and N-$(C)_3$ (Chang et al., 2018) belonging to pDOPA. Generation of AgNPs were confirmed by $Ag3d_{3/2}$ and $Ag3d_{5/2}$ peaks at B. E. 372.09eV and 366.09eV respectively, having 6.0eV doublet slitting which is a characteristic of metallic AgNPs.

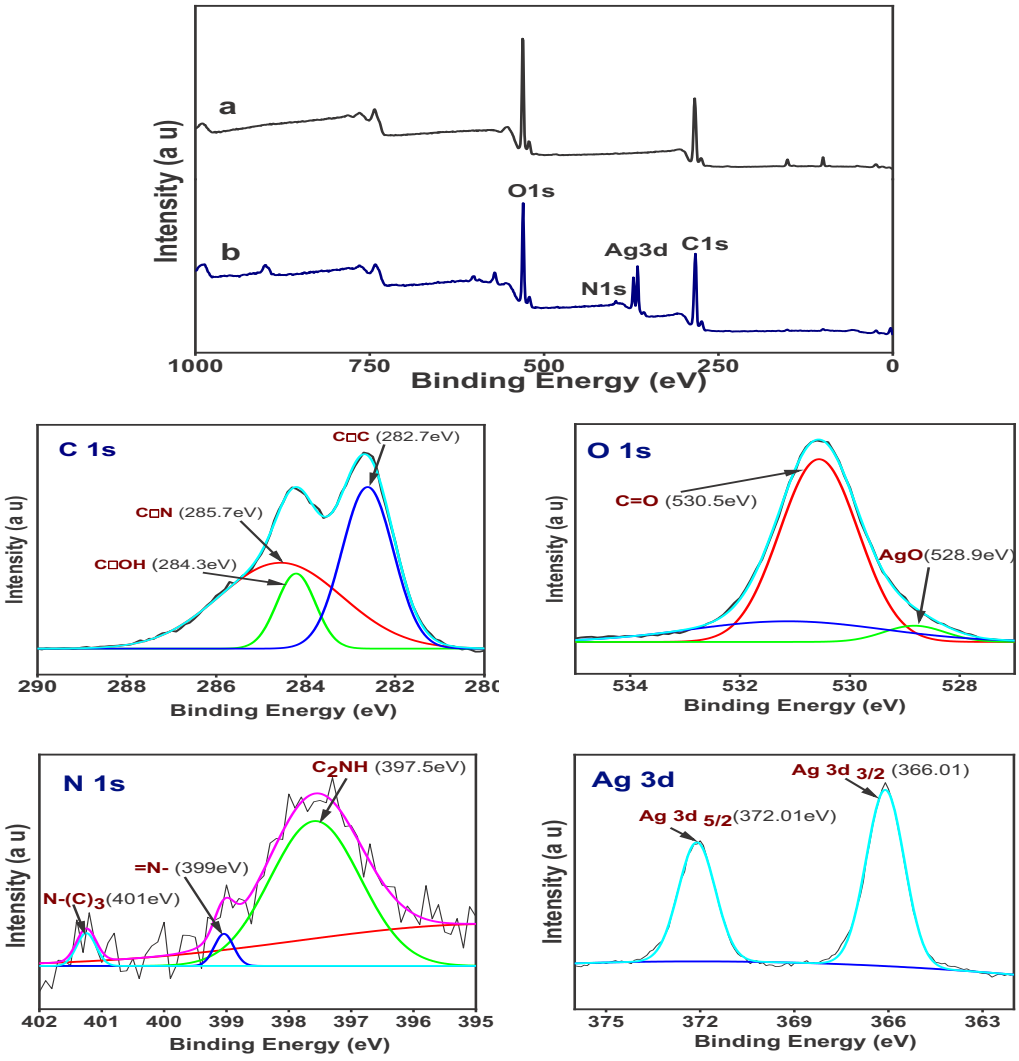

Figure 3.4 X-ray photoelectron spectroscopy (XPS) spectra of (a) modified CA (b) CA/AgNP nanofibers (narrow spectrum belongs to CA/AgNP)

3.4.5 TEM analysis

The TEM image of CA/AgNP given in Figure 3.5 illustrates CA nanofibers decorated with AgNPs. The TEM image depicts AgNPs having spherical shape. Sizes of the AgNPs calculated using ImageJ software were distributed between 10nm to 45nm having an average size of 22.68nm.

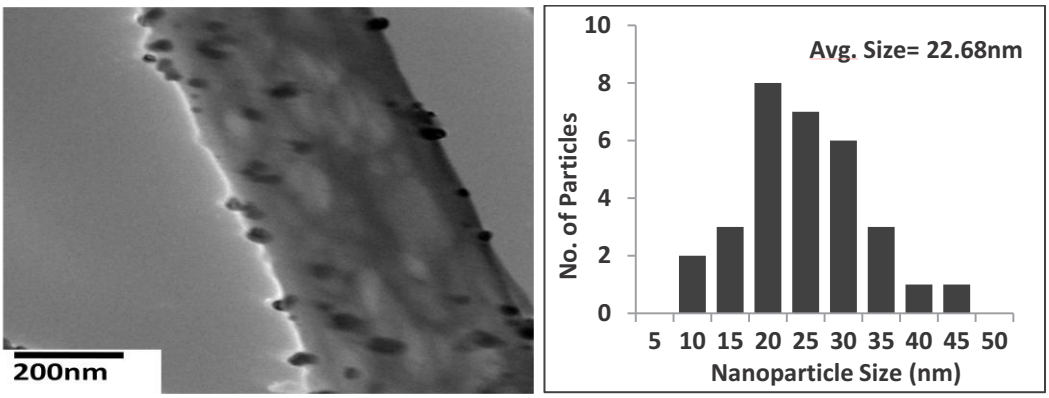

Figure 3.5 Transmission electron microscopy (TEM) image of CA/AgNP and size distribution of AgNPs

3.4.6 FTIR analysis

Surface modification of CA (deacetylation) and chemical modifications due to pDopa were studied using FTIR analysis (Figure 3.6). The CA spectrum (Figure 3.6a) shows a peak for stretching vibration of carbonyl groups (C=O) at 1750 cm^{-1}. A peak at 1370 cm^{-1} is assigned to CH_3 bending vibrations and the C-O-C stretching vibration peaks are present at 1237 cm^{-1} and 1050 cm^{-1}. The deacetylation treatment with NaOH removes the acetyl groups (CH_3CO) and generates hydroxyl groups (OH). In the surface modified CA, a broad peak at 3350cm^{-1} is assigned to stretching vibrations of OH groups which confirm surface modification and thus deacetylation process. Also broader peaks at 1000 cm^{-1} to 1200cm^{-1} are representative of deacetylated CA (cellulose structure). The three peaks at 1450cm^{-1}, 1350cm^{-1} and 813cm^{-1} are due to pDOPA. The peak at 1450cm^{-1} is assigned to stretching vibrations of aromatic C-C, at 1350cm^{-1} is assigned to C-N stretching vibrations and at 813cm^{-1} is assigned to NH_2 wagging. Weakening of OH stretching vibration peak at 3350 cm^{-1} in CA/AgNP (Figure 3.6c) may be due to electrostatic interaction of hydroxyl groups with AgNPs.

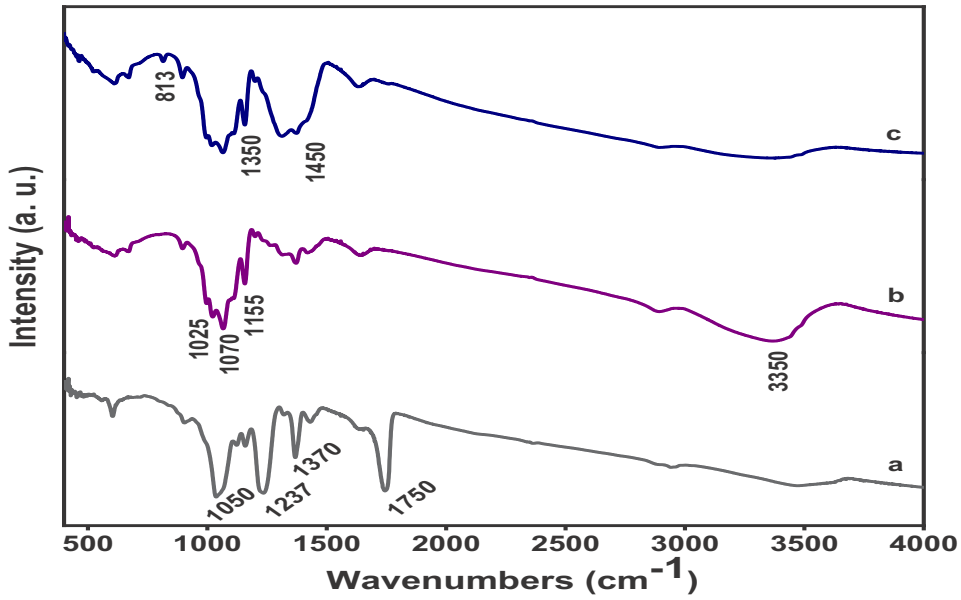

Figure 3.6 FTIR spectrum of (a) CA (b) surface modified CA (c) CA/AgNP

3.5 Antibacterial test

The antibacterial test results (disk diffusion method, halo width, mm) reported in Table 3.2 and Figure 3.7 show very good antibacterial activity of the CA/AgNP against both the Gram-negative bacteria (*E. coli*) and Gram-positive bacteria (*S. aureus*). The antibacterial agents such as AgNPs form an inhibition zone demonstrating an area inhibiting growth of the bacteria. A larger area (hallow width) means higher antibacterial activities. The net CA nanofibers show bacteria populations grown over the samples as well while the CA/AgNP samples demonstrated 1.79 mm and 1.78 mm inhibition zone (hallow width) against *E. coli* and *S. aureus* strains respectively which indicates substantial antibacterial properties of the CA/AgNP nanofibers.

Table 3.2 Antibacterial test (disk diffusion method) results of CA/AgNP against *E. coli* and *S. aureus*

Bacterial Strain	Halo Width (mm)	Halo Width (mm)	Halo Width (mm)	Mean Halo Width (mm)
E. coli	1.84	1.7	1.83	1.79
S. aureus	1.77	1.85	1.71	1.78

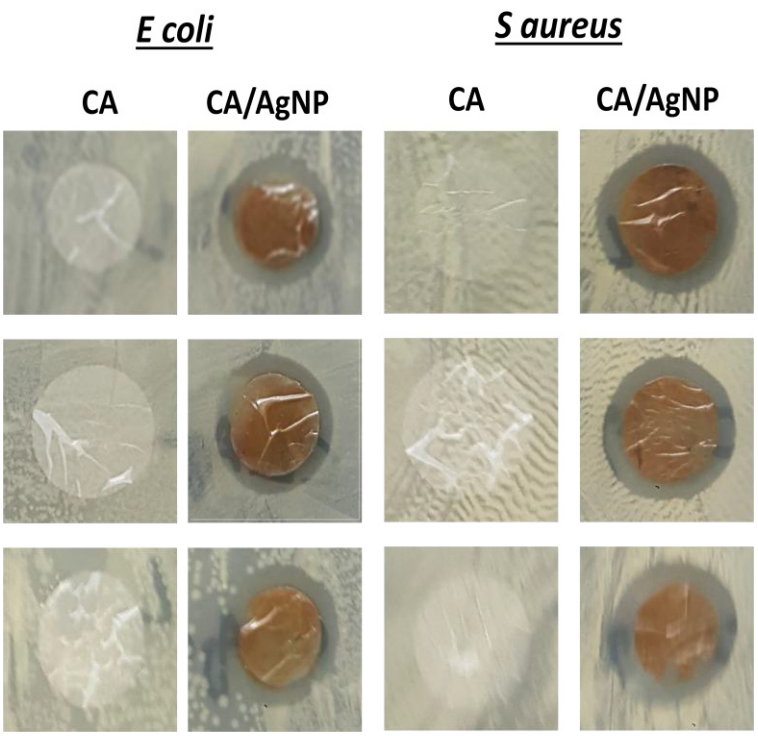

Figure 3.7 Photographic images of antibacterial test results (disk diffusion method) exhibiting halo width formed around CA/AgNP samples

The quantitative bactericidal activity results given in Figure 3.8A show 100% bactericidal activities of the CA/AgNP samples against both the *E. coli* (a Gram-negative bacteria) and *S. aureus* (a Gram-positive bacteria) revealing 0% viable bacterial cells. The relative cell viability (%) of the CA samples against the *E. coli* and *S. aureus* strains were 94% and 92% respectively. The AgNPs rupture bacterial cell walls either by direct contact or silver ions which when released into the bacterial species bind with adenosine triphophate (ATP) synthesizing enzymes and deoxyribonucleic acid (DNA) and obstruct their respiratory systems thereby produce antibacterial effect.

Bacterial growth inhibition properties of the CA/AgNP in liquid medium were also studied. The results given in Figure 3.8B demonstrated excellent *E. coli* and *S. aureus* growth inhibition potential of the CA/AgNP composite nanofibers. These results illustrate that the AgNPs owing to their larger surface area and gradual release of the silver ions are able to efficiently and effectively stop the bacteria reproduction and thus hinder their growth.

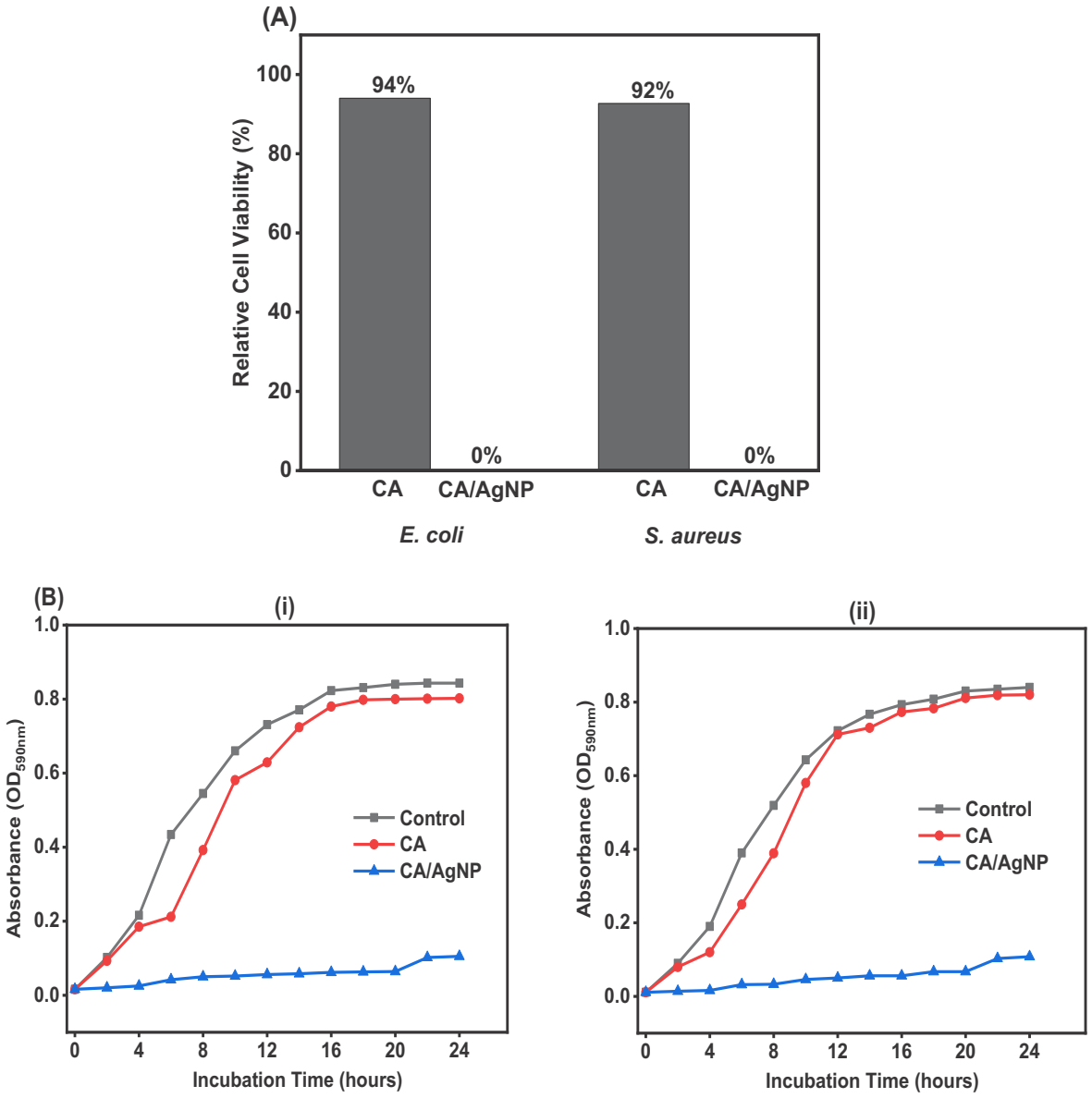

Figure 3.8 Antibacterial activities of the nanofiber samples (A) Relative cell viability results (B) Absorbance (OD_{590nm}) values obtained against (i) *E. coli* (ii) *S. aureus* strains

3.6 Conclusions

The research concludes synthesis of AgNPs on CA nanofibers by a green approach exploiting Dopa as reducing agent and stabilizing agent. Synthesis of spherical AgNPs decorated on CA/AgNP having 20nm crystallite sizes (Debye-Sherrer method) and 14.98 wt. % AgNP were confirmed by XRD, XPS, TEM and EDX analysis. The antibacterial test results confirmed very good antibacterial activities of the CA/AgNP composite nanofibers. The CA/AgNP samples were effective in bacterial growth inhibition (both on agar plates and in liquid medium) and bactericidal activities. Thus the research results suggest CA/AgNP as prospective bio-composite for antibacterial applications.

References

[1] R. Konwarh, N. Karak, M. Misra, Electrospun cellulose acetate nanofibers: the present status and gamut of biotechnological applications, Biotechnology advances 31(4) (2013) 421-437.

[2] M. Gopiraman, A.W. Jatoi, S. Hiromichi, K. Yamaguchi, H.-Y. Jeon, I.-M. Chung, K.I. Soo, Silver coated anionic cellulose nanofiber composites for an efficient antimicrobial activity, Carbohydrate polymers 149 (2016) 51-59.

[3] J.S. Devi, B.V. Bhimba, Silver nanoparticles: Antibacterial activity against wound isolates & invitro cytotoxic activity on Human Caucasian colon adenocarcinoma, Asian Pacific Journal of Tropical Disease 2 (2012) S87-S93.

[4] M. Hao, M. Tang, W. Wang, M. Tian, L. Zhang, Y. Lu, Silver-nanoparticle-decorated multiwalled carbon nanotubes prepared by poly (dopamine) functionalization and ultraviolet irradiation, Composites Part B: Engineering 95 (2016) 395-403.

[5] E.K. Jeon, E. Seo, E. Lee, W. Lee, M.-K. Um, B.-S. Kim, Mussel-inspired green synthesis of silver nanoparticles on graphene oxide nanosheets for enhanced catalytic applications, Chemical Communications 49(33) (2013) 3392-3394.

[6] Y. Ma, H. Niu, X. Zhang, Y. Cai, One-step synthesis of silver/dopamine nanoparticles and visual detection of melamine in raw milk, Analyst 136(20) (2011) 4192-4196.

[7] M. Sureshkumar, D.Y. Siswanto, Y.C. Chen, C.K. Lee, M.J. Wang, Antibacterial and biocompatible surfaces based on dopamine autooxidized silver nanoparticles, Journal of Polymer Science Part B: Polymer Physics 51(4) (2013) 303-310.

[8] Y.-r. Ma, H.-y. Niu, Y.-q. Cai, Colorimetric detection of copper ions in tap water during the synthesis of silver/dopamine nanoparticles, Chemical Communications 47(47) (2011) 12643-12645.

[9] G. Wang, X. Huang, P. Jiang, Mussel-inspired fluoro-polydopamine functionalization of titanium dioxide nanowires for polymer nanocomposites with significantly enhanced energy storage capability, Scientific Reports 7 (2017) 43071.

[10] J.r. Liebscher, R. Mrówczyński, H.A. Scheidt, C. Filip, N.D. Hădade, R. Turcu, A. Bende, S. Beck, Structure of polydopamine: a never-ending story?, Langmuir 29(33) (2013) 10539-10548.

[11] X. Chang, J. Yang, D. Han, B. Zhang, X. Xiang, J. He, Enhancing Light-Driven Production of Hydrogen Peroxide by Anchoring Au onto C3N4 Catalysts, Catalysts 8(4) (2018) 147.

CHAPTER 4

Cellulose Acetate/AgNP Composite Nanofibers by Thermal Treatment and DMF Assisted Process

4.1 Introduction

This chapter reports synthesis of CA/AgNP composite nanofibers by thermal treatment and DMF assisted process for antibacterial activities. The CA nanofibers were produced by electrospinning and deacetylated with sodium hydroxide to convert acetyl groups into hydroxyl groups for improved silver ion (Ag^{+}) adsorption. The deacetylated CA nanofibers were treated with silver nitrate. Generation of AgNPs was accomplished with a thermal treatment and DMF assisted procedures. The samples were characterized with SEM, FTIR, XRD, EDX, XPS, TEM and antibacterial assays. Effect of these methods on mechanical properties, thermal stabilities (DTA analysis) and swelling of the CA nanofibers was also studied. Both the processes were observed to be effective and efficient in generation of AgNPs on the CA nanofiber surfaces having higher contents and good spatial distributions. The DMF induced process generated AgNPs with comparatively larger sizes. The antibacterial test confirmed excellent antibacterial performance of the CA/AgNPs against *S. aureus* and *E. coli*. The CA/AgNP nanofibers well decorated with AgNPs having good spatial distribution and excellent antibacterial performance suggests CA/AgNPs as promising candidates for efficient antimicrobial activities.

4.2 Research background

CA is a well known biopolymer which possesses good hydrophilicity, biocompatibility and biodegradability. To improve adsorption of silver ions on CA surfaces, its acetyl groups need to be converted into hydroxyl groups by a suitable treatment in order to improve absorbency, chemical reactivity and surface functionality.

Electrospinning of the CA into nanofibers ensure its extended performances due to the inherent structural characteristics of nanofibers such as higher surface area, nano-scale diameter, porosity, breathability and mechanical strength which enables these nanocomposites ideal material in numerous applications. Furthermore, higher absorbency and moisture retaining properties of the deacetylated CA nanofibers produce moist environment and soothing effect in wound healing which enables CA as a desirable material particularly in wound healing applications[1].

Silver is a well known antimicrobial agent. Its nanoparticles (AgNPs) possess excellent antibacterial activities which depend on size of the AgNPs. Smaller sized AgNPs due to their larger contact areas

exhibit better antibacterial performance. Apart from antibacterial applications, the AgNP/nanofiber have also been used in other applications such as in biological protections, chemical protections, conductive nanocomposites, filtration, catalysis and in tissue engineering scaffolds for bone defect repairs. Functional performances of these composite nanofibers depend on size, shape, contents and spatial distribution of AgNPs[2].

AgNPs can be incorporated into/onto electrospun nanofiber structures by different methods. Such as adding synthesized AgNPs into the polymer solution, mixing silver salt into the solution and subsequently reducing into nanoparticles before electrospinning, adding silver salts into the solution and reduction procedure after electrospinning and dip coating of silver ions on nanofibers followed by a suitable reduction method. However, for better bioavailability post electrospun coating procedures are more effective. AgNP/nanofiber composites with uniformly distributed AgNPs over nanofibers are more likely to produce better performance in antibacterial applications. For reduction of the silver ions into AgNPs, several methods such as chemical reduction, biological reduction, irradiation and polysaccharides methods can be used.

This chapter proposes thermal treatment and DMF induced reduction process for synthesis of AgNPs on CA nanofibers. Both the methods generated AgNPs on CA nanofibers with good spatial distribution and higher contents. These simple reduction methods were effective and efficient in synthesis of AgNPs. No stabilizing agent, capping agent or any co-reducing agent was used. The antibacterial test results revealed excellent antibacterial activities by the CA/AgNP nanocomposites.

4.3 Synthesis of CA/AgNP composite nanofibers

The deacetylated CA nanofibers were produced as reported earlier in chapter 2. The CA samples were coated with silver by immersing into 200mM silver nitrate ($AgNO_3$) solution for 24 hours at 23 ^{0}C to prepare silver coated CA nanofibers (CA/Ag^+). The $CEAg^+$ were dried for two hours in an oven dryer at 40 ^{0}C before reduction process.

The thermal reduction process for CA/AgNP was carried out at 160 ^{0}C in a laboratory drying oven for 1 hour, 1.5 hours and 2 hours to prepare CA/AgNP1, CA/AgNP2 and CA/AgNP3 nanocomposite. In the DMF induced method the samples were intermittently soaked in DMF while heating at boiling point temperature of DMF. The intermittent soaking of silver coated CA nanofibers in DMF was performed after every fifteen (15) minutes and the samples were treated for 45 minutes (CA/AgNP4), 1hour (CA/AgNP5) and 1.5h (CA/AgNP6). Description of the processes is given in Table 4.1 as well.

Table 4.1 Description of the samples

Samples	Process Time	Temperature (^{0}C)	Thermal/DMF Process
CA/AgNP1	1h	160^{0}C	Thermal
CA/AgNP2	1.5h	160^{0}C	Thermal
CA/AgNP3	2h	160^{0}C	Thermal
CA/AgNP4	45min.	160^{0}C	DMF
CA/AgNP5	1h	160^{0}C	DMF
CA/AgNP6	1.5h	160^{0}C	DMF

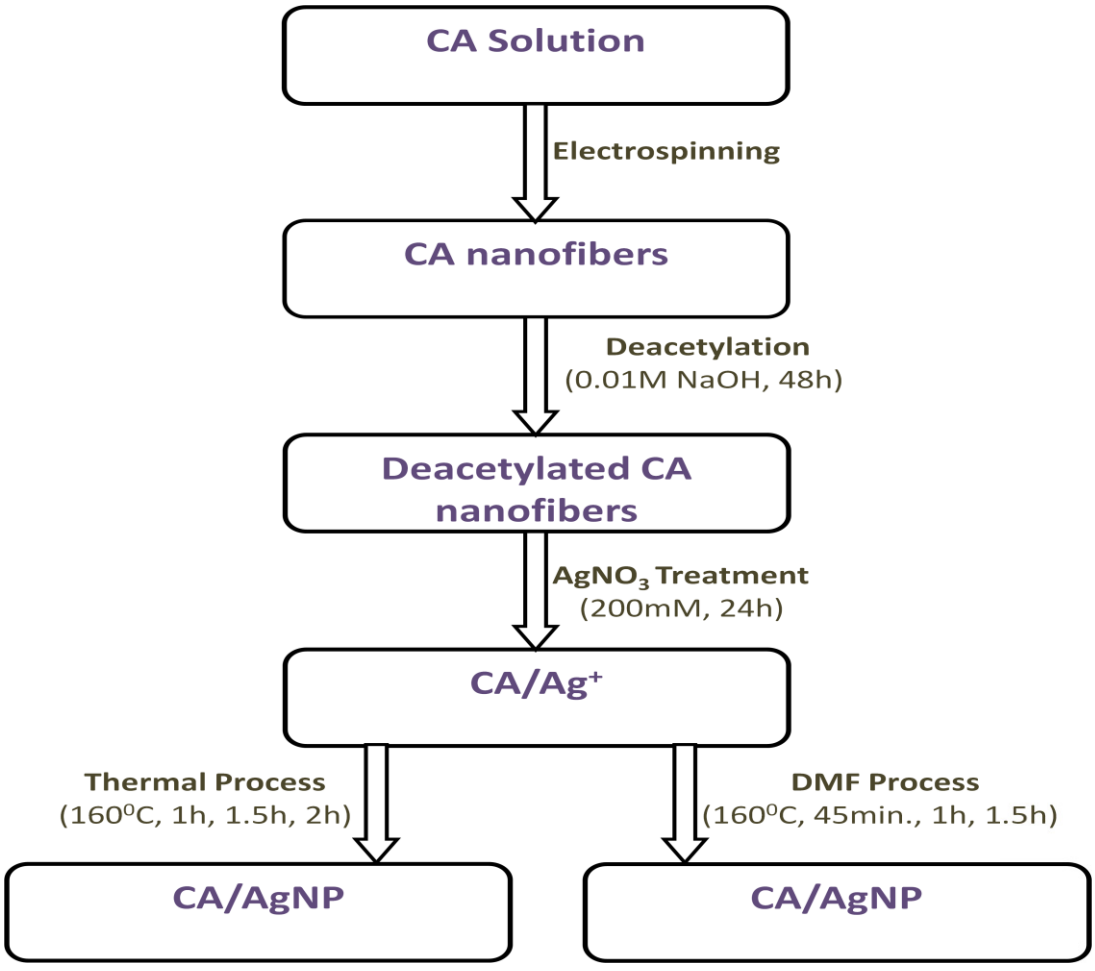

Scheme 4.1 Schematic diagram for preparation of CA/AgNP samples

4.4 Results and discussions

4.4.1 Characterization of CA nanofibers

SEM images of CA nanofibers show smooth and regular morphology of the nanofibers. Average diameter of CA was 291nm (Figure 4.1a) while that of modified CA was 289nm (Figure 4.1b). The results suggest alkaline deacetylation process having insignificant effect on morphology of the nanofibers.

Deacetylation of CA was studied with FTIR analysis. Characteristic FTIR peaks of cellulose acetate can be evidenced in the CA spectra (Figure 4.2Aa) at 1740 cm^{-1} for stretching vibrations of carbonyl group (C=O), 1375 cm^{-1} for CH_3 bending vibrations and at 1236 cm^{-1} and 1050 cm^{-1} for C-O-C stretching vibrations. These peaks disappeared in the modified CA spectra (Figure 4.2Ab). The broader peaks at 1000-1200 cm^{-1} are characteristics of deacetylated CA. Appearance of a peak at 3350cm^{-1} is due to stretching vibrations of hydroxyl (OH) groups, which further confirms conversion of acetyl group (CH_3CO) into hydroxyl (OH) groups. The peaks at 2910 cm^{-1}, 1306 cm^{-1} and 1432 cm^{-1} are assigned to CH stretching vibrations, CH wagging and CH_2 deformation respectively belonging to CA. A peak at 604cm^{-1} in both CA and modified CA is due to CH bending deformations. The residual acetyl contents in the modified CA (deacetylated CA) were 2.7% (Table 4.2, Figure 4.3).

The XRD results (Figure 4.2B) validates FTIR analysis results. The XRD pattern of CA shows Bragg's angles (2θ) at 9.18^0 and 17.3^0 for (110) and (200) reflections which correspond to CA structure. While the XRD pattern of deacetylated CA exhibit diffraction angles (2θ) at 12.1^0, 20.1^0 and 22.0^0 representing 7.19 Å, 4.42 Å and 4.04 Å d-spacing which are characteristics of deacetylated CA (cellulose-II).

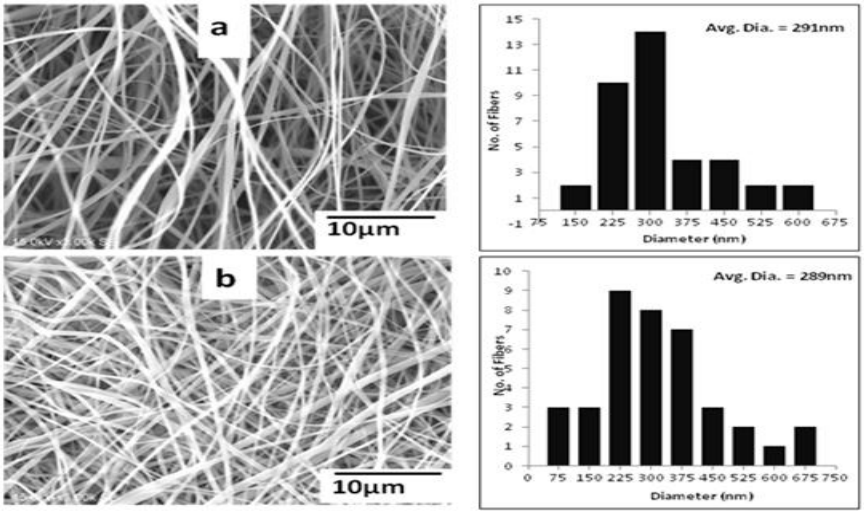

Figure 4.1 SEM images of nanofibers (a) CA (b) deacetylated CA

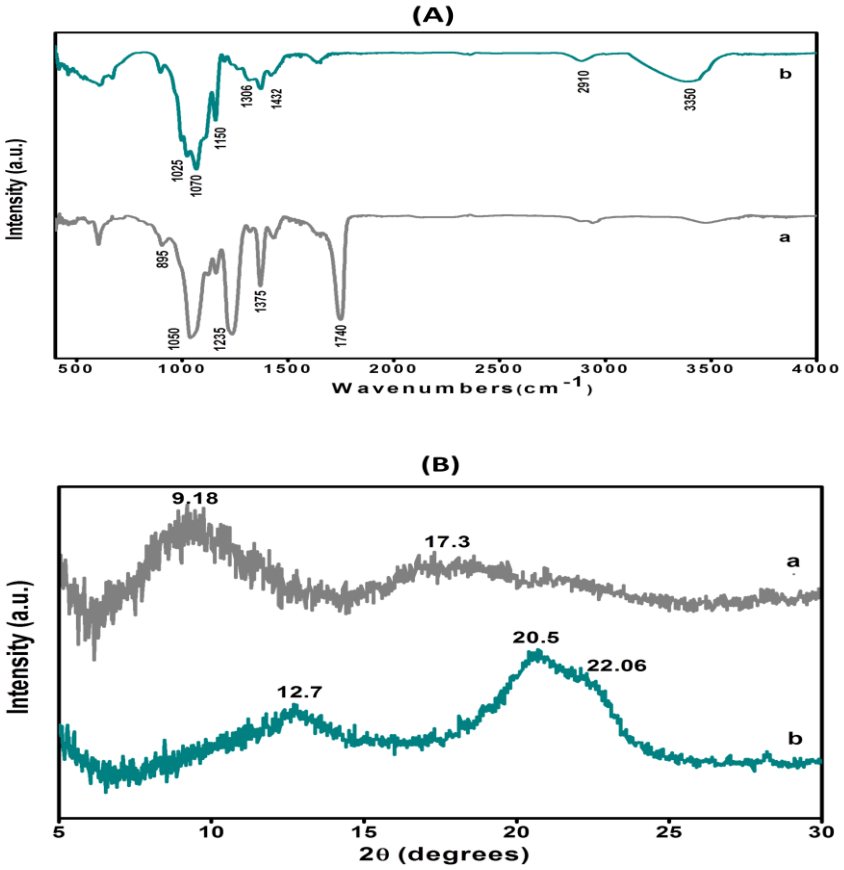

Figure 4.2 (A) FTIR spectrum of the nanofibers (a) CA (b) deacetylated CA

(B) XRD patterns of nanofiber (a) CA (b) deacetylated CA

Table 4.2 Calculation of residual acetyl contents

Sample	**A1740**	**A1030**	**Residual acetyl contents (%)**
CA	1.26	1.26	100
Deacetylated CA	0.39	1.4	2.7
CA/AgNP-P	0.118	2	5.9

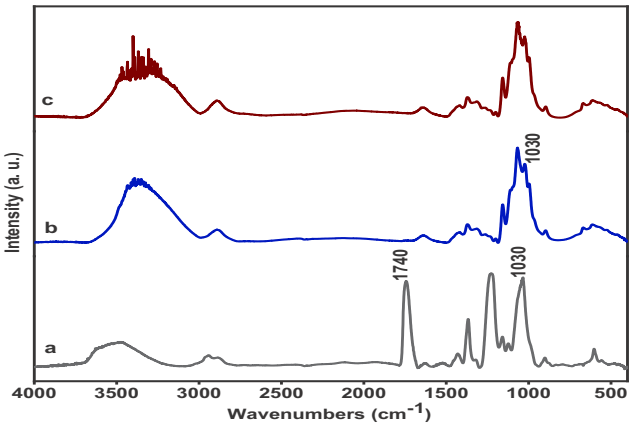

Figure 4.3 FTIR spectrum of (a) CA (b) deacetylated CA (c) CA/AgNP-P

4.4.2 CA/AgNP composite nanofibers

4.4.2.1 XRD analysis of CA/AgNP

Synthesis of AgNPs was primarily confirmed by XRD analysis and results are given in Figure 4.4. The results show all samples contain metallic AgNPs. Heat treatment has potential of reducing the silver ions into metallic silver as well as DMF is a potential reducing agent for silver. The samples show Bragg's angles (2θ) at 38.6^0, 44.5^0, 64.9^0 and 77.7^0 which were indexed as (111), (200), (220) and (311) crystal planes of metallic AgNPs with FCC (face centered cubic) crystal structure. At sufficiently high temperature the ionic silver reduce, nucleate and coalesce to form larger AgNPs[3]. The sizes of AgNPs calculated by Debye-Sherrer method and their specific surface area are reported in Table 4.3. The results demonstrated size of AgNPs moderately increase with increasing treatment time in both the thermal treatment and DMF induced reduction. Average sizes of AgNPs in CA/AgNP1, CA/AgNP2, CA/AgNP3, CA/AgNP4, CA/AgNP5 and CA/AgNP6 were 2.176nm, 2.586nm, 4.0198nm, 4.27nm, 4.81nm and 7.388nm respectively. Increase in size of AgNPs over extended heat treatment time may be result of stepwise mechanism for generation of metal AgNPs such as initiation of reduction and synthesis of small metal clusters (as small as 1nm) which grow to generate larger particles[4]. Sharpening of the peaks in both the Figures 4.4A and 4.4B from 'a' to 'c' suggests increase of AgNP sizes with processing time. Specific surface area of the synthesized AgNPs (Table 4.3) were $2.06x10^5$ m^2/g, $2.09x10^5$ m^2/g, $1.42153x10^5$ m^2/g, $1.3382x10^5$ m^2/g, $1.188x10^5$ m^2/g and $7.7345x10^4$ m^2/g in CA/AgNP1, CA/AgNP2, CA/AgNP3, CA/AgNP4, CA/AgNP5 and CA/AgNP6 respectively.

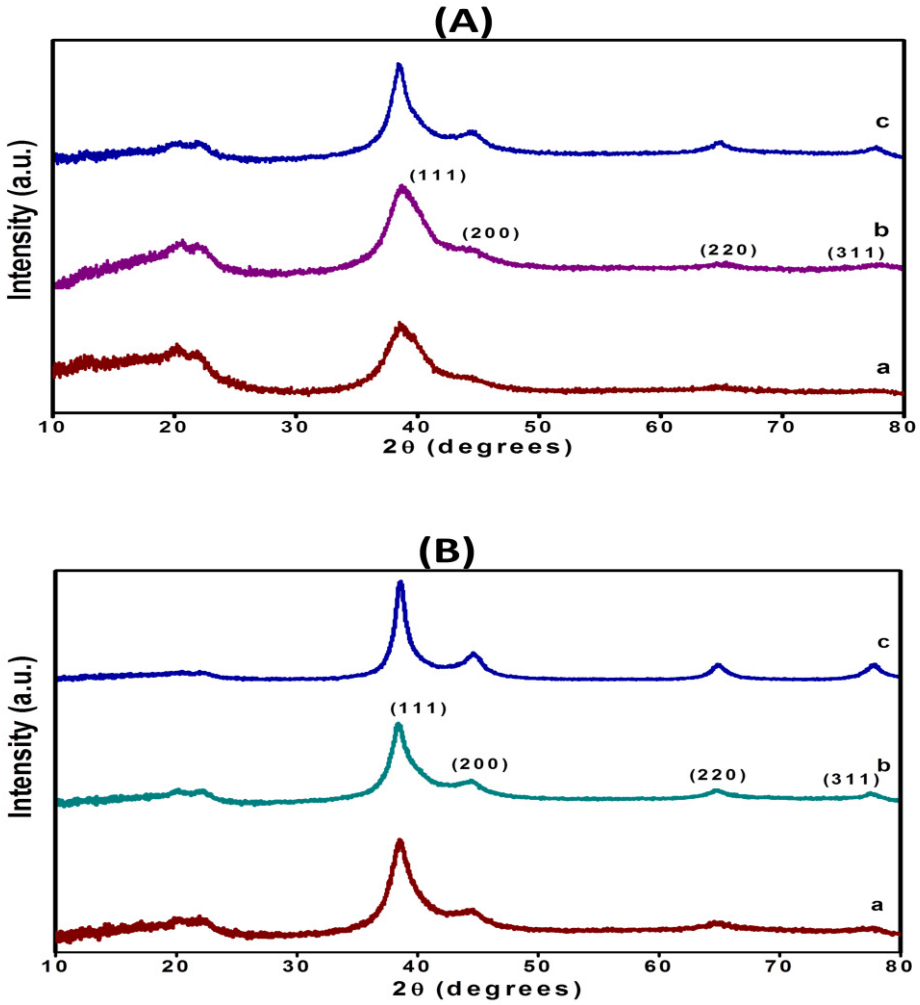

Figure 4.4 X-ray diffraction patterns of CA/AgNP synthesized by (A) thermal treatment (a) CA/AgNP1 (b) CA/AgNP2 (c) CA/AgNP3 (B) DMF reduction (a) CA/AgNP4 (b) CA/AgNP5 (c) CA/AgNP6

Table 4.3 Sizes of AgNPs (Debye-Sherrer method) and their respective specific surface area (m^2/g)

Samples	Size of AgNPs, A (nm)	Specific Surface Area (m^2/g)
CA/AgNP1	2.176	$2.06x10^5$
CA/AgNP2	2.586	$2.09x10^5$
CA/AgNP3	4.0198	$1.42153x10^5$
CA/AgNP4	4.27	$1.33824x10^5$
CA/AgNP5	4.81	$1.188x10^5$
CA/AgNP6	7.388	$7.7345x10^4$

4.4.2.2 EDX results

Quantitative elemental compositions and EDX spectrum of CA/AgNP1, CA/AgNP2, CA/AgNP3, CA/AgNP4, CA/AgNP5 and CA/AgNP6 are given in Table 4.4 and Figure 4.5 respectively. The mass percentage of AgNPs in CA/AgNP1, CA/AgNP2, CA/AgNP3, CA/AgNP4, CA/AgNP5 and CA/AgNP6 were 30.24 %, 33.29%, 35.47%, 35.14 %, 38.55% and 40.15% respectively. The results revealed a moderate increase in mass percentage of AgNPs with process time in both thermal treatment and DMF induced reduction methods. Furthermore, DMF reduction method samples (CA/AgNP4, CA/AgNP5 and CA/AgNP6) exhibited comparatively higher AgNP contents. The EDX spectrum reported in Figure 4.5 further validates the findings.

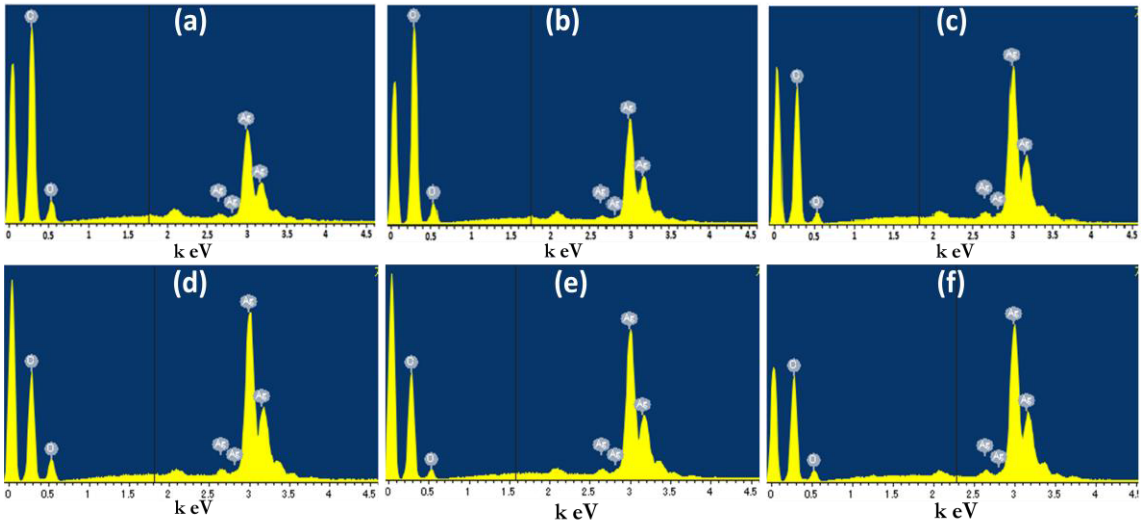

Figure 4.5 EDX spectrum of (a) CA/AgNP1 (b) CA/AgNP2 (c) CA/AgNP3 (d) CA/AgNP4 (e) CA/AgNP5 (f) CA/AgNP6

Table 4.4 Elemental compositions of CA/AgNP1, CA/AgNP2 and CA/AgNP3

Elements	Samples											
	CA/AgNP1		CA/AgNP2		CA/AgNP3		CA/AgNP4		CA/AgNP5		CA/AgNP6	
	Mass (%)	Atoms (%)	Mass (%)	Atoms (%)	Mass (%)	Atoms (%)	Mass (%)	Atoms (%)	Mass (%)	Atoms (%)	Mass (%)	Atoms (%)
CK	51.62	75.25	50.18	75.69	54.94	83.13	43.34	68.34	50.21	79.77	48.03	78.26
OK	18.13	19.84	16.53	18.72	9.59	10.89	21.53	25.49	11.24	13.41	11.82	14.46
AgL	30.24	4.91	33.29	5.59	35.47	5.98	35.14	6.17	38.55	6.82	40.15	7.28
Total	100	100	100	100	100	100	100	100	100	100	100	100

4.4.2.3 XPS evaluations

Further study on chemical states of the CA, CA/AgNP1, CA/AgNP2, CA/AgNP3, CA/AgNP4, CA/AgNP5 and CA/AgNP6 was conducted using XPS analysis and the results are reported in Figure 4.6 and Figure 4.7. The deacetylated CA contains C-OH, C=O, C-O-C, C-C and CH functional groups in its structure. The respective peaks at binding energy (B.E.) of 283.3 eV and 531.3 eV for C1s and O1s represent the chemistry of CA. The C1s peak at B.E 283.3 eV ascertains presence of C-O-C, C-OH, C-H, C-C and C=O groups. Presence of the C-OH and C=O groups may similarly be confirmed by O1s peak at B.E. 531.3 eV [5]. The XPS spectra of CA/AgNP1, CA/AgNP2 and CA/AgNP3, CA/AgNP4, CA/AgNP5 and CA/AgNP6 show peaks of Ag (3d) at B.E. 365.9 eV (Ag $3d_{3/2}$) and 371.9 eV (Ag $3d_{5/2}$). These peaks correspond to the representative peaks of metallic silver at 368.1 eV and 374.1 eV with a 6.0 eV doublet slitting [3, 5]. Thus the XPS results confirm deacetylation of CA and synthesis of CA/AgNP nanofibers both in thermal treatment and DMF induced reduction procedures.

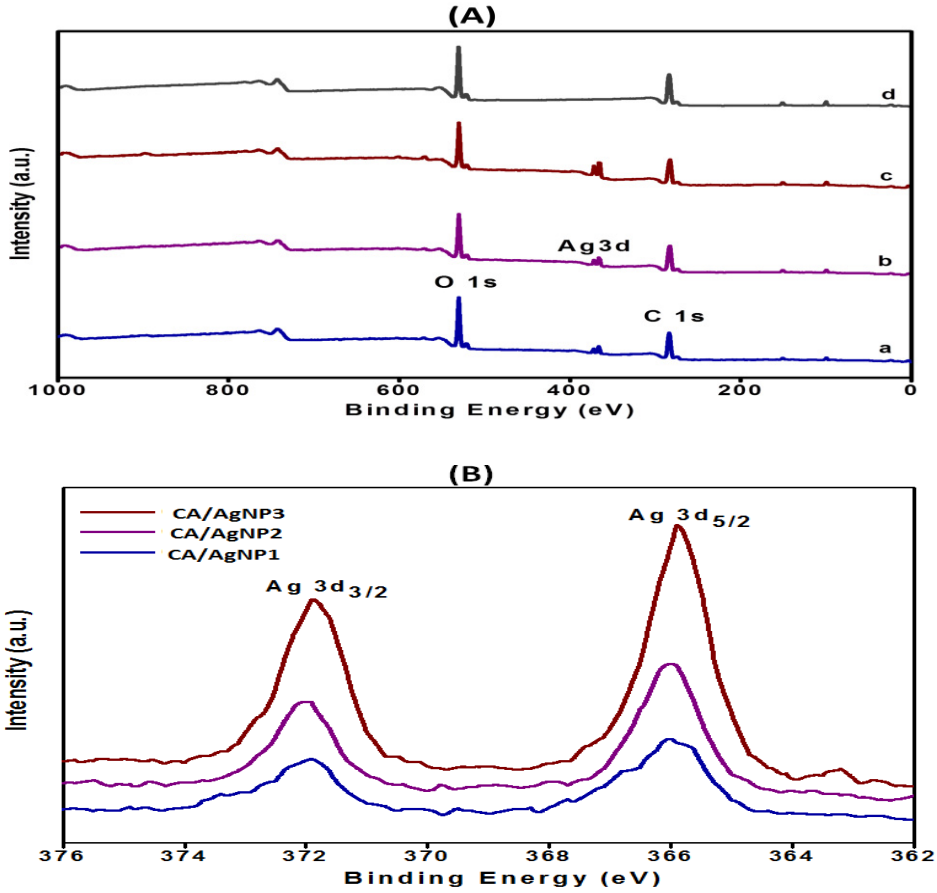

Figure 4.6 (A) X-ray photoelectron spectroscopy (XPS) spectrum of (a) CA/AgNP1 (b) CA/AgNP2 (c) CA/AgNP3 (d) CA nanofibers

(B) Magnified XPS spectrum of CA/AgNP1, CA/AgNP2 and CA/AgNP3 exhibiting Ag 3d peaks

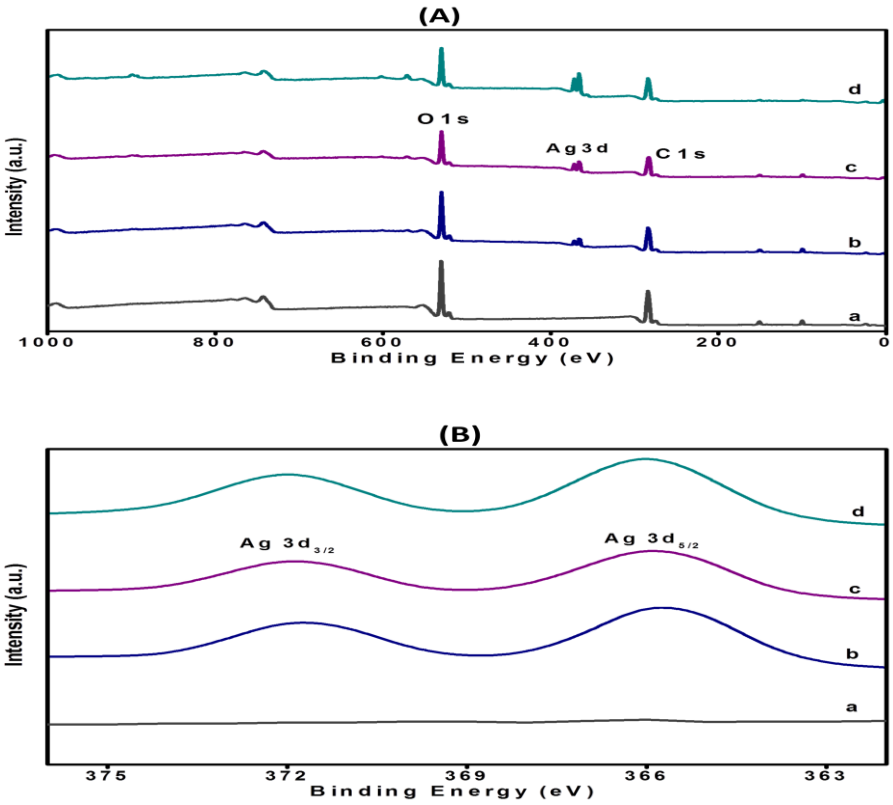

Figure 4.7 (A) XPS spectrum of (a) CA (b) CA/AgNP4 (c) CA/AgNP5 and (d) CA/AgNP6 (B) magnified XPS spectrum for Ag3d peaks (a) CA (b) CA/AgNP4 (c) CA/AgNP5 and (d) CA/AgNP6

4.4.2.4 TEM observations

To confirm synthesis of AgNPs, observe their shapes and spatial distributions, transmission electron microscopic (TEM) analysis was conducted. The results given in Figure 4.8, depict CA/AgNP samples highly decorated with well dispersed AgNPs. Sizes of the AgNPs in CA/AgN1 were between 1.5nm to 3.5nm having an average size of 2.22nm. Similarly, in the CA/AgNP3, the AgNP sizes were between 3nm to 6.5nm having an average size of 4.12nm. In both the samples a deviation of ±1.5nm from the average size was observed. Average size of the AgNPs on the CA/AgNP4 was calculated to be 4.28nm which increased to 7.4nm in CA/AgNP6. Thus DMF induced thermal treatments generated AgNPs on CA nanofibers with moderately larger sizes. Increase in the sizes of AgNPs over extending process time may be due to tendency of AgNPs to aggregate and form larger clusters due to coalescence. These results are in close agreement with the results of Debye-Sherrer method. The TEM images depicted spherical shape of AgNPs in both the thermal treatment and DMF reduction methods. Furthermore, the TEM images indicate CA nanofibers having very good spatial distribution of AgNPs.

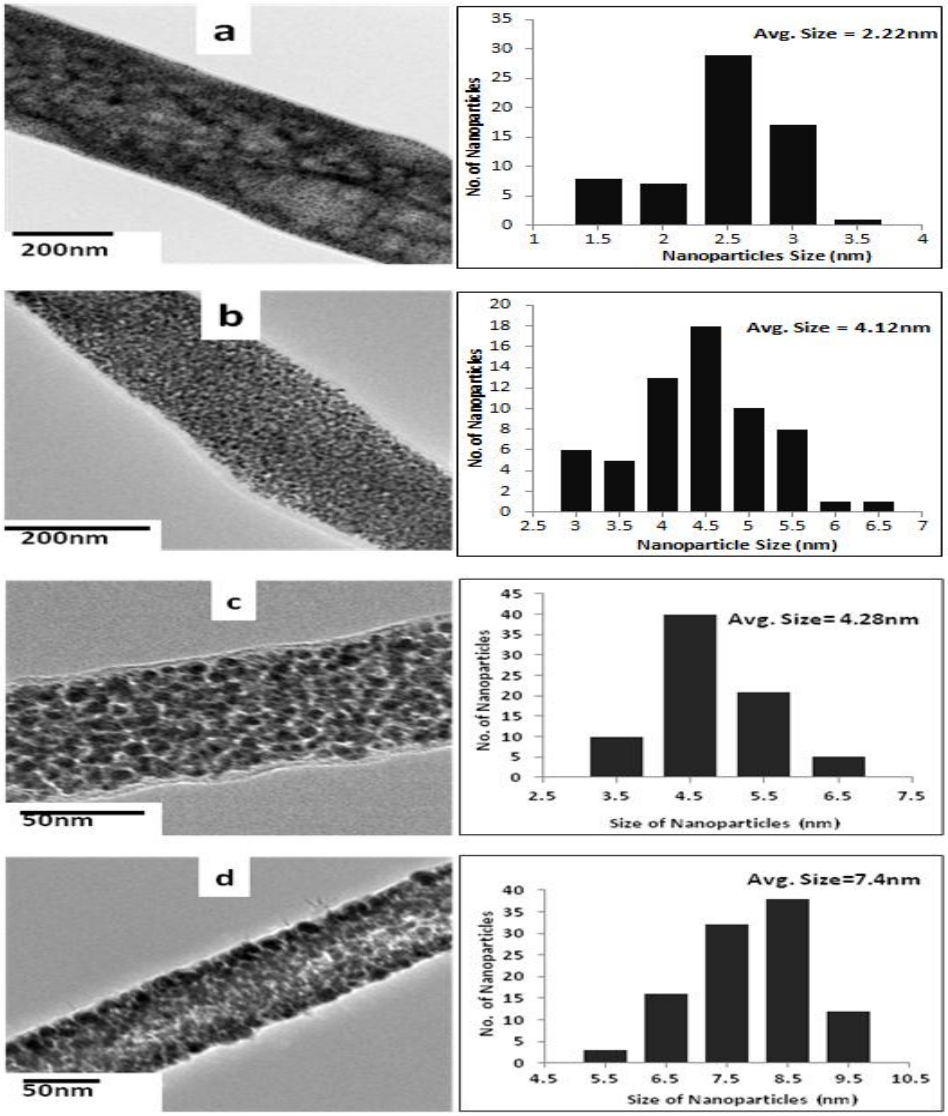

Figure 4.8 Transmission electron microscopy (TEM) image of (a) CA/AgNP1 (b) CA/AgNP3 (c) CA/AgNP4 (d) CA/AgNP6

4.4.3 Antibacterial activities of CA/AgNP

Antibacterial performance of the CA/AgNP samples determined by disk diffusion test method (inhibition zone) reported in Figure 4.9 and Table 4.5 exhibit excellent antibacterial performance of the CA/AgNP samples produced via thermal treatment (CA/AgNP1, CA/AgNP2 and CA/AgNP3) and DMF assisted process (CA/AgNP4, CA/AgNP5 and CA/AgNP6). The samples are observed to show higher antibacterial activity (larger area of inhibition zone) against *Gram-positive* bacteria (*S. aureus*) than the *Gram-negative* bacteria (*E. coli*). These results are consistent with previously reported antibacterial activities of AgNPs against *E. coli* and *S. aureus* [6-7]. Furthermore, area of the inhibition zone is correlated with processing time and hence AgNP contents in the CA/AgNP samples. The area of inhibition against *S. aureus* by CA/AgNP1 was 270.345mm^2 which increased to

347.1305mm^2 in CA/AgNP3 and against *E. coli* was 223.76mm^2 in CA/AgNP1 which increased to 269.9637mm^2 in CA/AgNP3. Similarly, it was 269.6893mm^2 in CA/AgNP4 which increased to 293.3707mm^2 in CA/AgNP6 against *S. aureus* and 186.0683mm^2 in CA/AgNP4 which increased to 268.014mm^2 in CA/AgNP6 against *E. coli*. The EDX results (Table 4.3) revealed higher silver contents in DMF treated samples (CA/AgNP4, CA/AgNP5 and CA/AgNP6) than thermal treatment samples (CA/AgNP1, CAAgNP2 and CA/AgNP3), however, sizes of AgNPs were smaller in later process. Higher antibacterial activities by thermally treated samples may be due to small sized AgNPs. This may be effect of sizes of AgNPs. Generally, smaller sized nanoparticles possess larger surface area and have been reported to show better antibacterial performances [8]. The TEM images (Figure 4.7) show sizes of AgNPs in CA/AgNP1 and CA/AgNP3 centered around 2.5nm and 4.5nm respectively, however, the same in CA/AgNP4 and CA/AgNP 6 were centered around 4.5nm and 8.5nm respectively.

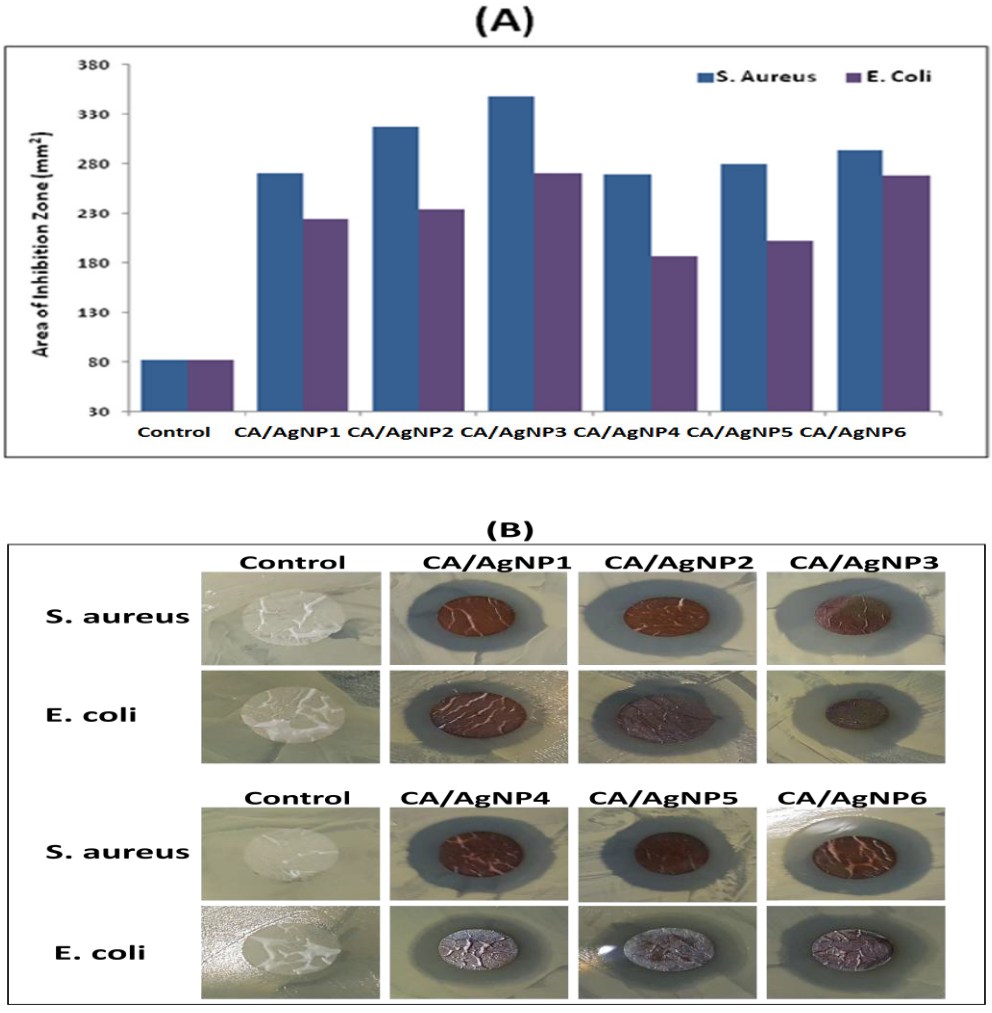

Figure 4.9 Antibacterial activities of CA/AgNP nanofiber samples (A) Area of inhibition zone (mm^2) (B) Photographic images of the samples incubated with *S. aureus* and *E. coli* strains

Table 4.5 Antibacterial activities of CA/AgNP nanofibers (area of inhibition zone in mm^2)

Sample	Area of inhibition zone (mm^2)	
	S. aureus	***E. coli***
Control (CA)	81.87	81.87
CA/AgNP1	270.345	223.76
CA/AgNP2	316.884	234.227
CA/AgNP3	347.1305	269.9637
CA/AgNP4	269.6893	186.0683
CA/AgNP5	279.5643	202.1973
CA/AgNP6	293.3707	268.014

Antibacterial activities of the samples were further investigated by quantitative bactericidal assay (relative viable cell counting, Figure 4.10) and liquid medium bacteria growth inhibition (OD_{590nm}, Figure 4.11). All of the CA/AgNP samples demonstrated 100% bactericidal properties (0% viable cells) and were effective in growth inhibition of the *E. coli* and *S. aureus* strains.

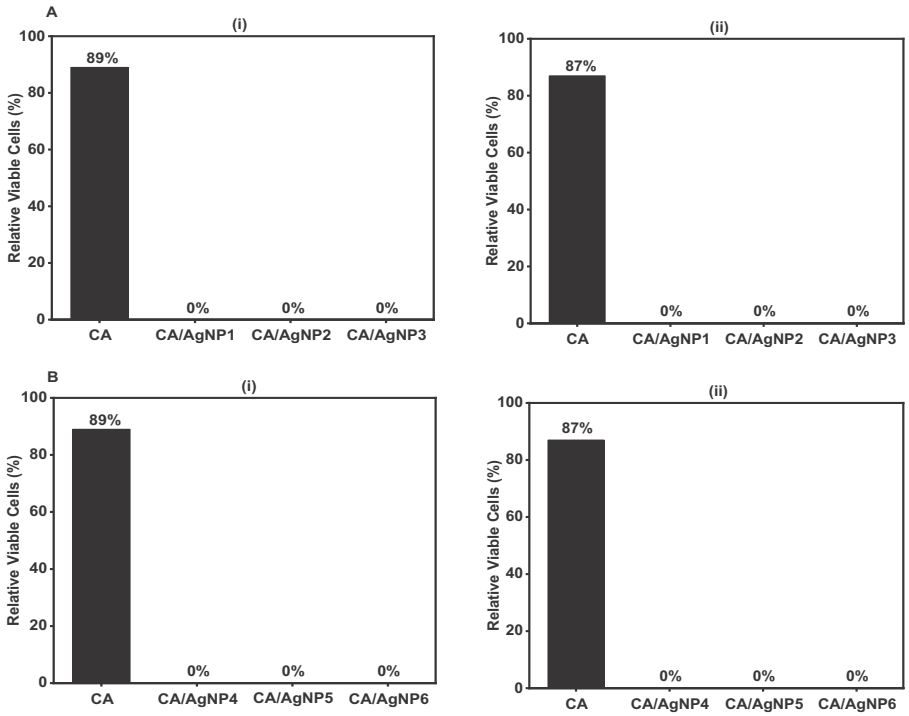

Figure 4.10 Quantitative bactericidal test results against (i) *E. coli* (ii) *S. aureus* (A) heat treated samples (B) DMF induced process

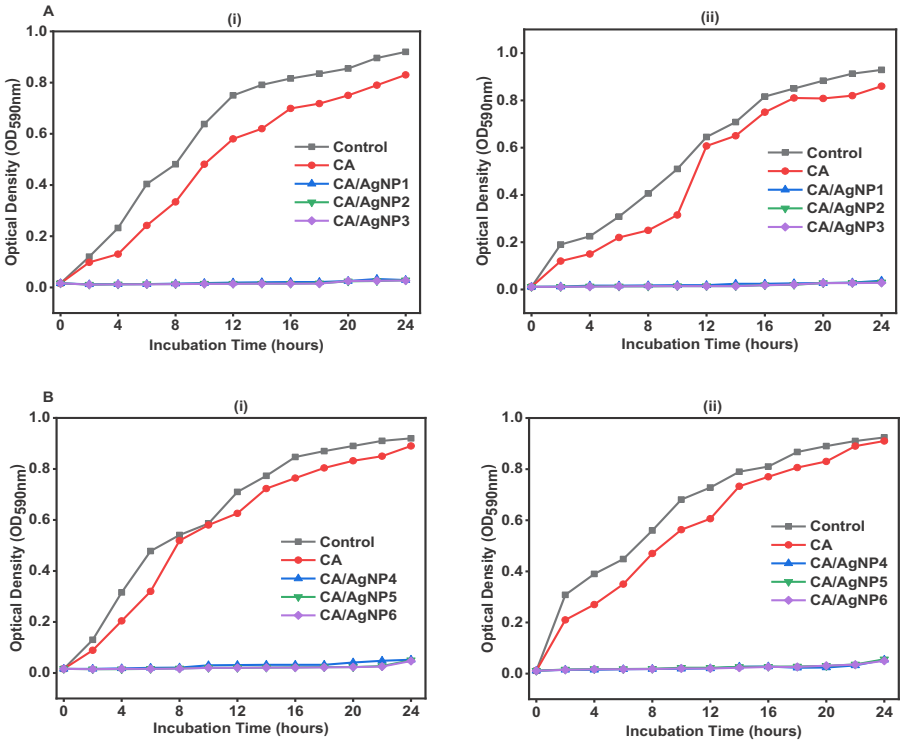

Figure 4.11 Liquid medium bacterial growth inhibition test results, optical density OD_{590nm}, against (i) *E. coli* (ii) *S. aureus* (A) heat treatment process (B) DMF induced process.

Thus antibacterial test results suggest potential of CA/AgNPs in antibacterial application domain. Apart from antibacterial applications, due to good spatial distribution and higher contents of AgNPs, the CA/AgNP may also be exploited in conductive applications where high conductivity of metallic silver, non-toxicity of AgNPs towards human cell and resemblance of nanofiberous structure with extracellular matrix (ECM) should serve the functionality.

4.4.4 SEM observations and FTIR studies of CA/AgNP nanofibers

SEM images of the CA/AgNP1, CA/AgNP2, CA/AgNP3, CA/AgNP4, CA/AgNP5 and CA/AgNP6 were taken for observing effect of the thermal treatments and DMF induced reduction method on morphology of the nanofibers. The results shown in Figure 4.12 indicate that the proposed methods for synthesis of AgNPs do not significantly affect morphology of the nanofibers except for a change in their diameters. Nanofiber diameters in thermal treatment process were observed to decrease while those in DMF method increased in comparison to parent CA nanofibers. The average diameters of the CA/AgNP1, CA/AgNP2 and CA/AgNP3 were 265nm, 257nm and 251nm respectively while diameters of CA/AgNP4, CA/AgNP5 and CA/AgNP6 were 297nm, 302nm and 320nm respectively. The decrease in nanofiber diameter by thermal treatment may be due to thermal relaxation and removal of residual solvent and/or moisture from the samples. However, in DMF

reduction method, the DMF may have swollen the nanofibers resulting in increase of their diameters.

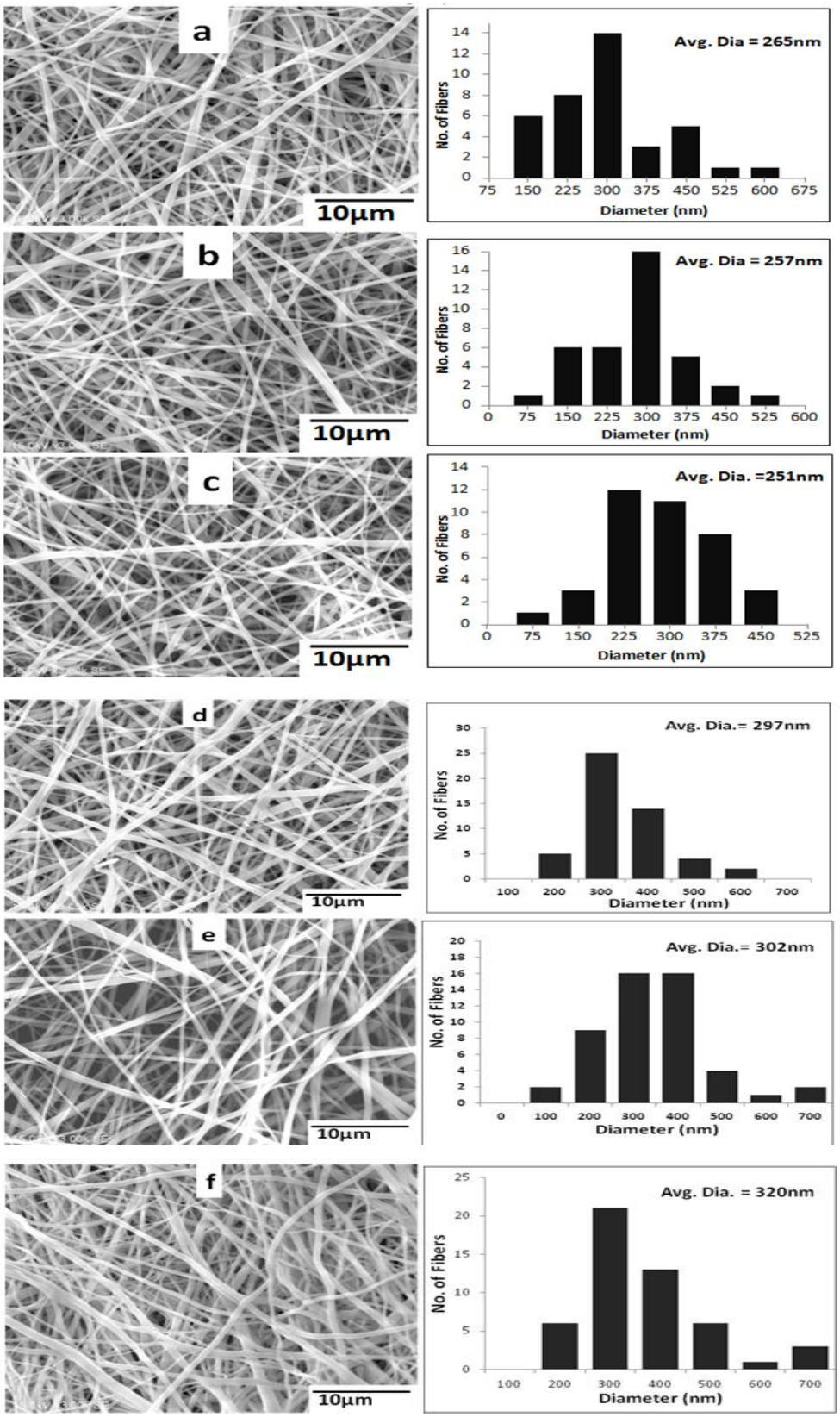

Figure 4.12 SEM images of CA/AgNP nanofibers (a) CA/AgNP1 (b) CA/AgNP2 (c) CA/AgNP3 (d) CA/AgNP4 (e) CA/AgNP5 (f) CA/AgNP6

The FTIR spectrum of CA/AgNP1, CA/AgNP2, CA/AgNP3, CA/AgNP4, CA/AgNP5 and CA/AgNP6 (Figure 4.13) confirms that both the thermal treatments and DMF induced reduction do not change chemical structure of CA nanofibers. Presence of all the characteristic peaks of CA illustrates that the thermal treatment and DMF induced reduction method does not alter chemistry of the respective CA/AgNP nanofibers. A moderate decrease in intensity of 3350 cm^{-1} peak in all the samples, which represents the stretching vibrations of hydroxyl groups, compared with deacetylated CA nanofibers may be due to electrostatic interaction with the AgNPs.

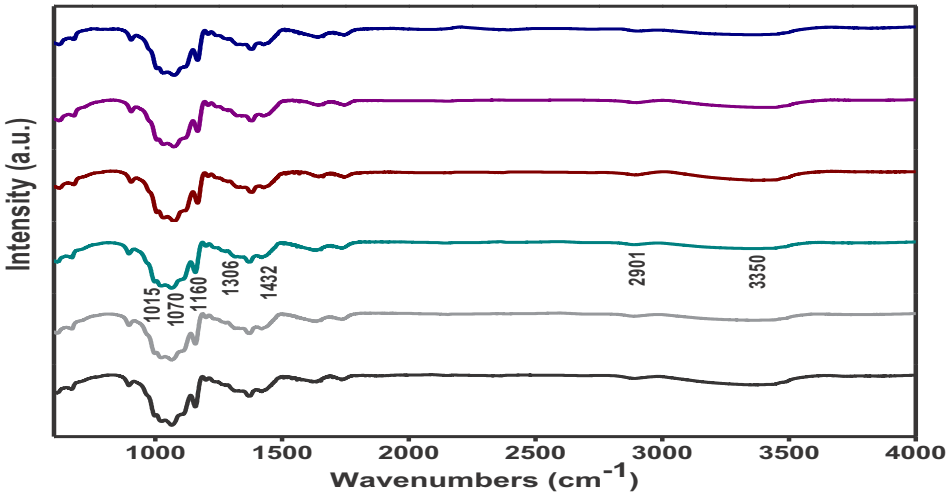

Figure 4.13 FTIR spectrum of (a) CA/AgNP1 (b) CA/AgNP2 (c) CA/AgNP3 (d) CA/AgNP4 (e) CA/AgNP5 (f) CA/AgNP6

Influence of deacetylation of CA on its morphology in DMF induced method for synthesis of AgNPs was further studied using FESEM analysis. The CA samples were deacetylated with 0.01M NaOH over 30 hours to prepare partially deacetylated templates (CA/AgNP-P) and for 48 hours in order to produce completely deacetylated samples (CA/AgNP-F). The results given in Figure 4.14 indicate CA/AgNP-P samples formed spherical protrusions on the CA/AgNP nanofiber surfaces which may be due to residual CA contents. The residual acetyl contents in the CA/AgNP-P were 5.9% (Table 4.2, Figure 4.3). Since CA is soluble in DMF while the deacetylated CA is insoluble, during the AgNP synthesis process the residual CA contents are solubilized. As the DMF evaporates these residual CA contents solidify and form spherical protrusion over the CA/AgNP nanofibers. The CA/AgNP-F exhibited smooth morphology without such protrusions.

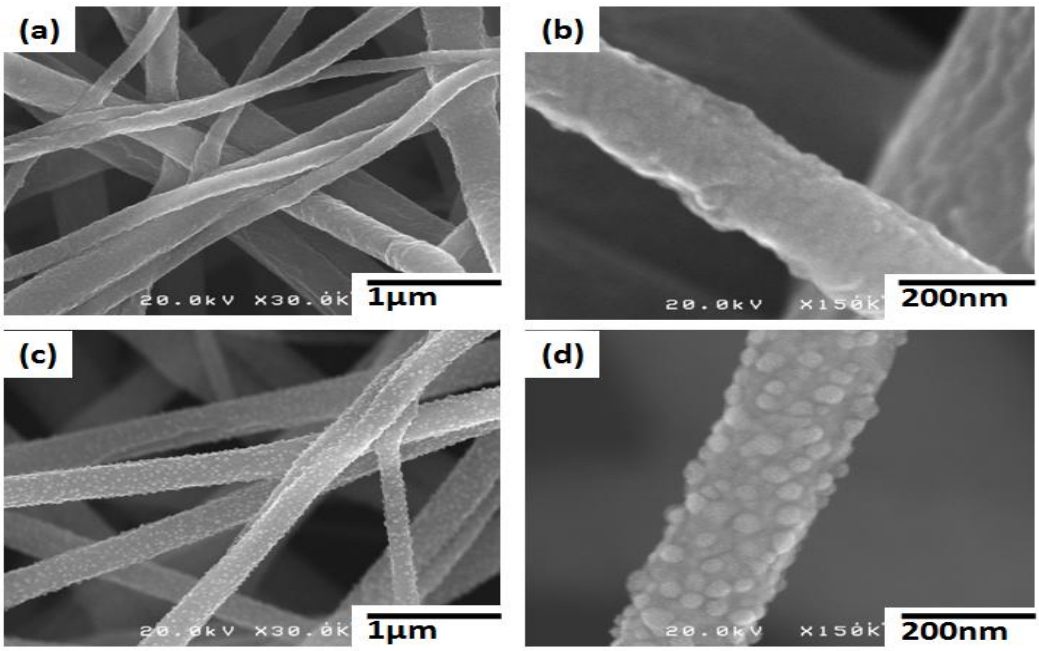

Figure 4.14 FESEM images of (a) CA/AgNP-F low magnification image (b) CA/AgNP-F high magnification image (c) CA/AgNP-P low magnification image (d) CA/AgNP-P high magnification image.

4.4.5 Mechanical properties, swelling test and DTA analysis

The mechanical properties of the samples were determined in terms of tensile strength at break (MPa) and elongation (%) at break (Figure 4.15A). The samples treated for longest times (CA/AgNP3 and CA/AgNP6) were chosen for mechanical analysis. The tensile strength (MPa) of the deacetylated CA, CA/AgNP3 and CA/AgNP6 samples were 6.86MPa, 4.76MPa and 4.92MPa respectively. Elongation at break (%) of deacetylated CA, CA/AgNP3 and CA/AgNP6 samples were 6.5%, 2.14% and 3.42% respectively. The results indicate decrease in tensile strength and elongation at break of the samples in thermal and DMF induced reduction methods. However, the mechanical properies seem sufficient for antibacterial applications. The reduction in tensile strength and elongation was higher in thermal reduction method than the DMF process.

Similar to mechanical properties, both the thermal and DMF induced methods of AgNP generation decreased swelling ratio (%) of the deacetylated CA samples (Figure 4.13B-D). Decrease in swelling ratio (%) was higher in thermal treatment than the DMF process. Since the generation of AgNPs took lesser time in DMF method than the thermal treatment, the samples were exposed to heat for less time. Also some heat was consumed in heating DMF. Thus the DMF process shows comparatively lower effect on mechanical properties and swelling ratio of the CA/AgNP nanofibers.

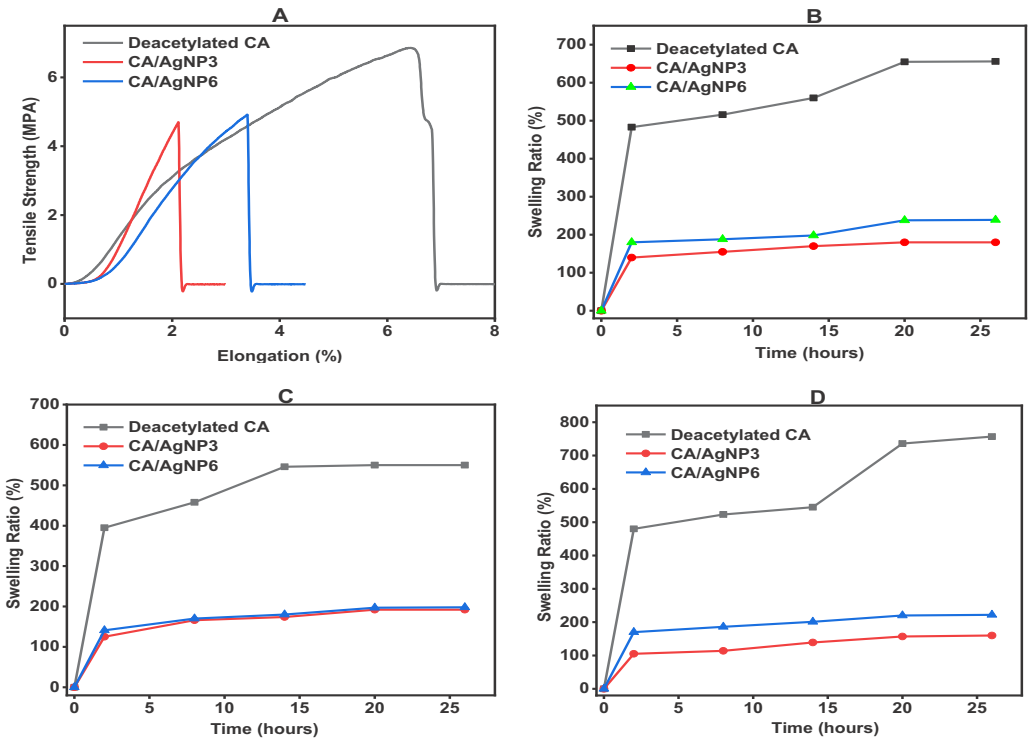

Figure 4.15 (A) Tensile strength-elongation diagram, swelling ration of the samples in different pH (B) pH 5.0 (C) pH 7.4 and (D) pH 8.0

For studying thermal stability of the samples, DTA analysis was carried out (Figure 4.16). For this study, the samples treated for longest times (CA/AgNP3 and CA/AgNP6) were chosen. The deacetylated CA showed two exothermic peaks at 335^{0}C and 440^{0}C corresponding to thermal degradation of cellulose and char formation [9] respectively. The CA/AgNP3 and CA/AgNP6 samples exhibited maximum degradation temperatures at 335^{0}C and 344^{0}C respectively. The sharper and intense exothermic peaks of CA/AgNP3 and CA/AgNP6 may be result of AgNP crystallization [10]. May be due to decrease in the hydroxyl groups in CA/AgNP3 and CA/AgNP6, as a result of AgNP adsorption, the initiation of thermal degradation temperatures shifted towards left [11]. However, due to crystallization of AgNPs, the final degradation temperatures increased to higher values demonstrating thermal stability of the CA/AgNP composite nanofibers [11-12].

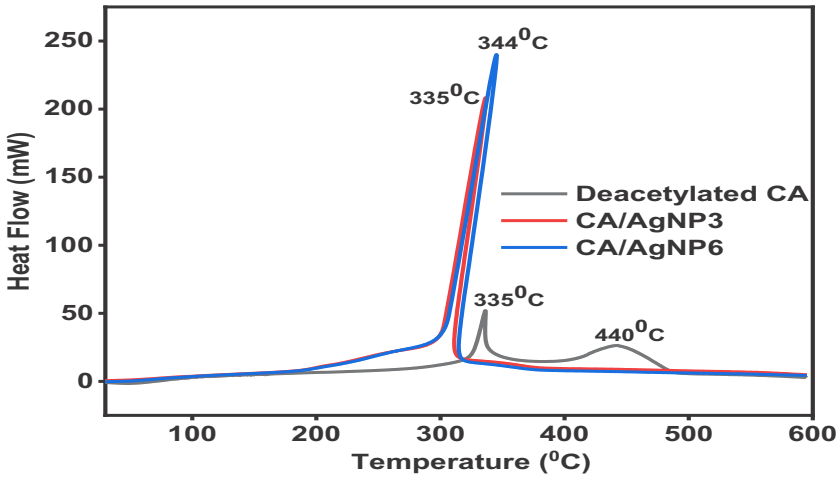

Figure 4.16 DTA thermogram of deacetylated CA, CA/AgNP3 and CA/AgNP6 nanofibers

4.5 Conclusions

The CA/AgNP composite nanofibers were successfully synthesized by thermal treatment and DMF induced reduction method for antibacterial applications. Synthesis of the metallic AgNPs was confirmed from XRD, XPS and TEM results. The diffraction angles (2θ) at 38.6^0, 44.5^0, 64.9^0 and 77.7^0 representing the (111), (200), (220) and (311) planes of metallic AgNPs demonstrated FCC crystal structure. Average sizes of the AgNPs on CA/AgNP samples produced by thermal treatment were 2.176nm, 2.586nm and 4.02nm (CA/AgNP1, CA/AgNP2 and CA/AgNP3) while the DMF induced process generated AgNPs having comparatively larger sizes (4.27nm, 4.81nm and 7.39nm in CA/AgNP4, CA/AgNP5 and CA/AgNP6 respectively). The antibacterial test results exhibited excellent antibacterial activities (area of inhibition zone) by all the samples against *S. aureus* and *E. coli*. May be due to smaller sizes of AgNPs, the CA/AgNP1, CA/AgNP2 and CA/AgNP3 (thermal treatment) produced larger area of inhibition zone compared to CA/AgNP4, CA/AgNP5 and CA/AgNP6 (DMF reduction) samples. All the CA/AgNP samples effectively inhibited growth of *E. coli* and *S. aureus* in liquid medium tests as well and demonstrated excellent bactericidal properties. Excellent antibacterial activities, smaller sizes and higher contents of AgNPs confirm CA/AgNPs as potential candidates for efficient antibacterial applications.

References

[1] M. Ke, J.A. Wahab, B. Hyunsik, K.-H. Song, J.S. Lee, M. Gopiraman, I.S. Kim, Allantoin-loaded porous silica nanoparticles/polycaprolactone nanofiber composites: fabrication, characterization, and drug release properties, RSC Advances 6(6) (2016) 4593-4600.

[2] J.H. Kim, H. Lee, A.W. Jatoi, S.S. Im, J.S. Lee, I.-S. Kim, Juniperus chinensis extracts loaded PVA nanofiber: Enhanced antibacterial activity, Materials Letters 181 (2016) 367-370.

[3] R. Li, M. He, T. Li, L. Zhang, Preparation and properties of cellulose/silver nanocomposite fibers, Carbohydrate polymers 115 (2015) 269-275.
[4] J.r. Polte, X. Tuaev, M. Wuithschick, A. Fischer, A.F. Thuenemann, K. Rademann, R. Kraehnert, F. Emmerling, Formation mechanism of colloidal silver nanoparticles: analogies and differences to the growth of gold nanoparticles, Acs Nano 6(7) (2012) 5791-5802.
[5] M. Gopiraman, D. Deng, S. Saravanamoorthy, I.-M. Chung, I.S. Kim, Gold, silver and nickel nanoparticle anchored cellulose nanofiber composites as highly active catalysts for the rapid and selective reduction of nitrophenols in water, RSC Advances 8(6) (2018) 3014-3023.
[6] M. Guzman, J. Dille, S. Godet, Synthesis and antibacterial activity of silver nanoparticles against gram-positive and gram-negative bacteria, Nanomedicine: Nanotechnology, Biology and Medicine 8(1) (2012) 37-45.
[7] R. Veerasamy, T.Z. Xin, S. Gunasagaran, T.F.W. Xiang, E.F.C. Yang, N. Jeyakumar, S.A. Dhanaraj, Biosynthesis of silver nanoparticles using mangosteen leaf extract and evaluation of their antimicrobial activities, Journal of Saudi Chemical Society 15(2) (2011) 113-120.
[8] J. Yan, A.M. Abdelgawad, M.E. El-Naggar, O.J. Rojas, Antibacterial activity of silver nanoparticles synthesized In-situ by solution spraying onto cellulose, Carbohydrate polymers 147 (2016) 500-508.
[9] S. Hu, Y.-L. Hsieh, Synthesis of surface bound silver nanoparticles on cellulose fibers using lignin as multi-functional agent, Carbohydrate Polymers 131 (2015) 134-141.
[10] M.A.M. Khan, S. Kumar, M. Ahamed, S.A. Alrokayan, M.S. AlSalhi, Structural and thermal studies of silver nanoparticles and electrical transport study of their thin films, Nanoscale research letters 6(1) (2011) 434.
[11] A.K. Vipin, B. Fugetsu, I. Sakata, A. Isogai, M. Endo, M. Li, M.S. Dresselhaus, Cellulose nanofiber backboned Prussian blue nanoparticles as powerful adsorbents for the selective elimination of radioactive cesium, Scientific reports 6 (2016) 37009.
[12] R.G. Chaudhary, H.D. Juneja, R. Pagadala, N.V. Gandhare, M.P. Gharpure, Synthesis, characterisation and thermal degradation behaviour of some coordination polymers by using TG–DTG and DTA techniques, Journal of Saudi Chemical Society 19(4) (2015) 442-453.

CHAPTER 5

Cellulose Acetate/TiO_2/AgNP Composite Nanofibers

5.1 Introduction

Silver nanoparticles (AgNPs) are effective antimicrobial agents however excess release of silver may cause rapid silver depletion and prolonged contact with AgNPs may induce side effects such as *carcinoma*, *allergies*, *argyria* and *argyrosis*. An strategy to avoid these detrimental side effects is immobilization of AgNPs on several organic and inorganic substrates. This chapter reports fabrication and characterization of CA/TiO_2/AgNP nanofiber composite containing AgNPs anchored on TiO_2 nanoparticles. The AgNPs anchored on TiO_2 nanoparticles were synthesized by an environmentally green process using dopamine hydrochloride (Dopa) as an adhesive and reducing agent. The TiO_2 nanoparticles were first treated with Dopa solution followed by a treatment in $AgNO_3$ solution. Then, the TiO_2/AgNP nanocomposites were added into CA solution and electrospun to fabricate CA/TiO_2/AgNP composite nanofibers. The samples have been characterized by XRD, TEM, XPS, SEM, EDX, FTIR and antibacterial assays. Synthesis of TiO_2/AgNP and its loading into CA nanofibers were confirmed by XRD, XPS, TEM and EDX analysis. SEM images indicated regular morphology of the nanofibers. The antibacterial test results confirmed CA/TiO_2/AgNP composite nanofibers having excellent antibacterial performances for 36hours and substantial bacterial growth inhibition for 72hours.

5.2 Research background

Titanium dioxide is a well known semiconducting material used in catalysis, optical, energy, environment and photonic applications. It is a popular photocatalyst available in three phases namely anatase, rutile and brookite. The TiO_2 has been reported to posses photo-induced bactericidal properties as well which are more prominent under ultraviolet (UV) light. Under UV irradiation, the TiO_2 produces reactive oxygen species i.e. superoxide and hydroxide radicals which disrupt the bacterial cell walls and block their respiratory systems. However, due to faster electron hole recombination rate in TiO_2, generation of ROS is limited. Immobilizing the noble metals such as silver on TiO_2 surface reduces electron-hole recombination rate thus improves generation of ROS[1].

Characteristic advantages of silver and AgNPs, discussed in previous sections, are highly suitable for many applications in general and excellent particular in antibacterial activities. However, silver induces harmful effects to the human cell when released in excess; *carcinoma*, *allergies*, a*rgyria* and *argyrosis* are the well known examples of excess silver release and prolonged contact with AgNPs. At

the same time earlier silver depletion may produce comparatively limited time antibacterial activities. One of the strategies to avoid these side-effects is anchoring the AgNPs on varying organic or inorganic surfaces to reduce the reported problems maintaining their antibacterial performances for extended times. Immobilization of the AgNPs on TiO_2 nanoparticles improves the UV light induced antibacterial properties of TiO_2 nanoparticles and helps to avoid adverse effects of excess release of silver ions[2].

Owing to, already discussed, highly desirable properties of CA it was chosen as a polymer to prepare CA/TiO_2/AgNP composite nanofibers. Advantages of electrospun nanofiberous structures have also been discussed in previous chapters.

In general, antibacterial nanocomposites inhibit bacteria colonization by release of the antibacterial agents, generation of reactive oxygen species (ROS), contact killing and oxidative stress[3]. The proposed bactericidal mechanism of CA/TiO_2/AgNP nanocomposite is based on generation of reactive oxygen species such as super oxides, hydroxide radicals, per oxides and singlet oxygen radicals[2]. The TiO_2/AgNP composite nanoparticles were synthesized using dopamine hydrochloride (Dopa) to form a polydopamine coating (pDopa) on the TiO_2 nanoparticles which when treated with $AgNO_3$ solution generated metallic AgNPs. Dopamine is a biomaterial, composed of catechol and amine groups, which possesses excellent adhesive, film forming and metal ion reducing capabilities. The hydroxyl groups of catechol moiety during oxidation into quinone lose their electrons to metal ions thereby generate corresponding metal nanoparticles[4]. Its amine groups on the other hand help to avoid aggregation of the metal ions. Thus, dopamine forms an adhesive coating on the TiO_2 nanoparticles which ensures adequate adsorption of silver ions on the TiO_2 and subsequently generates AgNPs. The dopamine process is a simple, environmentally benign and efficient route for generation of AgNPs. The CA/TiO_2/AgNP composite nanofibers have been observed to produce long term antibacterial performances.

5.3 Synthesis of TiO_2/AgNP composite nanoparticles

The TiO_2/AgNP composite nanoparticles were prepared using the adhesive film forming and reducing properties of dopamine hydrochloride (DOPA). For synthesis of TiO_2/AgNP nanoparticles, 300mg of DOPA were dissolved in 150mL of 1M Tris HCl buffer (2mg DOPA/mL of the buffer) then 200mg of TiO_2 nanoparticles were added into the solution. The mixture was rigorously stirred on magnetic stirrer for 18hours. The DOPA coated TiO_2 nanoparticles were obtained by centrifugation at 3000rpm for 15 minutes which were then washed multiple times with DI water. The DOPA coated TiO_2 nanoparticles were then added into 0.2M silver nitrate solution (350mL) and kept under strong

stirring for 18 hours. The TiO_2/AgNP composite nanoparticles were obtained by centrifugation at 3000 rpm for 20 minutes. The TiO_2/AgNP nanoparticles were dried in an oven dryer at 60 ^{0}C for 12hours.

5.4 Fabrication of CA/TiO_2 and CA/TiO_2/AgNP

For fabricating CA/TiO_2/AgNP composite nanofibers, a 17% CA solution was first prepared in DMF/acetone (1:2) solvents. Afterwards 5 wt. % (CA/TiO_2/AgNP1) and 10 wt. % (CA/TiO_2/AgNP2) of TiO_2/AgNP nanoparticles were added into the CA solution and rigorously stirred on the magnet stirrer. The solutions were sonicated for one hour. The CA/TiO_2 samples were similarly fabricated using 10 wt. % of TiO_2 nanoparticles. The electrospinning process and conditions were same as described in chapter 2.

5.5 Results and discussions

5.5.1 TiO_2/AgNP nanoparticles

Synthesis of TiO_2/AgNP nanocomposite particles was first confirmed by X-ray diffraction studies. The TiO_2 nanoparticles used in the research had rutile phase (size <100nm). The XRD pattern of TiO_2 given in Figure 5.1 shows diffraction angles, 2θ values, at 27.24^0, 36.1^0, 41.13^0, 54.3^0, 56.62^0, 62.56^0, 64.09^0, 69.05^0 and 69.81^0 which represent the (110), (101), (111), (211), (220), (002), (310), (301) and (112) planes of rutile phase titanium di oxide[5]. XRD patterns of TiO_2/AgNP shows corresponding 2θ values of metallic AgNPs, 38.1^0, 44.19^0, 64.47^0, 77.28^0 which are indexed as (111), (200), (220) and (311) demonstrating face centred cubic crystal structure of AgNPs [6], as well as corresponding diffraction angles of rutile phase TiO_2. The absence of any other peak in the XRD patterns of TiO_2 and TiO_2/AgNP illustrates purity of nanoparticles.

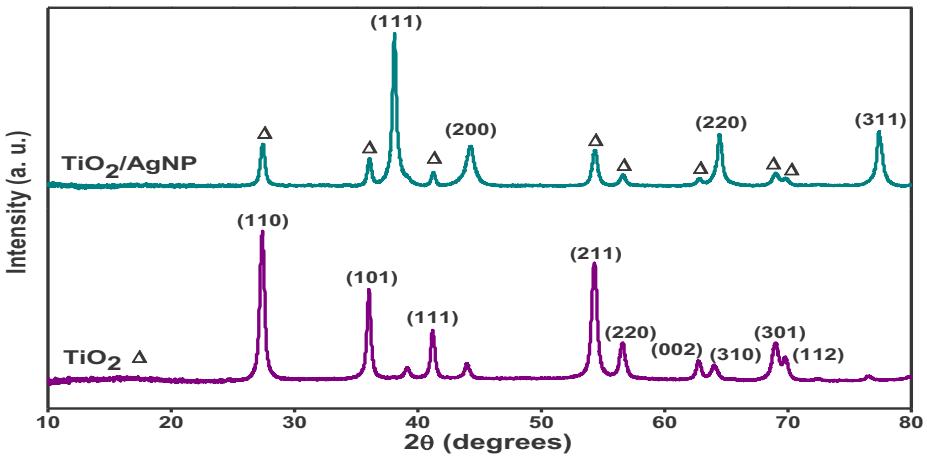

Figure 5.1 XRD patterns of TiO_2 nanoparticles and TiO_2/AgNP composite nanoparticles

Transmission electron microscopy images were taken to confirm synthesis and morphology of TiO_2 and TiO_2/AgNP (Figure 5.2). The HRTEM image of the AgNPs given in Figure 5.2d depicts (111) lattices of the AgNPs having 0.241nm lattice size confirming spherical shape and crystallinity of the AgNPs. The TEM image show TiO_2 nanoparticles (Figure 5.2a) having spherical and rod-like shapes. The TiO_2 nanoparticles had sizes between 20nm~100nm with average size of 36.12nm. The TEM images of TiO_2/AgNP (Figure 5.2b-5.2c) show spherical AgNPs densely decorated on the surface of TiO_2 nanoparticles. Average particle sizes of the AgNPs were 5.9nm while their sizes were dispersed between 4nm ~12nm; mainly between 6nm ~8nm, demonstrating poly-dispersity in the AgNPs.

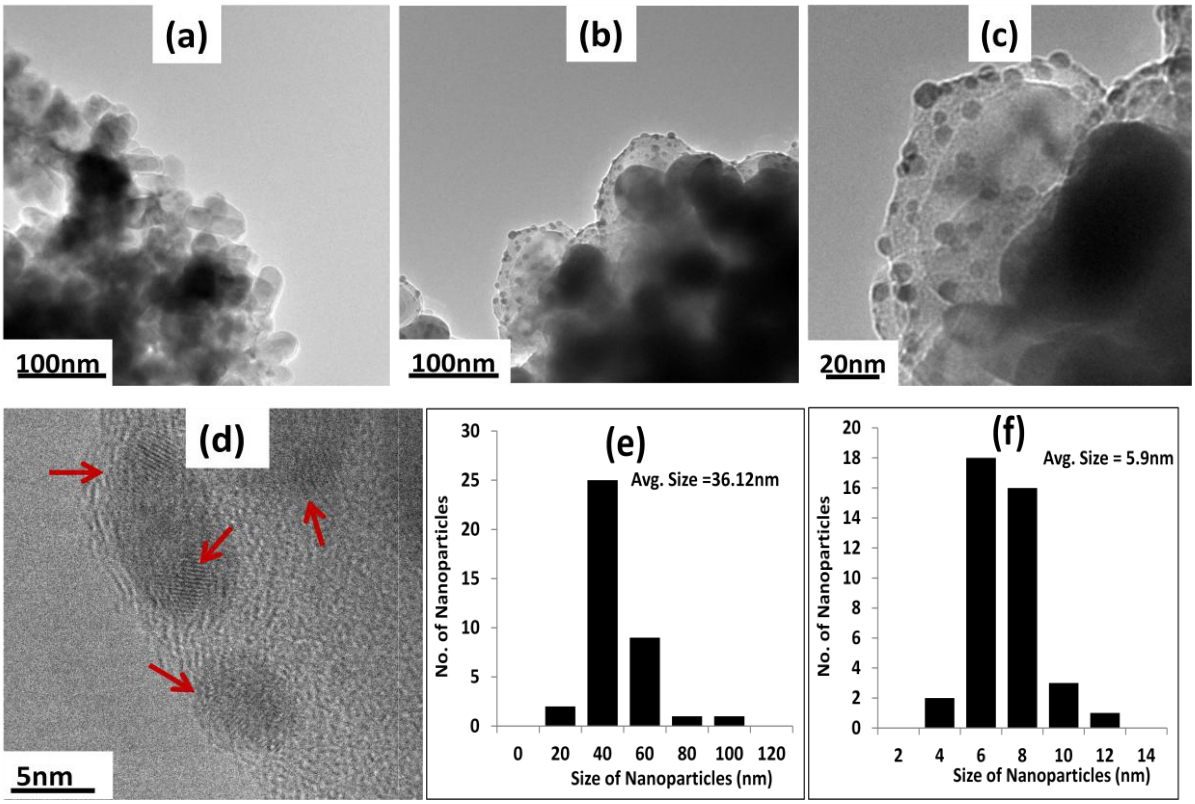

Figure 5.2 TEM images of (a) TiO_2 nanoparticles (b, c) TiO_2/AgNP nanocomposite particles (d) HRTEM image of the AgNPs (e) size distribution of TiO_2 nanoparticles (f) size distribution of AgNPs decorated on TiO_2 nanoparticles.

Analysis of TiO_2/AgNP by X-ray photoelectron spectroscopy (XPS) reveals chemisorptions of pDopa on TiO_2 nanoparticles and subsequent generation of AgNPs by pDopa. The XPS wide scan spectrum of the composite nanoparticles (Figure 5.3) shows C 1s, O 1s, N 1s, Ag 3d and Ti 2p peaks. The de-convoluted C 1s narrow spectrum exhibits peaks at binding energies (B. E.) of 282.66eV, 283.96eV, 285.08eV and 286.08eV representing C-C, C=O, C-OH and CN groups of pDopa. The C=O group confirms oxidation of C-OH into quinone. De-convolution of O 1s spectrum shows two peaks at B.E. 530.27eV and 531.01eV which belong to C=O and C-OH groups of pDopa. The N 1s narrow scan

spectrum further confirms pDopa structure on TiO_2 exhibiting N-H and =N- peaks at B.E. 398.11eV and 400.5eV respectively. A peak at B.E. 396.22eV for N-Ti reveals chemisorptions of pDopa on TiO_2 nanoparticles [7].The peaks at B.E. 456.7eV and 462.4eV represent the Ti 2p $_{3/2}$ and Ti 2p $_{1/2}$ states of titanium dioxide. The Ti 2p $_{3/2}$ and Ti 2p $_{½}$ had a doublet slitting of 5.7eV corresponding to TiO_2 nanoparticles. A peak at B.E. 457.6eV is due to Ti-N which demonstrates chemical interaction between pDopa and TiO_2 nanoparticles [8]. The two peaks at B.E. 372.36eV and 366.36eV belong to Ag 3d $_{3/2}$ and Ag 3d $_{5/2}$ having doublet slitting of 6.0eV which is characteristic of AgNPs.

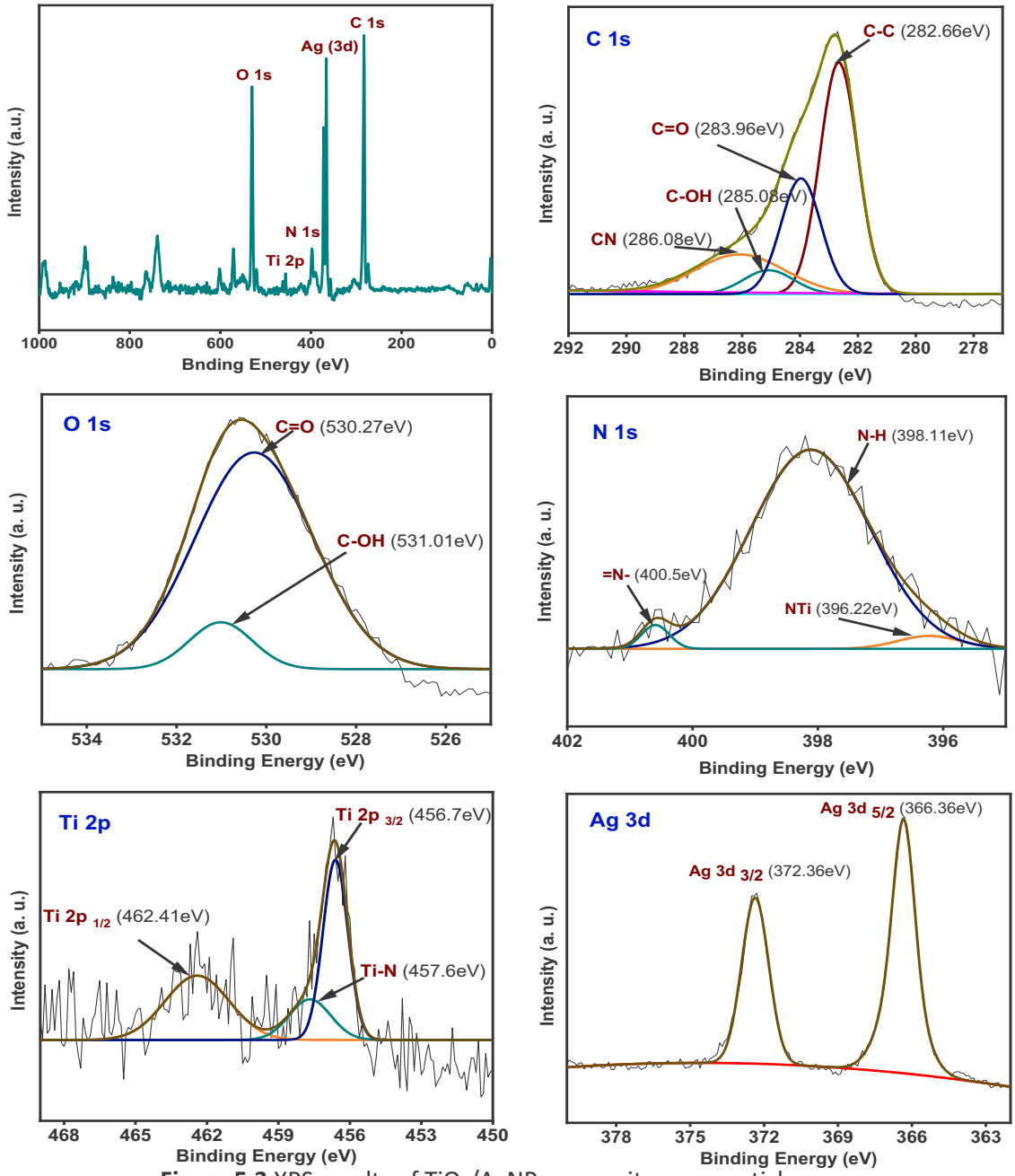

Figure 5.3 XPS results of TiO_2/AgNP composite nanoparticles

The EDX analysis of the TiO_2/AgNP composite nanoparticles was taken to get an insight into elemental compositions of the nanoparticles. The elemental compositions given in Table 5.1 validate contents of TiO_2, AgNPs and dopamine in the nanocomposite. The weight percentage of AgL and TiK were 32.91% and 25.62%. The CK and NK contents belong to the dopamine.

Table 5.1 Elemental composition of TiO_2/AgNP composite nanoparticles

Elements	Weight %age	Atomic %age
CK	4.73	11.03
NK	4.26	8.52
OK	32.48	56.92
TiK	25.62	14.99
AgL	32.91	8.55
Total	**100**	**100**

5.5.2 CA/TiO_2/AgNP composite nanofibers

The scanning electron microscopy images of CA, CA/TiO_2 and CA/TiO_2/AgNP nanofibers are given in Figure 5.4. The SEM images show regular and bead free morphologies of the nanofibers. May be due to increased conductivity of the solutions by addition of the nanoparticles, diameters of the CA/TiO_2, CA/TiO_2/AgNP1 and CA/TiO_2/AgNP2 were found to reduce in comparison to CA nanofibers. However, diameters of the CA/TiO_2/AgNP2 composite nanofibers were larger in comparison to CA/TiO_2/AgNP1 samples. This may be due to higher concentration of TiO_2/AgNP composite nanoparticles embedded in the CA matrix.

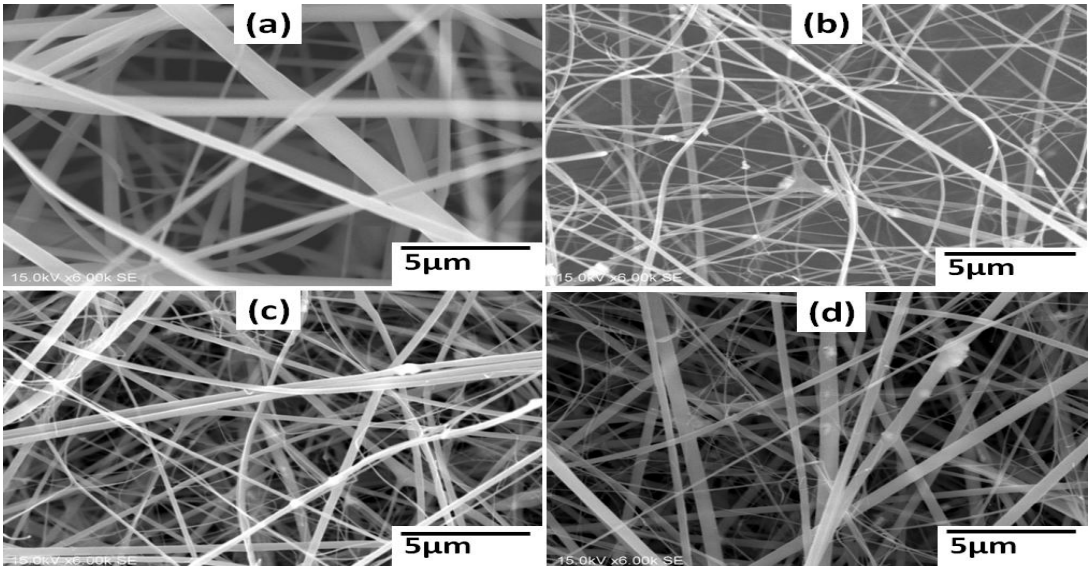

Figure 5.4 SEM images of the nanofibers (a) CA (b) CA/TiO_2 (c) CA/TiO_2/AgNP1 (d) CA/TiO_2/AgNP2

CA/TiO_2 and CA/TiO_2/AgNP samples were studied with XRD analysis to confirm the TiO_2 and TiO_2/AgNP loading in the CA nanofibers (Figure 5.5A). The CA/TiO_2 sample shows 2θ values (diffraction angles) at 27.24^0, 36.1^0, 41.13^0, 54.3^0, 56.62^0 and 69.05^0 indexed as (110), (101), (111), (211), (220) and (301) planes of TiO_2 (rutile). These results confirm TiO_2 nanoparticle's loading in CA/TiO_2 composite nanofibers. The XRD patterns of CA/TiO_2/AgNP nanocomposite, in addition to diffraction angles of TiO_2, exhibit corresponding AgNP's 2θ values at 38.1^0, 44.19^0, 64.47^0 and 77.28^0 for (111), (200), (220) and (311) planes of metallic silver nanoparticles. Existence of TiO_2 and AgNP peaks in CA/TiO_2/AgNP confirms that the samples are loaded with TiO_2/AgNP composite nanoparticles.

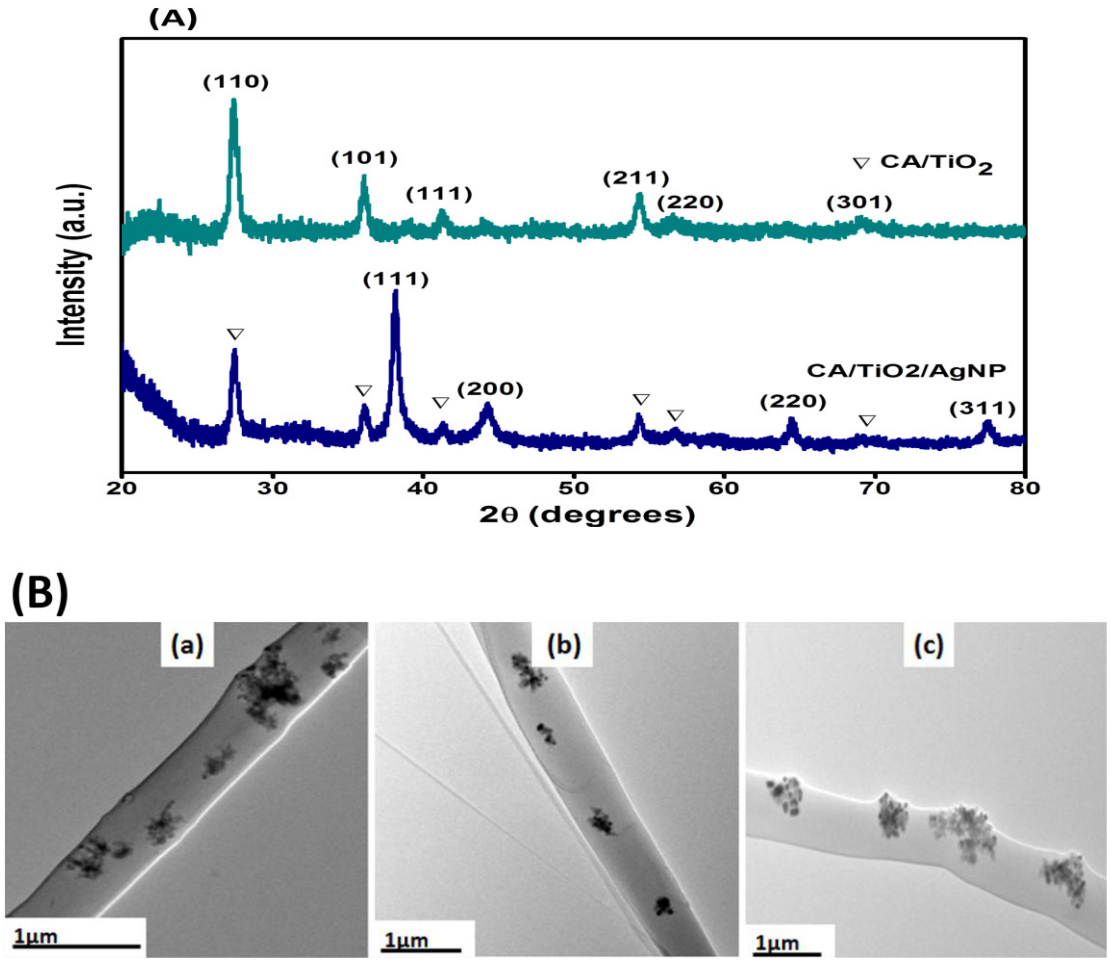

Figure 5.5 (A) XRD patterns of CA/TiO_2 and CA/TiO_2/AgNP1 composite nanofibers
(B) TEM images of (a) CA/TiO_2 (b) CA/TiO_2/AgNP1 (c) CA/TiO_2/AgNP2

TEM analysis was conducted to observe TiO_2 nanoparticles and TiO_2/AgNP composite nanoparticles loading in the CA nanofibers. The results given in Figure 5.5B show TiO_2 nanoparticles (Figure 5.5Ba) and TiO_2/AgNP (Figure 5.5B b-c) composite nanoparticles embedded in the CA nanofiber matrix. Anchoring of AgNPs on TiO_2 nanoparticle surfaces and their embedding inside the CA polymer matrix

are expected to ensure antibacterial performance for longer time span due to reduced propensity of silver leaching from the nanofiber mats. The TiO_2 and TiO_2/AgNP nanoparticles were well dispersed in the CA nanofiber matrix. Owing to higher concentrations of TiO_2/AgNP nanoparticles in CA/TiO_2/AgNP2 (in comparison to CA/TiO_2/AgNP1), its TEM image depicted larger TiO_2/AgNP agglomerates having moderately shorter distance between them. The elemental composition results (Table 5.2) revealed 9.49 wt. % of Ti in CA/TiO_2 samples, while the CA/TiO_2/AgNP1 samples contained 2.09 wt. % and 2.74 wt. % of Ti and Ag contents respectively. Due to higher concentration of TiO_2/AgNP nanocomposite particles in CA/TiO_2/AgNP2, the Ti and Ag contents were found to be 4.69 wt. % and 5.12 wt. % respectively. Thus, the TEM images and elemental compositions show that the CA nanofibers were adequately loaded with TiO_2 nanoparticles and TiO_2/AgNP composite nanoparticles.

Table 5.2 Elemental compositions of nanofiber samples

Element	Samples					
	CA/TiO_2		**CA/TiO_2/AgNP1**		**CA/TiO_2/AgNP2**	
	Mass Percentage (%)	Atomic Percentage (%)	Mass Percentage (%)	Atomic Percentage (%)	Mass Percentage (%)	Atomic Percentage (%)
CK	41.42	51.35	46.61	55.56	45.08	55.87
OK	49.09	45.7	48.56	43.45	45.11	41.97
TiK	9.49	2.95	2.09	0.63	4.69	1.46
AgL	-----	-----	2.74	0.36	5.12	0.71
Total	100	100	100	100	100	100

To observe the chemical structure and possible chemical changes in the structure of CA by incorporation of TiO_2 nanoparticles and TiO_2/AgNP, FTIR studies were conducted. The FTIR results given in Figure 5.6 show the spectrum of CA, CA/TiO_2 and CA/TiO_2/AgNP nanofibers. All the three samples show corresponding peaks of cellulose acetate. A peak at 1745 cm^{-1} is assigned to stretching vibrations of carbonyl (C=O) group. A peak at 1370cm^{-1} is due to CH_3 bending vibration. The two peaks at 1236 cm^{-1} and 1045 cm^{-1} are assigned to stretching vibrations of C-O-C groups. The CA/TiO_2 and CA/TiO_2/AgNP samples do not show any new peak or any peak shift which demonstrates that the nanoparticles do not have chemical interaction with CA polymer chains and do not induce any chemical change.

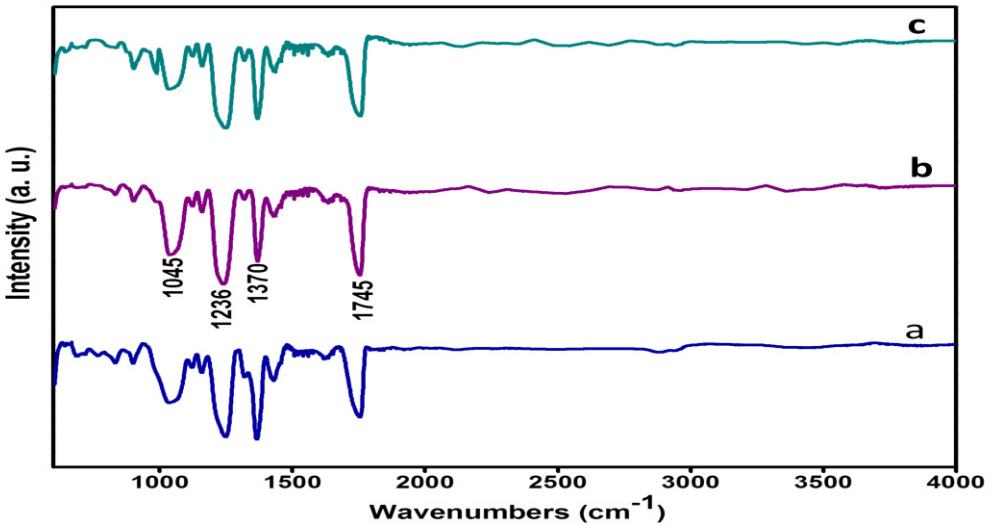

Figure 5.6 FTIR spectrum of (a) CA (b) CA/TiO_2 (c) CA/TiO_2/AgNP nanofibers (CA/TiO_2/AgNP2)

5.5.3 Antibacterial tests

Antibacterial activity test results (inhibition zone; halo width (mm)) are given in Table 5.3. The results indicate CA/TiO_2/AgNP nanocomposite fibers having sufficiently higher antibacterial properties. The AgNPs are effective in inhibition of bacteria colonization by disruption of bacteria cell wall, denature their DNA and by blocking the respiratory systems. Although the AgNPs are highly efficient and effective antimicrobial agents, however, excess release of silver induces harmful effects to human cells. The reported side-effects of excess use of silver are *carcinoma*, *allergies*, *argyria* and *argyrosis [9]*. To avoid the harmful side effect of silver, immobilization of AgNP on several organic and inorganic substrates have been proposed [2]. Thus, in this research AgNPs were immobilized on TiO_2 nanoparticles and were subsequently loaded into the CA nanofibers. Although, TiO_2 reportedly possesses antibacterial properties, however, may be due to experimental conditions, in our results CA/TiO_2 nanocomposites did not show any hollow width. The antibacterial properties of TiO_2 nanoparticles are initiated under ultra violet (UV) illuminations [3]while our experiments were conducted in dark. The CA/TiO_2/AgNP1 and CA/TiO_2/AgNP2 show very good antibacterial activities (halo width) against both the *E. coli* and *S. aureus*. The CA/TiO_2/AgNP1 depicted 1.61mm and 1.47mm halo widths against *S. aureus* and *E. coli* respectively. The CA/TiO_2/AgNP2, which was prepared with higher concentrations of TiO_2/AgNP nanoparticles, formed halo widths of 1.8mm and 1.73mm respectively.

Table 5.3 Antibacterial test results, halo width (mm), of the samples against *S. aureus* and *E. coli*

Bacterial Strain	Halo Width (mm)		
	CA/TiO_2	CA/TiO_2/AgNP1	CA/TiO_2/AgNP2
S aureus	N/A	1.61	1.8
E coli	N/A	1.47	1.73

The growth curves of both the *E. coli* and *S. aureus* were obtained with and without the nanofiber samples. Absorbance (OD_{590nm}) data given in Figure 5.7A (24 hours; OD_{590nm} taken every 3hours) and Figure 5.7B (72hours; OD_{590nm} taken after every 12 hours) demonstrated excellent antibacterial characteristics of CA/TiO_2/AgNP1 and CA/TiO_2/AgNP2 against both the *E. coli* and *S. aureus* strains. Against *E. coli* (Gram negative bacteria), the OD_{590nm} values, after 24hours of incubation (Figure 5.7A (i)), were 0.0387 and 0.01 for CA/TiO_2/AgNP1 and CA/TiO_2/AgNP2 respectively compared to 0.8 in control and 0.694 in CA samples. Similarly, against *S. aureus* (Gram positive bacteria), the OD_{590nm} values, after 24 hours incubation (Figure 5.7 A(ii)), were 0.035 and 0.007 for CA/TiO_2/AgNP1 and CA/TiO_2/AgNP2 respectively compared with 0.826 for control and 0.8 for CA samples. As observed from Figure 5.7B(i)-(ii), although both the CA/TiO_2/AgNP1 and CA/TiO_2/AgNP2 show substantial bactericidal performance up to 72 hours, however, their antibacterial activities were observed to be excellent until 36 hours against both the studied strains. This may be due to reduction in gradual release of silver from TiO_2 surface after 36 hours. Although, we consider antibacterial performance of CA/TiO_2/AgNP nanocomposite based on generation of reactive oxygen species (ROS), however, a moderate reduction in antibacterial performance after 36hours indicated gradual release of silver ions from the nanocomposites as well. Antibacterial performance of the CA/TiO_2/AgNP nanocomposites up to 72 hours suggested their suitability in applications desiring long term bactericidal performances.

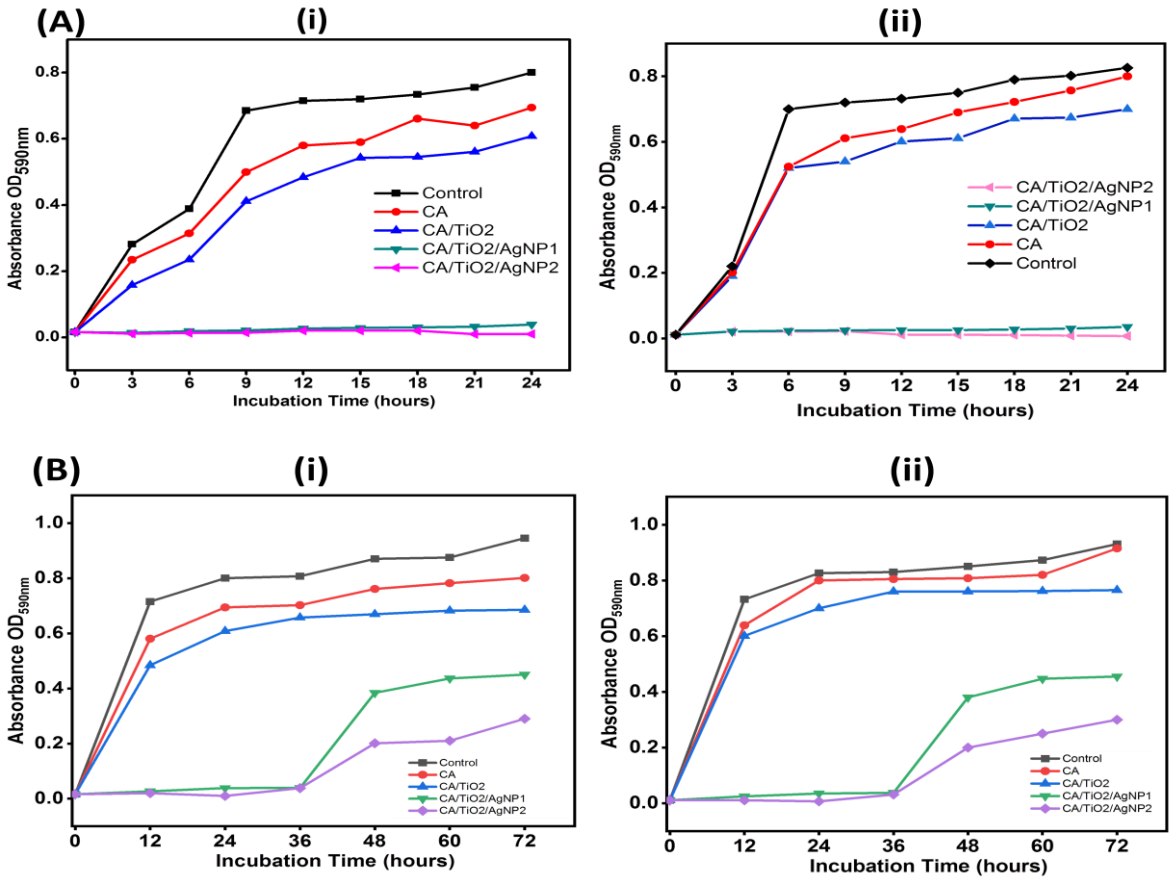

Figure 5.7 Bacterial growth curves of (i) *E .coli* (ii) *S. aureus* strains incubated with samples for (A) 24h (B) 72h (control sample represents OD_{590nm} of culture medium without nanofibers)

The relative cell viability (%) results of CA/TiO_2/AgNP1 given in Figure 5.8 show 10% and 2% viable *E. coli* and *S. aureus* bacterial cells respectively. However, the CA/TiO_2/AgNP2 exhibited 0.3% and 0.16% viable *E. coli* and *S. aureus* cells. Thus, CA/TiO_2/AgNP2 having almost 100% bactericidal performance against both the studied strains may be taken as best sample.

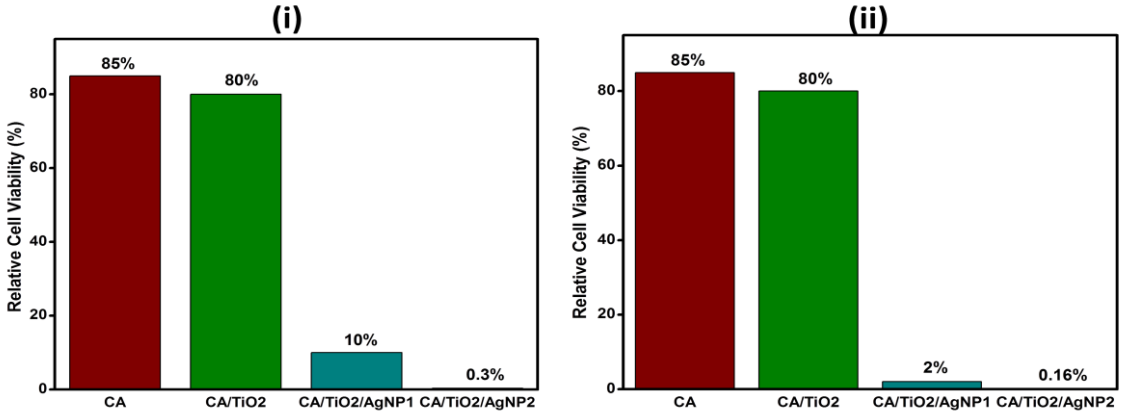

Figure 5.8 Relative cell viability (%) of the samples incubated in (i) *E. coli* (ii) *S. aureus*

The bactericidal activities of CA/TiO_2/AgNP2 could also be confirmed from the SEM images (Figure 5.9) of the samples, where, numerous dead *E. coli* (Figure 5.9 (ii)) and *S. aureus* (Figure 5.9 (iv)) cells can be observed in comparison to less number of dead cell on CA/TiO_2/AgNP1 nanofiber samples (Figure 5.9 (i) and (iii)).

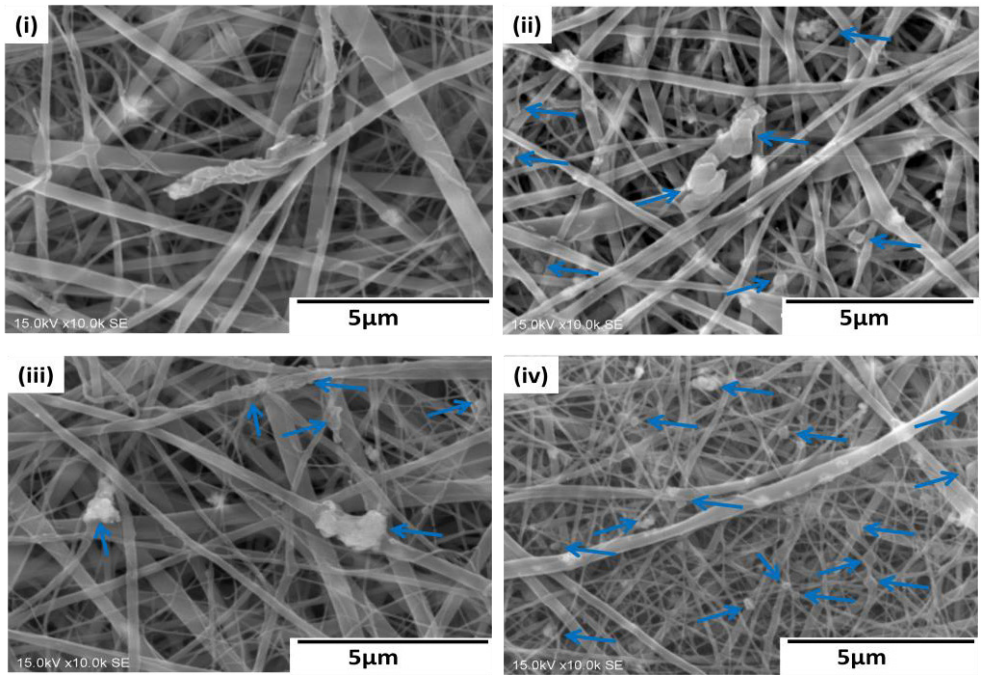

Figure 5.9 SEM images of (i) CA/TiO_2/AgNP1 incubated with *E. coli* (ii) CA/TiO_2/AgNP2 incubated with *E. coli* (iii) CA/TiO_2/AgNP1 incubated with *S. aureus* (iv) CA/TiO_2/AgNP2 incubated with *S. aureus*

5.6 Conclusions

The cellulose acetate nanofibers embedded with TiO_2/AgNP composite nanoparticles for long term excellent antibacterial applications were successfully synthesized. XPS results revealed chemisorption of pDopa on TiO_2 nanoparticles and generation of metallic AgNPs. TEM images depicted TiO_2 nanoparticles, having 36.12nm average size, densely decorated with AgNPs having an average size of 5.9nm. The TEM images and XRD patterns of CA/TiO_2/AgNP nanocomposites exhibited successful loading of TiO_2/AgNPs in CA nanofiber matrix while the SEM images confirmed regular morphology of the nanofiber samples. The antibacterial test results demonstrated substantial *E. coli* and *S. aureus* growth inhibition (OD_{590nm}) by the CA/TiO_2/AgNP nanocomposite for up to 72 hours and excellent growth inhibition for up to 36 hours. The CA/TiO_2/AgNP2 samples owing to higher halo width, excellent growth inhibition (OD_{590nm}) and lowest cell viability (%) of *E. coli* and *S. aureus* are proposed as potential nanocomposite for biologically safe and long term excellent antibacterial applications.

References

[1] H.A. Foster, I.B. Ditta, S. Varghese, A. Steele, Photocatalytic disinfection using titanium dioxide: spectrum and mechanism of antimicrobial activity, Applied microbiology and biotechnology 90(6) (2011) 1847-1868.

[2] A.W. Jatoi, Y.K. Jo, H. Lee, S.G. Oh, D.S. Hwang, Z. Khatri, H.J. Cha, I.S. Kim, Antibacterial efficacy of poly (vinyl alcohol) composite nanofibers embedded with silver-anchored silica nanoparticles, Journal of Biomedical Materials Research Part B: Applied Biomaterials 106(3) (2018) 1121-1128.

[3] Z. Wang, G. Li, H. Peng, Z. Zhang, X. Wang, Study on novel antibacterial high-impact polystyrene/TiO2 nanocomposites, Journal of materials science 40(24) (2005) 6433-6438.

[4] Y. Liao, Y. Wang, X. Feng, W. Wang, F. Xu, L. Zhang, Antibacterial surfaces through dopamine functionalization and silver nanoparticle immobilization, Materials Chemistry and Physics 121(3) (2010) 534-540.

[5] K. Thamaphat, P. Limsuwan, B. Ngotawornchai, Phase characterization of TiO2 powder by XRD and TEM, Kasetsart J.(Nat. Sci.) 42(5) (2008) 357-361.

[6] K. Kalimuthu, R.S. Babu, D. Venkataraman, M. Bilal, S. Gurunathan, Biosynthesis of silver nanocrystals by Bacillus licheniformis, Colloids and Surfaces B: Biointerfaces 65(1) (2008) 150-153.

[7] R. Asahi, T. Morikawa, Nitrogen complex species and its chemical nature in TiO2 for visible-light sensitized photocatalysis, Chemical Physics 339(1-3) (2007) 57-63.

[8] V. Raja, L. Shiamala, K. Alamelu, B.J. Ali, A study on the free radical generation and photocatalytic yield in extended surfaces of visible light active TiO2 compounds, Solar Energy Materials and Solar Cells 152 (2016) 125-132.

[9] N.R. Panyala, E.M. Peña-Méndez, J. Havel, Silver or silver nanoparticles: a hazardous threat to the environment and human health?, Journal of Applied Biomedicine (De Gruyter Open) 6(3) (2008).

CHAPTER 6

Cellulose Acetate/MWCNT/AgNP Composite Nanofibers

6.1 Introduction

This chapter reports synthesis and characterization of CA/CNT/AgNP composite nanofibers for long-time antibacterial applications. The cellulose acetate (CA) nanofibers loaded with silver nanoparticles anchored multiwall carbon nanotubes (CNT/AgNP) were fabricated by electrospinning. Synthesis of CNT/AgNP, fabricated of CA/CNT/AgNP composite nanofibers and their characterizations have been studied and discussed. Synthesis of the CNT/AgNP was studied using XPS, XRD and TEM analysis. The CA/CNT/AgNP composite nanofibers were studied with SEM, XRD, TEM, FTIR analysis and characterized for their antibacterial performances.

6.2 Research background

A brief literature survey, need and suitability of silver and silver anchored hybrid nanoparticles have already been discussed in chapter 5. Cellulose acetate and cellulose acetate based nanocomposites have also been discussed in previous sections. However, main focus of this chapter is synthesis and characterizations of AgNP immobilized multiwall carbon nanotubes (CNT/AgNP), fabrication of CA/CNT/AgNP composite nanofibers and investigating their antibacterial performances.

Similar to TiO_2, the CNTs provide an effective platform to immobilize silver nanoparticles due to their excellent thermal, electrical, mechanical, electronic properties [1-3]. The CNTs which were first revealed by Iijima in 1990 [4] have very good chemical and physical stability and are reported to possess contact-killing based antibacterial properties [5-8]. The pristine CNTs lack the functional groups for adsorption of silver ions (Ag^+), thus, a chemical treatment to generate functional groups such as carboxyl (COOH) and hydroxyl (OH) groups enhances adsorption of silver ions. A suitable reduction process afterwards generates AgNP on CNT surfaces [9-11].

Thus, CNT/AgNP composite nanoparticles were prepared and incorporated into the CA to fabricate CA/CNT/AgNP composite nanofibers. The CA/CNT/AgNP thus would be a highly desirable composite material having lower silver leaching due to its immobilized structure and embedding in the nanofiber polymer matrix. Similar to CA/TiO_2/AgNP, proposed antibacterial mechanism of the CA/CNT/AgNP mainly be due to generation of reactive oxygen species (ROS) such as peroxide ions, hydroxyl ions and oxygen radicals. The generated ROS produce bactericidal and bacterial inhibition functionalities.

6.3 Synthesis of CNT/AgNP composite nanoparticles

For synthesis of CNT/AgNP composite nanoparticles, the CNTs were first oxidized with a mixture of sulfuric acid and nitric acid. Typically, 0.5grams of CNTs were dispersed in 100mL of sulfuric acid and nitric acid (3:1; v/v) and sonicated at 60^0C for three hours in a sonication bath. The oxidized multi-wall carbon nanotubes were obtained by centrifugation at 5000 rpm for 20minutes and were dried in a drying oven at 70^0C.

Afterwards, 0.3g of oxidized CNTs were added into 100mL DI water and sonicated at 50^0C for one hour for forming a homogenous dispersion. A 100mL of 0.25M $AgNO_3$ solution was prepared and added into the dispersion. The solution was then kept under strong stirring on a magnetic stirrer for three hours. The CNTCOO/Ag^+ were obtained by centrifugation at 5000rpm for 20minutes and dried overnight in an oven at 50^0C. Finally, a heat treatment was carried out to produce CNTs decorated with silver nanoparticles (CNT/AgNP). For this purpose, the CNT-$COOAg^+$ were thermally treated in an oven at 210^0C for two hours.

6.4 Fabrication of CA/CNT/AgNP

To fabricate cellulose acetate (CA) nanofibers embedded with CNT/AgNP nanoparticles, a 17% of CA solution was prepared as reported in experimental section. Three different concentrations (wt.%) of CNT/AgNP nanoparticles such as 3% (CA/CNT/AgNP1), 5% (CA/CNT/AgNP2) and 8% (CA/CNT/AgNP3) were added into the CA solution prior to electrospinning. Electrospinning process and parameters used were similar to those reported for electrospinning of CA (section 2.3).

6.5 Results and discussions

6.5.1 CNT/AgNP composite nanoparticles

6.5.1.1 XPS evaluations

The XPS wide scan spectrum of pristine CNTs (Figure 6.1Aa) shows strong C 1s peak at binding energy (B. E.) 284eV while its de-convoluted narrow spectrum (Figure 1Ci) exhibited two peaks at B.E. 284.13eV and 284.57eV belonging to sp^2 and sp^3 carbons respectively. While the de-convoluted narrow scan spectrum of oxidized CNTs shows C=O (285.92eV), COOH (287.99eV) and π ->π^* (290.74eV) which confirms oxidation of the CNTs and formation of carboxyl groups on CNT surface. The XPS wide scan spectra of oxidized CNT (Figure 6.1Ab) shows a distinct O 1s peak at B.E. 532eV which was comparatively insignificant in the pristine CNT spectrum. De-convolution of the O 1s peak of oxidized CNT shows COOH peak at B.E. 531.11eV which evidences generation of carboxyl groups on oxidized CNTs as well. Generation of AgNPs on CNT surfaces could be confirmed from

appearance of Ag 3d peak in CNT/AgNP spectrum in Figure 6.1Ac. De-convolution of Ag 3d peak (Figure 6.1B) of CNT/AgNP exhibited Ag 3d $_{3/2}$ and Ag 3d $_{5/2}$ peaks at B.E. 372.9eV and 367.9eV belonging to metallic silver nanoparticles. A doublet-slitting of 6.0eV between Ag 3d $_{5/2}$ and Ag 3d $_{3/2}$ evidences metallic nature of the silver[12].

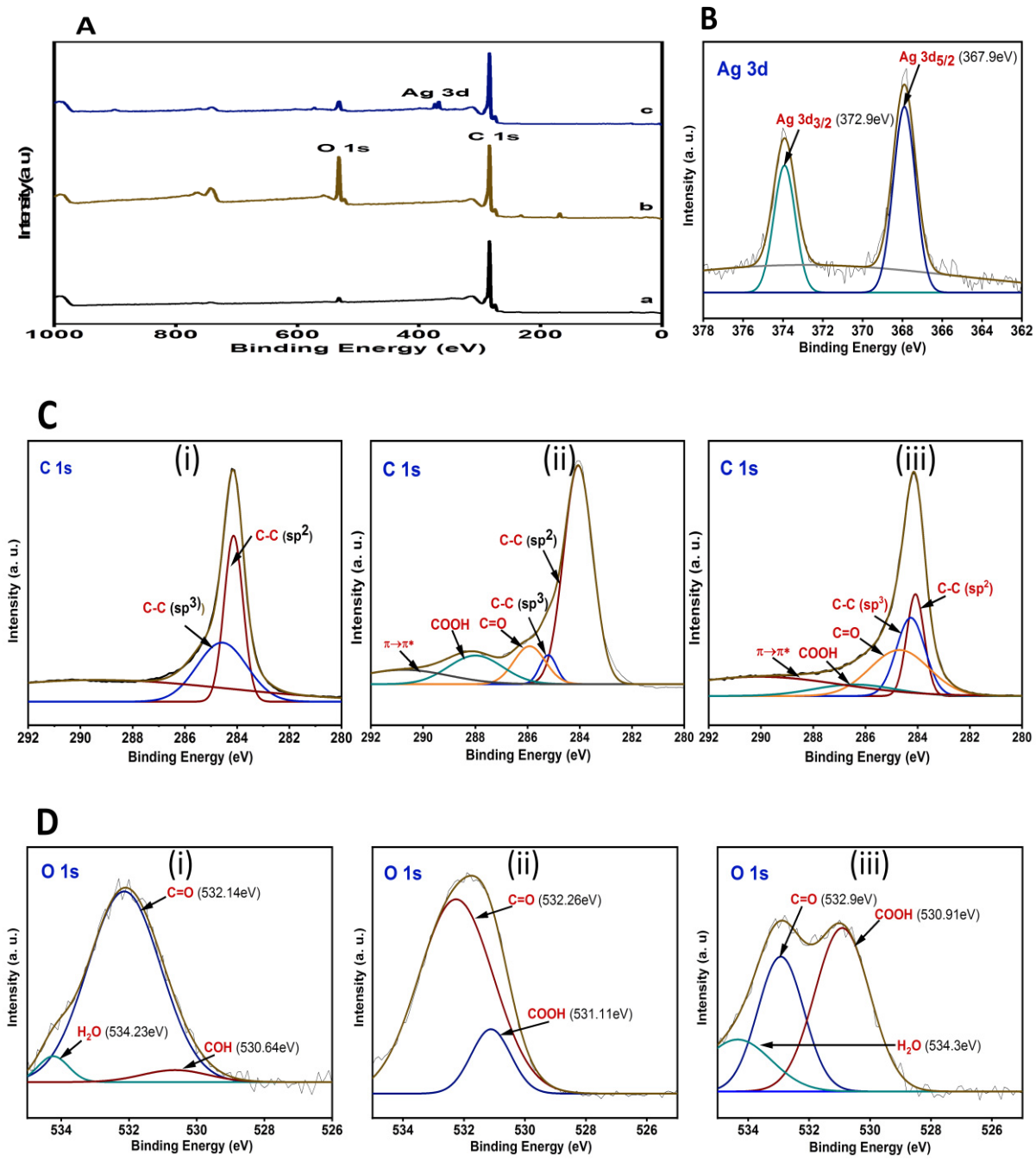

Figure 6.1 (A) XPS wide scan spectrum of (a) CNT (b) Oxidized CNT (c) CNT/AgNPs

(B) XPS C 1s narrow scan spectrum of (i) CNT (ii) Oxidized CNT (iii) CNT/AgNPs

(C) XPS O 1s narrow scan spectrum of (i) CNT (ii) Oxidized CNT (iii) CNT/AgNPs

(D) XPS Ag 3d narrow scan spectrum of CNT/AgNPs

6.5.1.2 X-ray diffraction studies

Synthesis of AgNPs on CNT surfaces was further studied using X-ray diffraction studies (Figure 6.2). The XRD patterns of oxidized CNTs (Figure 6.2a) show diffraction angles (2θ) at 26.159°, 42.66°, 44.58°, 54.397° and 77.6° which are indexed as (002), (100), (101), (004) and (006) planes of CNTs [13]. The XRD pattern of CNT/AgNPs (Figure 6.2b), in addition to confirmation of the CNT structure shows 2θ values at 38.207°, 44.32°, 64.64° and 77.42° which are indexed as (111), (200), (220) and (311) planes of metallic silver nanoparticles [14].

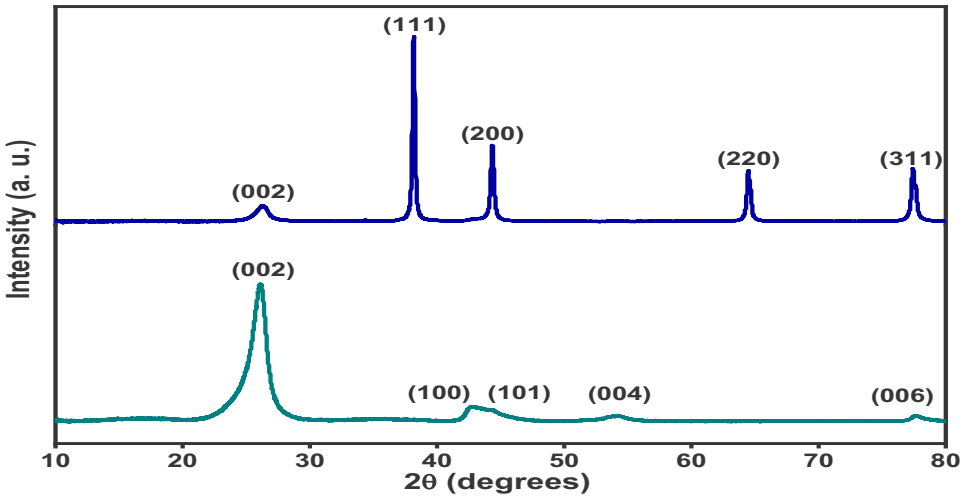

Figure 6.2 X-ray diffraction patterns of (a) CNT (b) CNT/AgNP

6.5.1.3 TEM analysis

The transmission electron microscopy (TEM) images were taken to observe generation and distribution of silver nanoparticles on CNT surfaces. The results given in Figure 6.3 depict the multiwall carbon nanotubes (CNTs) decorated with AgNPs. The TEM images show well distribution of spherical AgNPs on CNT surfaces. Thus the TEM images further validates XPS and XRD observations.

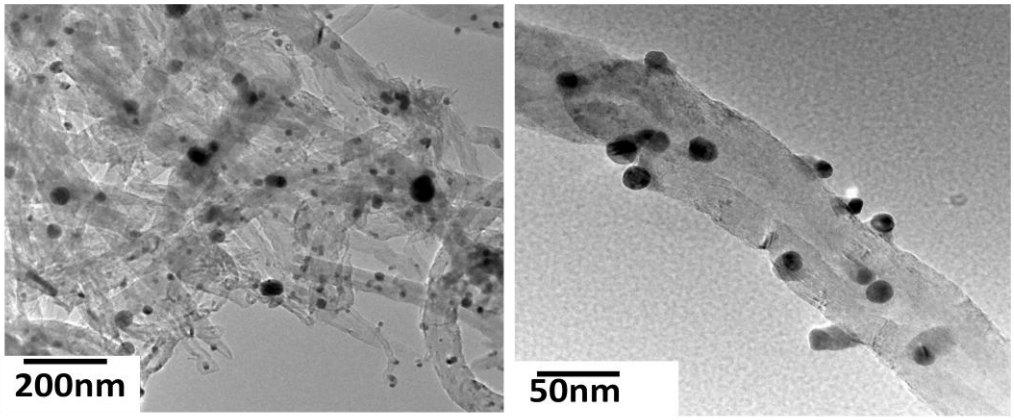

Figure 6.3 Transmission electron microscopy images of CNT/AgNP

6.5.2 CA/CNT/AgNP composite nanofibers

6.5.2.1 Morphology of CA/CNT/AgNP nanofibers

Morphologies of the nanofiber composites were observed using scanning electron microscopy. The results given in Figure 6.4 show regular and bead free nanofibers. As observed the diameters of nanofibers were decreased after addition of CNT/AgNP nanoparticles. The reduction in nanofiber diameters may be due to improvement in conductivity[15] of the electrospinning solution which when electrospun using electric voltage produced finer nanofibers.

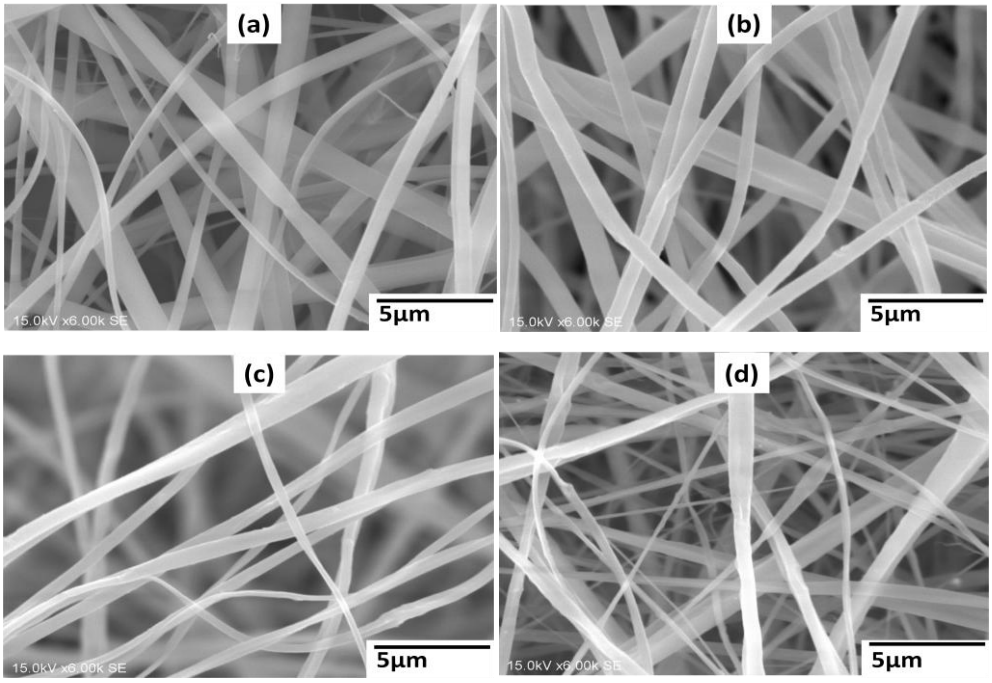

Figure 6.4 SEM images of (a) CA (b) CA/CNT/AgNP1 (c) CA/CNT/AgNP2 (d) CA/CNT/AgNP3

6.5.2.2 XRD analysis

The XRD studies were conducted in order to confirm CNT/AgNP contents in CA nanofibers. As observed from the XRD patterns, the CA/CNT/AgNP1, CA/CNT/AgNP2 and CA/CNT/AgNP3 samples (Figure 6.5b-6.5d) show XRD patterns of CNT and AgNPs. A diffraction peak at 2θ value of 26.35^{o} represents (002) planes of CNTs. The diffraction peaks (2θ) at 38.2^{o}, 44.32^{o}, 64.64^{o} and 77.42^{o} representing the (111), (200), (220) and (311) planes of AgNPs confirms presence of AgNPs. Intensity of CNT and AgNP peaks increased from CA/CNT/AgNP1 to CA/CNT/AgNP3 as the concentration of CNT/AgNP was increased in the CA solution. Thus the XRD patterns confirmed incorporation of CNT/AgNP nanoparticles in the CA nanofibers.

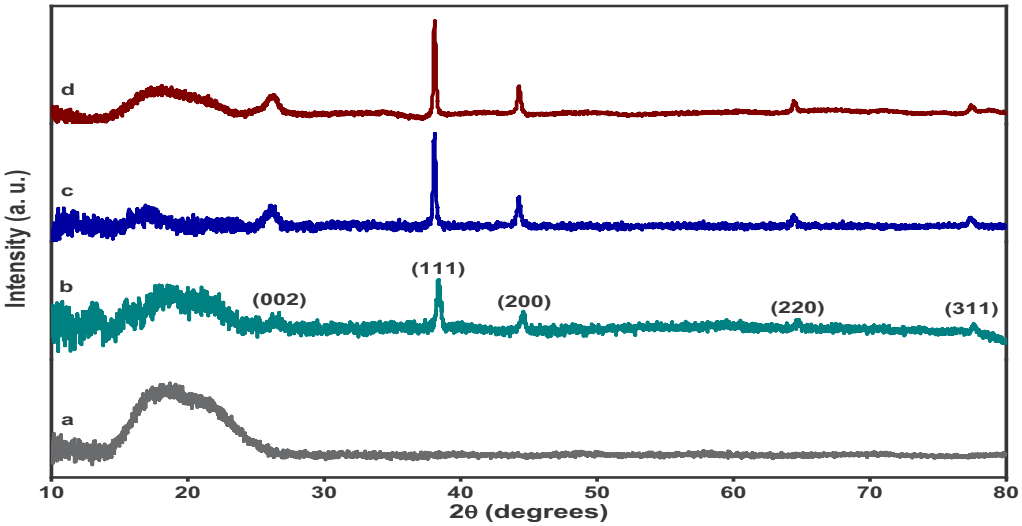

Figure 6.5 XRD patterns of (a) CA (b) CA/CNT/AgNP1 (c) CA/CNT/AgNP2 (d) CA/CNT/AgNP3

6.5.2.3 TEM observations

To confirm CNT/AgNP in CA nanofibers, the CA/CNT/AgNP samples were studied via TEM analysis. The TEM images given in Figure 6.6 exhibit presence of CNT/AgNP nanoparticles embedded in the CA nanofibers. Higher loading of CNT/AgNP from Figure 6.6b and Figure 6.6c in CA/CNT/AgNP2 and CA/CNT/AgNP3 respectively could be confirmed from the TEM images.

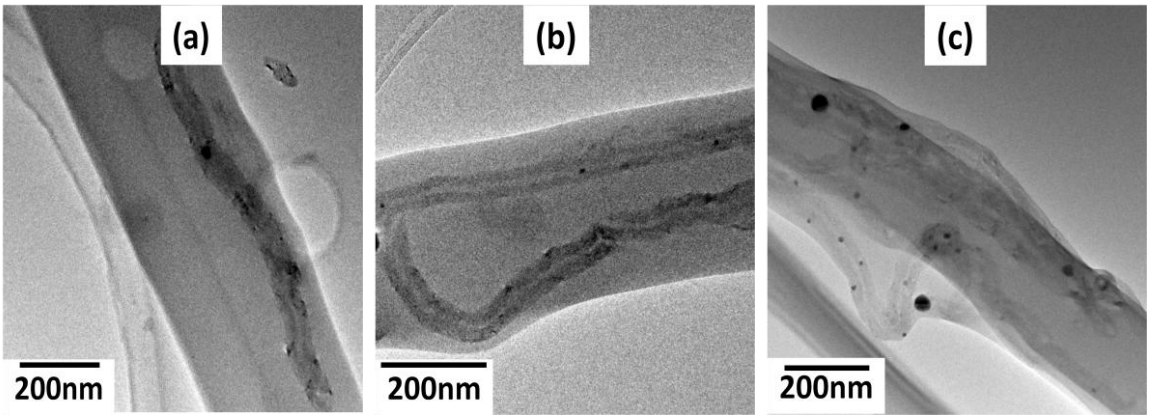

Figure 6.6 TEM images of (a) CA/CNT/AgNP1 (b) CA/CNT/AgNP2 (c) CA/CNT/AgNP3

6.5.2.4 FTIR studies

Fourier transform infrared spectroscopy analysis was carried out to determine chemical structure of the composite nanofibers. The results given in Figure 6.7 show all the samples exhibiting characteristic peaks of cellulose acetate. The peak at 1740cm^{-1} is due to stretching vibrations of carbonyl functional groups. The peak at 1367 cm^{-1} represents bending vibrations of methyl group (CH_3) groups. The two peaks at 1230 cm^{-1} and 1038 cm^{-1} appeared due to stretching vibrations in

glycosidic linkage (C-O-C)[16]. The CA/CNT/AgNP samples did not show any new peaks which demonstrate CNT/AgNP composite nanoparticles may be embedded in the CA polymer matrix, however, without chemical alterations.

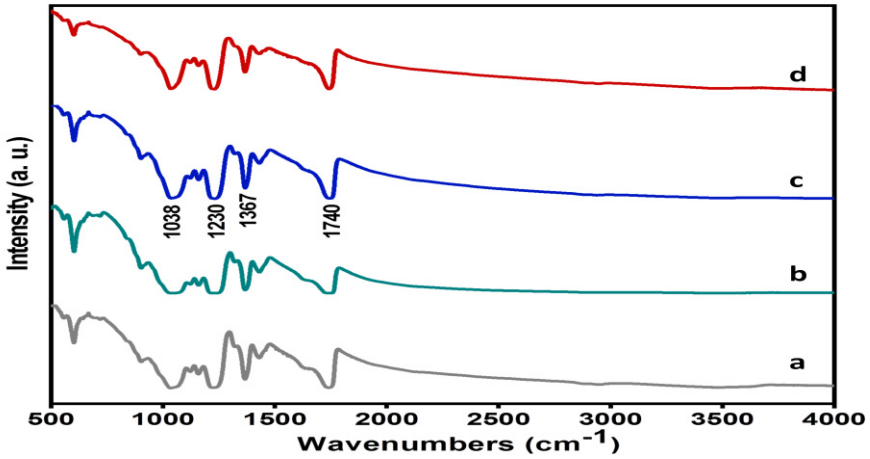

Figure 6.7 FTIR spectrum of (a) CA (b) CA/CNT/AgNP1 (c) CA/CNT/AgNP2 (d) CA/CNT/AgNP3 nanofibers

6.5.3 Antibacterial activities of CA/CNT/AgNP

Antibacterial performances of the CA/CNT/AgNP samples were studied against two popular bacterial strains namely *E. coli* and *S. aureus*. The CA/CNT/AgNP nanofiber samples were incubated with the strains on agar plates for 24 hours in order to measure *halo width* (inhibition zone) against the bacterial strains. The *halo widths* measured in mm are reported in Table 6.1 and related photographic images are given in Figure 6.8. The *halo width* formed by CA/CNT/AgNP1, CA/CNT/AgNP2 and CA/CNT/AgNP3 against *S. aureus* were 0.42mm, 0.73mm and 0.92mm respectively. While the *halo widths* against *E. coli* were 0.4mm, 0.62mm and 0.9mm. The results revealed slightly higher antibacterial activities of the CA/CNT/AgNP samples against *staphylococcus aureus*.

Table 6.1 Antibacterial test (inhibition zone) results of the CA/TiO_2/AgNP

Strain	Samples			
	CA	CA/CNT/AgNP1	CA/CNT/AgNP2	CA/CNT/AgNP3
S. aureus	-----	0.42	0.73	0.92
E. coli	-----	0.40	0.62	0.90

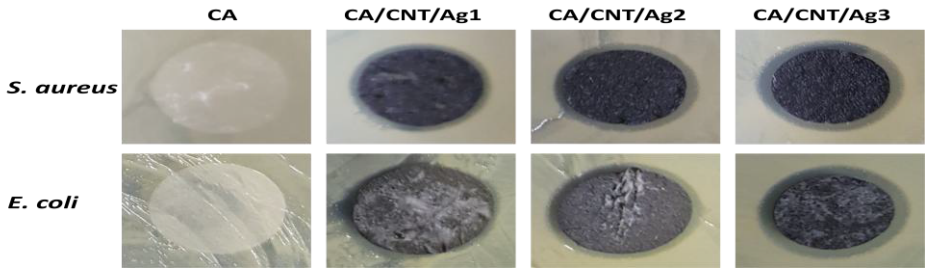

Figure 6.8 Photographic images of samples tested by disk diffusion method (*halo width*, mm)

The relative bacterial cell viability (%) results (Figure 6.9) were obtained in order to determine bactericidal performance of the CA/CNT/AgNP samples. The CA/CNT/AgNP3 sample exhibited 100% bactericidal performance (0% viable cells) against both the *E. coli* and *S. aureus* strains. The relative viable *S. aureus* cells after incubation with CA/CNT/AgNP1 and CA/CNT/AgNP2 were 27% and 12% respectively, while, those against *E. coli* were 29% and 15% respectively.

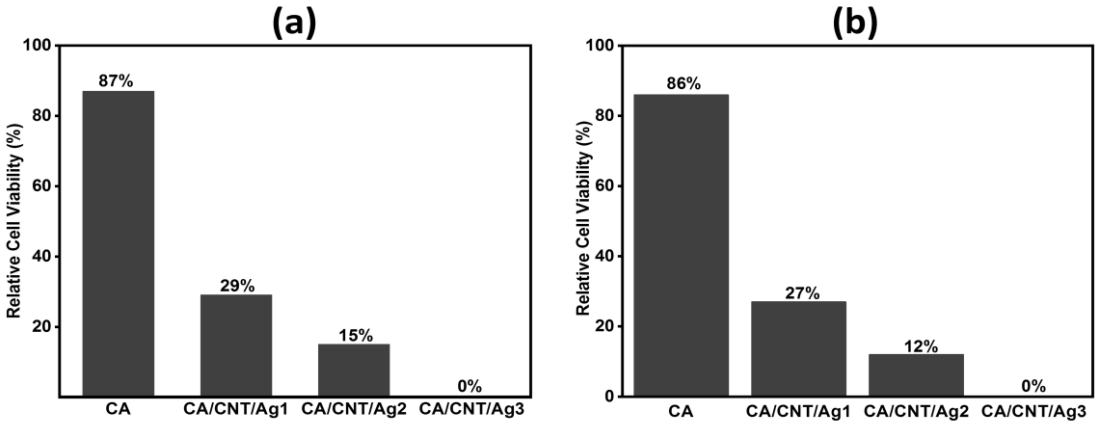

Figure 6.9 Relative cell viability (%) of bacterial cells incubated with the samples (a) *E. coli* (b) *S. aureus*

Bactericidal performance of the CA/CNT/AgNP composite nanofibers were also studied by obtaining growth curves of the *E. coli* and *S. aureus* strains (absorbance, OD_{590nm}) over a period of 48 hours (Figure 6.10). The results revealed all the CA/CNT/AgNP samples exhibiting excellent bactericidal growth inhibition activity up to 48 hours against *S. aureus*. Against the *E. coli* CA/CNT/AgNP2 and CA/CNT/AgNP3 demonstrated excellent antibacterial activity while CA/CNT/AgNP1 showed comparatively higher OD_{590nm} values. In general, samples showed lower absorbance (OD_{590nm}) against *S. aureus* than *E. coli* which elaborates comparative better growth inhibition tendency against *S. aureus* strains. It is suggested mechanism for antibacterial activities of CA/CNT/AgNP nanofiber composites is based on generation of reactive oxygen species (ROS) which may ensure antibacterial performances over extended time. The reactive oxygen species such as peroxide ions, oxygen radicals and hydroxyl ions rupture cell wall of bacterial species and damage their deriboxy nucleic acid (DNA) which leads to death and growth inhibition of bacteria populations.

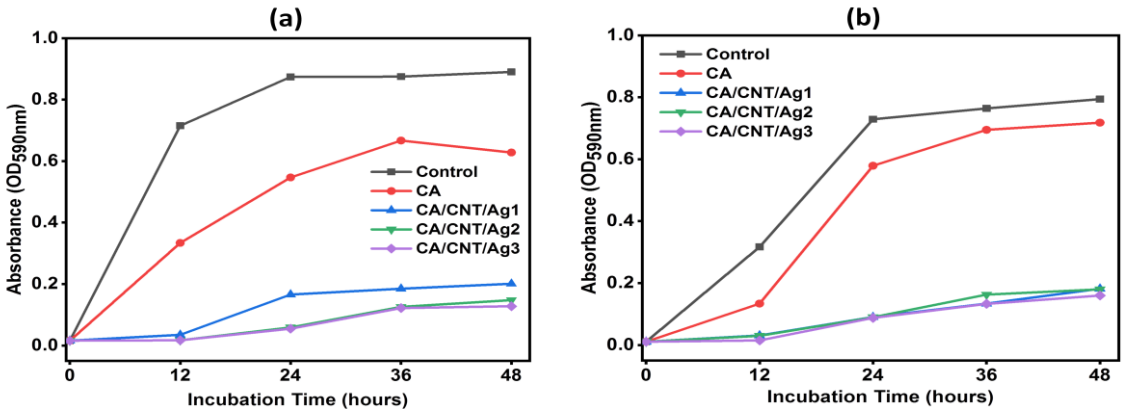

Figure 6.10 Absorbance (OD_{590nm}) values of samples incubated with (a) *E. coli* (b) *S. aureus* strains

6.6 Conclusions

The study on synthesis of AgNP decorated multiwall carbon nanotubes and their subsequent incorporation in to cellulose acetate to fabricate CA/CNT/AgNP nanofiber composite for long term antibacterial activities have been successfully concluded. The XPS, XRD and TEM analysis confirmed synthesis of CA/CNT/AgNP composite nanofibers. SEM images depicted regular morphology of the nanofibers. The antibacterial assay (OD_{590nm}) demonstrated effective antibacterial properties for up to 48 hours. The relative cell viability (%) test exhibited 100% bactericidal performance (0% viable cells) by CA/CNT/AgNP3 samples. Thus our current study suggests CA/CNT/AgNP composite nanofibers for long term excellent antibacterial applications.

References

[1] M. Kang, P. Chen, H.-J. Jin, Preparation of multiwalled carbon nanotubes incorporated silk fibroin nanofibers by electrospinning, Current Applied Physics 9(1) (2009) S95-S97.

[2] Q. Guo, X. Zhou, X. Li, S. Chen, A. Seema, A. Greiner, H. Hou, Supercapacitors based on hybrid carbon nanofibers containing multiwalled carbon nanotubes, Journal of Materials Chemistry 19(18) (2009) 2810-2816.

[3] J.J. Ge, H. Hou, Q. Li, M.J. Graham, A. Greiner, D.H. Reneker, F.W. Harris, S.Z. Cheng, Assembly of well-aligned multiwalled carbon nanotubes in confined polyacrylonitrile environments: electrospun composite nanofiber sheets, Journal of the American Chemical Society 126(48) (2004) 15754-15761.

[4] H. Hou, J.J. Ge, J. Zeng, Q. Li, D.H. Reneker, A. Greiner, S.Z. Cheng, Electrospun polyacrylonitrile nanofibers containing a high concentration of well-aligned multiwall carbon nanotubes, Chemistry of Materials 17(5) (2005) 967-973.

[5] R. Mohan, A. Shanmugharaj, R. Sung Hun, An efficient growth of silver and copper nanoparticles on multiwalled carbon nanotube with enhanced antimicrobial activity, Journal of Biomedical Materials Research Part B: Applied Biomaterials 96(1) (2011) 119-126.

[6] J.H. Jung, G.B. Hwang, J.E. Lee, G.N. Bae, Preparation of airborne Ag/CNT hybrid nanoparticles using an aerosol process and their application to antimicrobial air filtration, Langmuir 27(16) (2011) 10256-10264.

[7] S. Kang, M. Pinault, L.D. Pfefferle, M. Elimelech, Single-walled carbon nanotubes exhibit strong antimicrobial activity, Langmuir 23(17) (2007) 8670-8673.

[8] T. Makowski, D. Kowalczyk, W. Fortuniak, S. Brzezinski, D. Kregiel, Electrochemical deposition of silver nanoparticle and polymerization of pyrrole on fabrics via conducting multiwall carbon nanotubes, Cellulose 22(5) (2015) 3063-3075.

[9] A.J. Haider, M. Mohammed, E.A.J. Al-Mulla, D.S. Ahmed, Synthesis of silver nanoparticle decorated carbon nanotubes and its antimicrobial activity against growth of bacteria, Rendiconti Lincei 25(3) (2014) 403-407.

[10] B. Peng, M. Locascio, P. Zapol, S. Li, S.L. Mielke, G.C. Schatz, H.D. Espinosa, Measurements of near-ultimate strength for multiwalled carbon nanotubes and irradiation-induced crosslinking improvements, Nature nanotechnology 3(10) (2008) 626.

[11] Y. Xing, L. Li, C.C. Chusuei, R.V. Hull, Sonochemical oxidation of multiwalled carbon nanotubes, Langmuir 21(9) (2005) 4185-4190.

[12] M. Gopiraman, D. Deng, S. Saravanamoorthy, I.-M. Chung, I.S. Kim, Gold, silver and nickel nanoparticle anchored cellulose nanofiber composites as highly active catalysts for the rapid and selective reduction of nitrophenols in water, RSC Advances 8(6) (2018) 3014-3023.

[13] P. Gunawan, C. Guan, X. Song, Q. Zhang, S.S.J. Leong, C. Tang, Y. Chen, M.B. Chan-Park, M.W. Chang, K. Wang, Hollow fiber membrane decorated with Ag/MWNTs: toward effective water disinfection and biofouling control, Acs Nano 5(12) (2011) 10033-10040.

[14] A.B. Castle, E. Gracia-Espino, C. Nieto-Delgado, H. Terrones, M. Terrones, S. Hussain, Hydroxyl-functionalized and N-doped multiwalled carbon nanotubes decorated with silver nanoparticles preserve cellular function, Acs Nano 5(4) (2011) 2458-2466.

[15] J.D. Schiffman, M. Elimelech, Antibacterial activity of electrospun polymer mats with incorporated narrow diameter single-walled carbon nanotubes, ACS applied materials & interfaces 3(2) (2011) 462-468.

[16] M. Seki, Silver coated anionic cellulose nanofiber composites for, Biomaterials 25(7) (2016) 1319-1329.

CHAPTER 7

Polyvinyl Alcohol/Silica/AgNP Composite Nanofibers

7.1 Introduction

In this chapter synthesis of polyvinyl alcohol/silica/AgNP (PVA/silica/AgNP) composite nanofibers and their characterizations for antibacterial performance are reported. Silver nanoparticles anchored on silica nanoparticles were prepared by alcohol reduction method and incorporated into PVA nanofibers to fabricate silica/AgNP embedded PVA nanofibers (PVA/silica/AgNP). Synthesis of silica/AgNP composite nanoparticles is discussed at the beginning of chapter. Then characterization of PVA/silica/AgNP composite nanofibers have been reported. Antibacterial performances of the PVA/silica/AgNP composite nanofibers are given at the end.

7.2 Research background

As discussed previously, immobilization of AgNPs on a substrate controls silver release and ensures biological safety. Since silica nanoparticles possess certain antibacterial characteristics, therefore, were chosen for immobilization of AgNPs. Thus, silica nanoparticles would control silver release while retaining antibacterial activity of the nanocomposites [1]. The hybrid silica/AgNP composite nanoparticles are chemically stable, prevent aggregation of the AgNPs and are easier to handle [2].

PVA is a hydrophilic and semi-crystalline polymer with good biocompatibility, biodegradability, non-toxicity, and fiber formability. Due to this, it has been greatly exploited in cosmetic, biomedical, and pharmaceutical applications, wound dressings and impermanent skin covering materials [3-5]. The wound dressings require bacterial resistance for better healing of the wounds since the dressings provide ideal conditions such as moisture, nutrients and warmth for the growth of microorganism, which otherwise may impede healing process[6-8]. Bacterial infections induce inflammatory substances in addition to impeding the healing process[6, 9]. Bacterial cells may battle with normal cells for accessible nutrients and available oxygen [10].

Previously, Song et al.[11] synthesized silver/polyrhodanine-Silica nanoparticles and characterized for antibacterial performance where the antibacterial activity was attributed to the silver nanoparticles and polyrhodanine. Ma et al. [12] fabricated SiO_2 thereby grafted silver nanoparticles for antibacterial wound cover. Niu et el. Son et al.[13] fabricated silica and polyrhodanine coreshell nanoparticles and studied their antibacterial effects. Tian et al.[14] synthesized silver anchored on mesoporous silica nanoparticles for antibacterial applications.

In the present work, silica/AgNP embedded PVA composite nanofibers (PVA/silica/AgNP) have been synthesized and characterized for antibacterial applications.

7.3 Synthesis of silica/AgNP and fabrication of PVA/silica/AgNP

The silica/AgNP nanoparticles were synthesized following a previous method with slight modification [2]. Typically, NH_4OH solution (21.2 ml) was mixed with 250 ml ethanol. After mild stirring for 20 min., 10 g of TEOS were added in the solution while continuously stirring for 1 h. 2g of MPTMS was then added and the solution was kept under mild stirring for 6 h. The solution was centrifuged at 10,000 rpm for 15 min. in order to separate the thiol functionalized silica nanoparticles. To remove the un-reacted reagents, ethanol was utilized for washing the particles. Finally, sludge of thiol functionalized silica particles was obtained and subsequently used for synthesis of silica/AgNP by alcohol reduction process. 96 ml of ethanol was added in the synthesized silica sludge under agitation and sonication. Afterwards, 4 g of PVP K15 were added while mildly stirring for 2 h. After complete mixing of PVP, 10,000 ppm of $AgNO_3$ was added and kept under mild stirring for further six hours. The solution was then centrifuged twice at 10,000 rpm for 15 min. Finally, the obtained silica/AgNP were dispersed in 100 ml water and a solution with 1.1% silver (11,000 ppm) and 18.9 % silica nanoparticles was obtained.

These composite nanoparticles were then used to fabricate PVA/silica/AgNP nanofibers. Typically, 8 wt% of PVA solution was prepared in H_2O. After 12 h mixing on magnetic stirrer, glutaraldehyde (22 wt% of PVA), as a cross-linking agent, was added into the solution and kept under mild stirring for 3 h. Three different concentrations of the silica/AgNP (5 wt%, 10 wt% and 15 wt%; w/w) were then mixed in the PVA solution and kept under mild stirring for 3 h. The prepared solutions were then used to fabricate PVA/silica/AgNP nanofibers by electrospinning apparatus installed with high voltage supply (Har-100*12, Matsusada Co., Tokyo, Japan). The needle tip to collector distance was maintained at 12cm and a 12kV electric voltage was applied for electrospinning. After two days of drying at room temperature, the PVA/ silica/AgNP nanofibers were peeled-off from aluminum foil and fumed with HCl for 60 seconds to catalyze cross-linking reaction of PVA nanofibers.

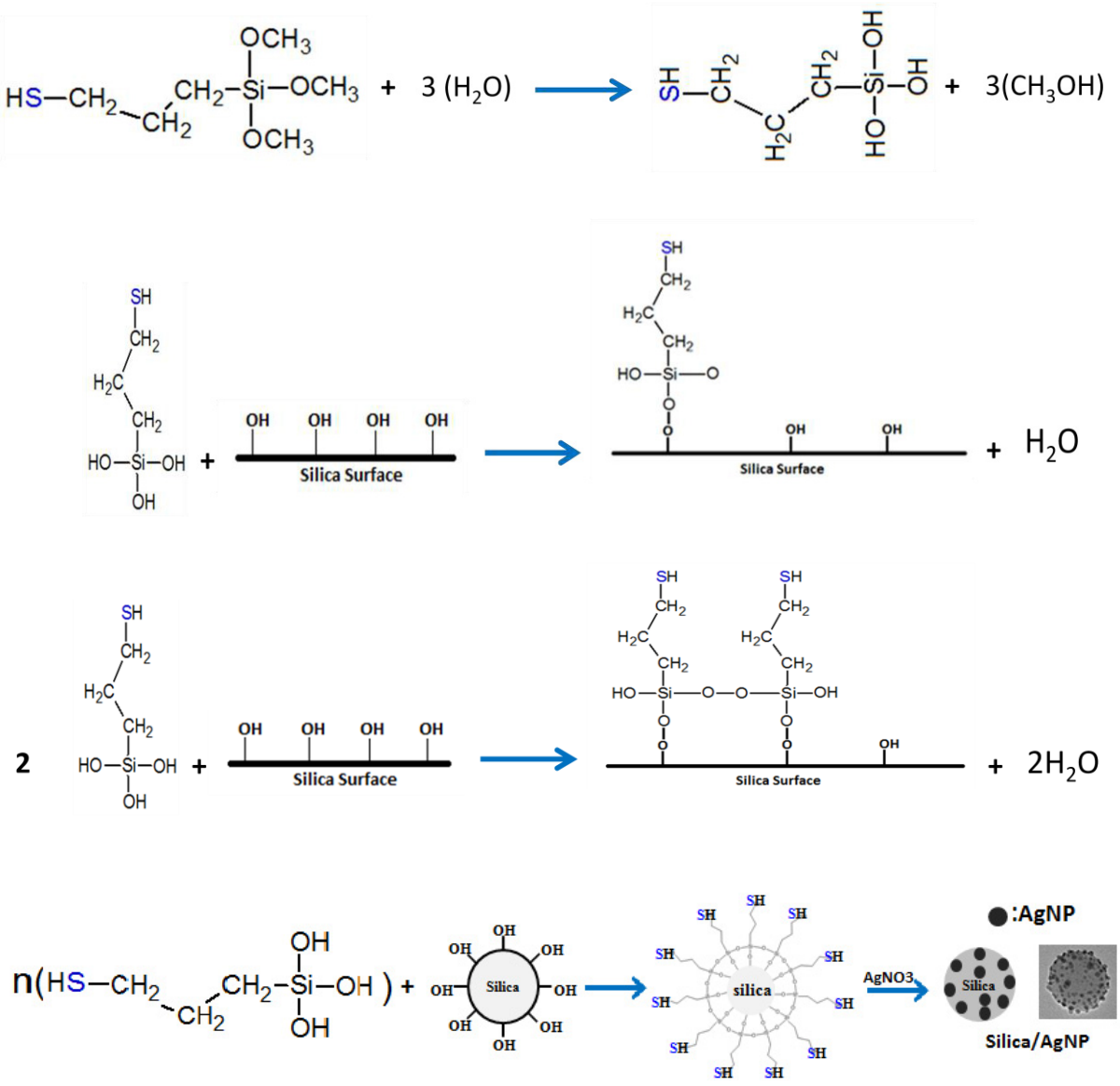

Scheme 7.1 Schematic representation of Silica/AgNP synthesis procedure

7.4 Results and discussions

7.4.1 Morphologies of the silica/AgNP and PVA/silica/AgNP

TEM images of the silica/AgNP nanoparticles given in the Figure 7.1, depict silver nanoparticles anchored on the spherical silica surface. Average sizes of the silica nanoparticles calculated by Image J software were 75.14 nm and those of the AgNPs were 3.93 nm.

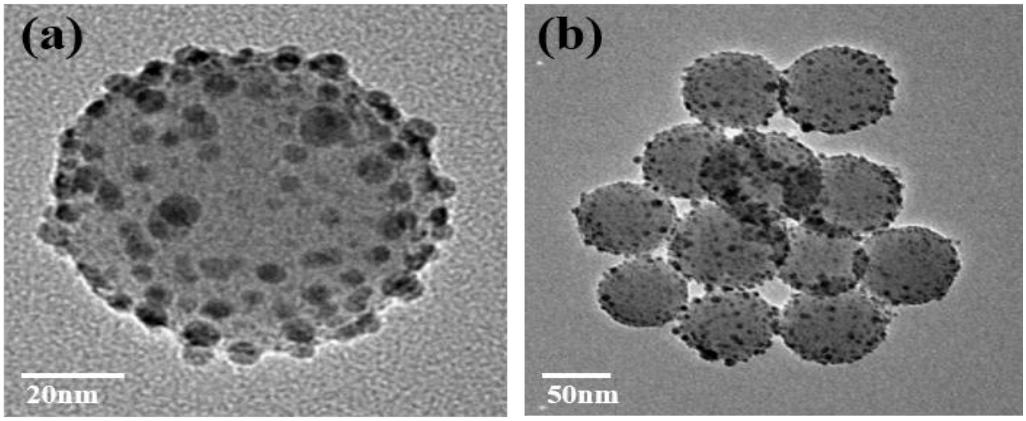

Figure 7.1 TEM images of sliver anchored silica nanoparticles (a) high and (b) low magnification.

The morphologies of the PVA/ silica/AgNP nanofibers have been presented in Figure 7.2. The results demonstrate smooth morphology and uniform structure of the nanofibers. Incorporation of silica/AgNP does not significantly affect morphology of the nanofibers except increasing the nanofiber diameters with successive addition of silica/AgNP (Figure 7.2b-7.2d). The average diameter of PVA nanofibers was around 170 nm, which increased to 277 nm in PVA/silica/AgNP having 15 wt% of silica/AgNP.

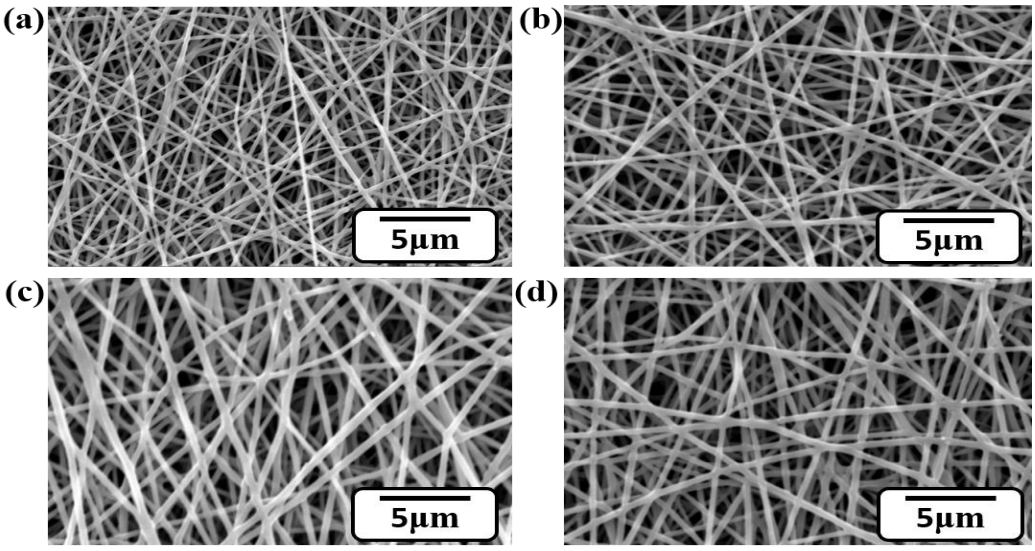

Figure 7.2 SEM images of PVA nanofibers with (a) 0 wt% (b) 5wt% (c) 10wt% and (d) 15wt% of silica/AgNP nanoparticles

Transmission electron microscopy images were taken to confirm the incorporation of silica/AgNP in the nanofiber (Figure 7.3). It is worth to note that the silica/AgNP were evenly distributed in the PVA nanofibers and the silica/AgNP protrude outside the nanofiber structure in the high concentration sample (15 wt% of silica/AgNP) (Figure 7.3c).

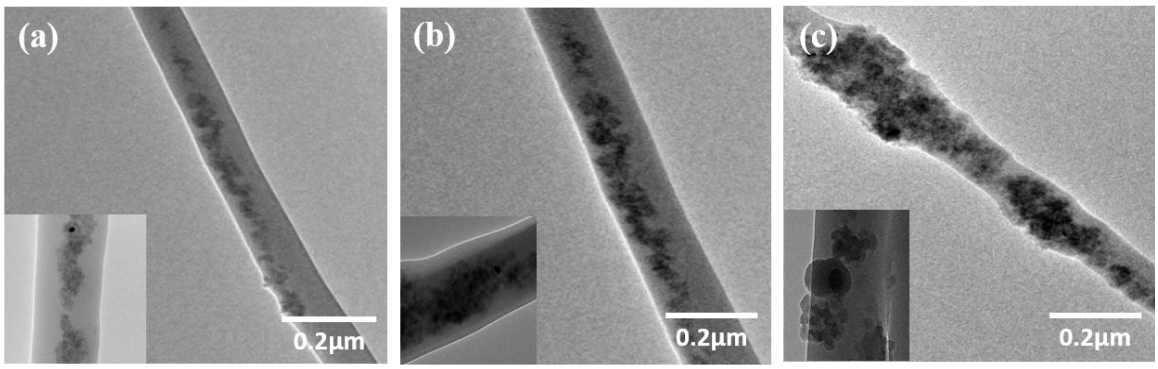

Figure 7.3 TEM images of PVA nanofibers with (a) 5wt% (b) 10wt% and (c) 15wt% of silica/AgNP nanoparticles.

Table 7.1 Summary of calculated swelling ratio, cross-linking density and average molecular weight between crosslinking points in cross-linked PVA nanofibers.

No.	Swelling ratio, Δm (%)		Crosslinking density, n (mol/cm^3)		Average molecular weight b/w cross-links, M_c	
	Δm	Mean Δm	n	Mean n	M_c	Mean M_c
1	304	307	4.11844×10^{-4}	4.089×10^{-4}	1214	1259
2	337		3.23574×10^{-4}		1545	
3	282		4.91181×10^{-4}		1018	

7.4.2 Cross-linking density of PVA/silica/AgNP

The PVA nanofibers were chemically crosslinked using glutaraldehyde which was added in the polymer solution prior to electrospinning. The crosslinking reaction initiated when the nanofibers were fumed with HCl that catalyzed the reaction. PVA has numerous hydroxyl groups which react with aldehyde groups in the presence of protons (H^+) catalysts and form acetal linkages (C-O-C)[15]. Table 1 summarized the calculated cross-linking density, swelling ratio and average molecular weight (M_c) between the cross-links. The results show 4.089 x 10^{-4} (mol/cm^3) and 1259 as mean cross-linking density and M_c of the cross-linked PVA respectively. These results demonstrate substantial cross-linking between the PVA polymer chains.

7.4.3 FTIR analysis of PVA/silica/AgNP nanofibers

The FTIR spectrum of PVA/ silica/AgNP demonstrates C-H and O-H bending vibrations at 848 cm^{-1} and 1420 cm^{-1}, respectively (Figure 7.4). Crosslinking of the PVA polymer chains with glutaraldehyde

catalyzed by HCl forms acetal linkages. The stronger peaks at 1110 cm^{-1} are due to C-O-C stretching vibrations [15] which is main feature of acetal linkage in crosslinked PVA nanofibers [16]. A peak at 3300 cm^{-1} is attributed to stretching of the –OH owing to strong inter-molecular and intra-molecular hydrogen bonds of PVA. The absorption band at 2925 cm^{-1} corresponds to $–CH_2$ symmetric and asymmetric stretching vibration [17]. The FTIR spectra confirmed cross-linking between PVA polymer chains.

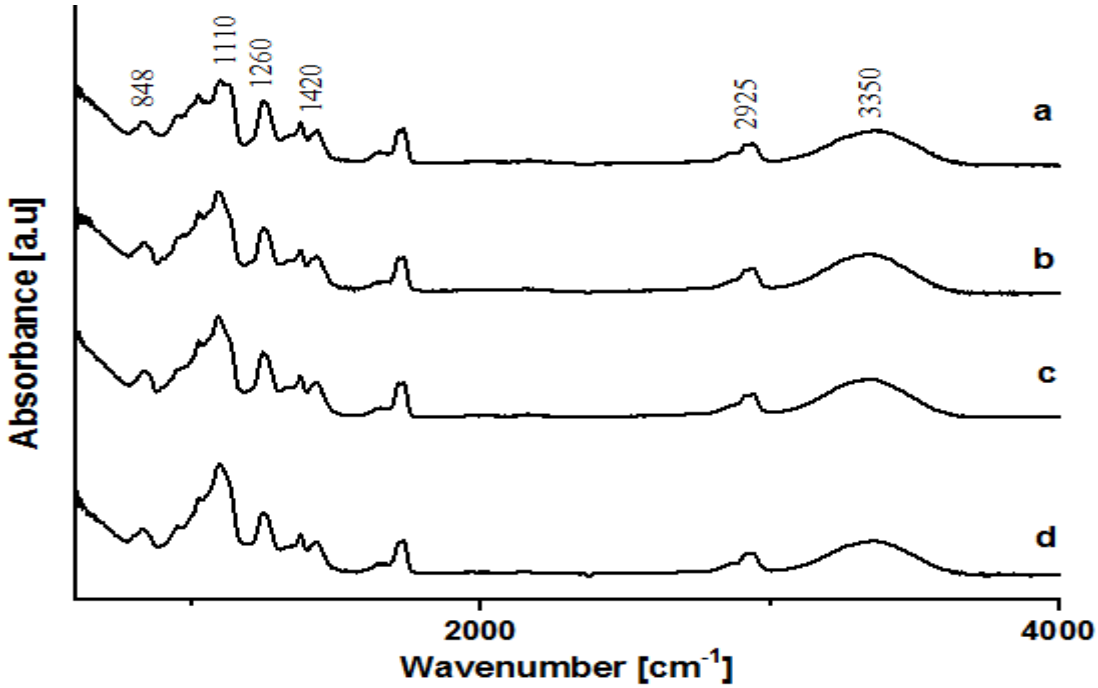

Figure 7.4 FTIR spectrum of PVA nanofibers with (a) 0wt% (b) 5wt% (c) 10wt% (d) 15wt% of silica/AgNP nanoparticles.

7.5 Antibacterial activities of PVA/silica/AgNP nanofibers

The antibacterial activity tests of the PVA/silica/AgNP nanofibers were conducted against *E. coli* as a representative of Gram-negative bacterium and *S. aureus* as a representative of Gram-positive bacterium. The disk diffusion test results of PVA/silica/AgNP nanofiber samples (Figure 7.5) exhibited significant inhibition zones, indicating the effective antibacterial activity against both bacterial strains. Notably, the area of inhibition zone of PVA/silica/AgNP nanofiber samples increased with increasing silica/AgNP loading concentrations in PVA nanofibers. The neat PVA nanofibers did not show any inhibition of bacterial growth which suggests that the antibacterial activities are due to silica/AgNP composite nanoparticles.

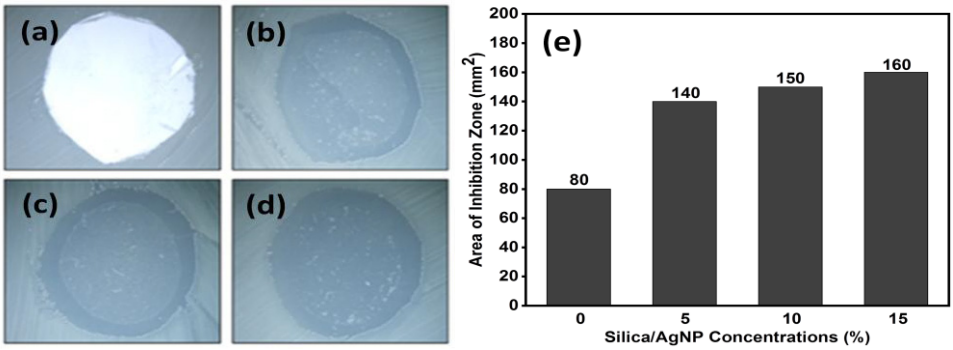

Figure 7.5 Disk diffusion test of PVA/ silica/AgNP nanofibers conjugated with (a) 0wt% (b) 5wt% (c) 10wt% (d) 15wt% silica/AgNP and (e) their area of inhibition zone

The bacterial growth-inhibiting activities of PVA/silica/AgNP nanofiber samples in liquid media (LB) with log-phase of *E. coli* and *S. aureus* were evaluated for 24 hours. Here, the surface of a bare cell culture plate was used as a negative control for normal growth condition of wild-type bacterial strains. Consistent with the results of disk diffusion test, the quantitative time profiles of bacterial growth demonstrated that the PVA/silica/AgNP nanofibers effectively inhibited growth of both the strains over the course of 24 h, while the bare PVA nanofiber did not show any growth-inhibiting activities against bacterial strains (Figure 7.6).

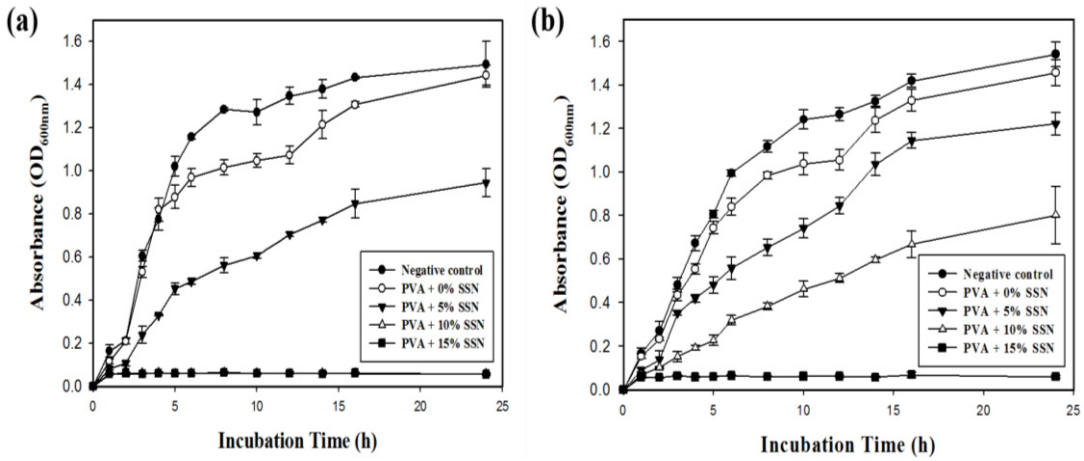

Figure 7.6 Bacterial growth time profiles of (a) *E. coli* (b) *S. aureus* strains incubated with PVA/silica/AgNP samples.

The bactericidal test results (Figure 7.7) indicated PVA/silica/AgNP having 15wt.% of silica/AgNP nanoparticles did not show any growth of *E. coli* and *S. aureus* strains over the tested time (24 hours). The PVA/silica/AgNP nanofibers conjugated with 10wt% of silica/AgNP nanoparticles depicted 0% *E. coli* viable cells; against *S. aureus* strains the same sample exhibited 4.8% relative cell viability. These results were consistent with qualitative liquid medium antibacterial activity results.

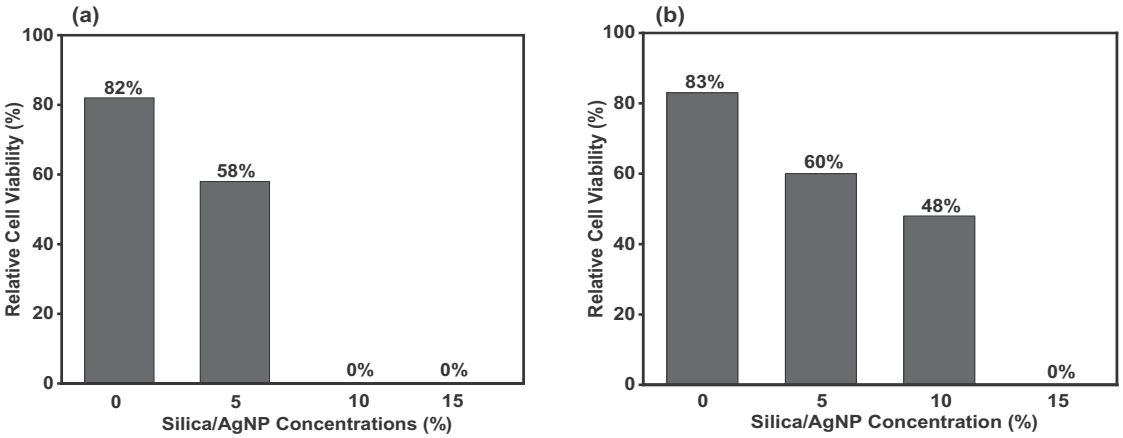

Figure 7.7 Bacterial cell viability of (a) *E. coli* (b) *S. aureus* strains incubated with PVA/silica/AgNP samples.

The significant reduction of viable cells confirmed the antibacterial activity of PVA/ silica/AgNP nanofibers against tested bacterial strains. The higher growth-inhibiting efficacy of PVA/silica/AgNP nanofibers toward Gram-negative (*E. coli*) may be due to the difference in the structures of Gram-negative and Gram-positive bacteria cell walls. The higher contents of peptidoglycan in the cell wall of Gram-positive bacteria show relatively higher resistance against antibacterial activities of silver [18-19]. However, contradictory results have also been reported. Our other works, i.e. CA/TiO_2/AgNP and CA/TiO_2/AgNP, demonstrated comparatively higher antibacterial activities against *S. aureus* in comparison to *E. coli*.

For qualitative analysis of antibacterial effects of PVA/silica/AgNP nanofibers, morphological changes in the bacteria after contact with the samples were observed via SEM analysis (Figure 7.8). The SEM images indicated clumping or aggregation of bacterial cells with the ruptured morphologies after incubation with PVA/silica/AgNP nanofibers conjugated with 15% silica/AgNP nanoparticles. The membrane rupture of bacterial cells on PVA/silica/AgNP nanofibers was inevitable, considering free radical reactions in a silver-based antibacterial mechanism for attacking bacterial cell membrane [18].

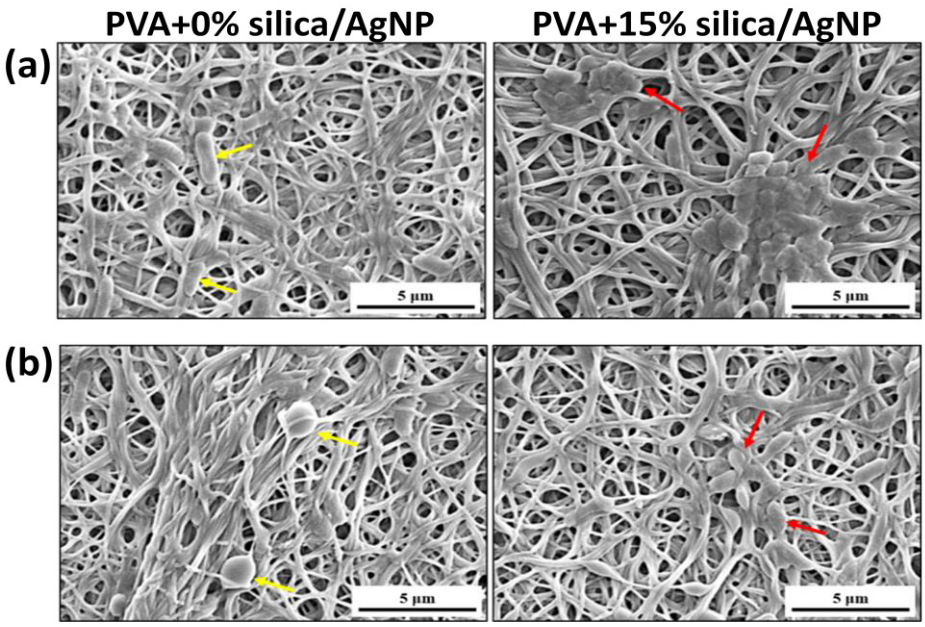

Figure 7.8 Morphologies of (a) Gram-negative *E. coli* and (b) Gram-positive *S. aureus* on PVA nanofibers conjugated with 0% silica/AgNP (left side) and 15% silica/AgNP (right side) observed by FE-SEM. Yellow arrows indicate viable bacterial cells and red arrows ruptured bacterial cells showing the abnormal morphologies of aggregates or clumps.

7.6 Conclusions

The research successfully concludes study on synthesis of silica/AgNP nanoparticles and their exploitation in fabricating PVA/silica/AgNP composite nanofibers. The SEM images depicted regular nanofibers. The TEM results depicted silica/AgNP loading in the PVA nanofibers. Incorporation of silica/AgNP nanoparticles in PVA increased diameters of PVA/silica/AgNP nanofibers. The PVA/silica/AgNP composite nanofibers showed substantial antibacterial activities against both Gram-positive (*S. aureus*) and Gram-negative bacteria (*E. coli*).

References

[1] S. Egger, R.P. Lehmann, M.J. Height, M.J. Loessner, M. Schuppler, Antimicrobial properties of a novel silver-silica nanocomposite material, Applied and environmental microbiology 75(9) (2009) 2973-2976.

[2] J.-M. Lee, D.-W. Kim, T.-H. Kim, S.-G. Oh, Facile route for preparation of silica–silver heterogeneous nanocomposite particles using alcohol reduction method, Materials Letters 61(7) (2007) 1558-1562.

[3] K. Shalumon, K. Anulekha, S.V. Nair, S. Nair, K. Chennazhi, R. Jayakumar, Sodium alginate/poly (vinyl alcohol)/nano ZnO composite nanofibers for antibacterial wound dressings, International Journal of Biological Macromolecules 49(3) (2011) 247-254.

[4] W.-C. Lin, D.-G. Yu, M.-C. Yang, Blood compatibility of novel poly (γ-glutamic acid)/polyvinyl alcohol hydrogels, Colloids and Surfaces B: Biointerfaces 47(1) (2006) 43-49.

[5] N.A. Peppas, J.E. Scott, Controlled release from poly (vinyl alcohol) gels prepared by freezing-thawing processes, Journal of controlled release 18(2) (1992) 95-100.

[6] D.J. Leaper, Silver dressings: their role in wound management, International wound journal 3(4) (2006) 282-294.

[7] C.L. Gallant-Behm, H.Q. Yin, S. Liu, J.P. Heggers, R.E. Langford, M.E. Olson, D.A. Hart, R.E. Burrell, Comparison of in vitro disc diffusion and time kill-kinetic assays for the evaluation of antimicrobial wound dressing efficacy, Wound repair and regeneration 13(4) (2005) 412-421.

[8] X. Liu, T. Lin, Y. Gao, Z. Xu, C. Huang, G. Yao, L. Jiang, Y. Tang, X. Wang, Antimicrobial electrospun nanofibers of cellulose acetate and polyester urethane composite for wound dressing, Journal of Biomedical Materials Research Part B: Applied Biomaterials 100(6) (2012) 1556-1565.

[9] S.A. Jones, P.G. Bowler, M. Walker, D. Parsons, Controlling wound bioburden with a novel silver-containing Hydrofiber® dressing, Wound repair and regeneration 12(3) (2004) 288-294.

[10] B.S. Atiyeh, M. Costagliola, S.N. Hayek, S.A. Dibo, Effect of silver on burn wound infection control and healing: review of the literature, Burns 33(2) (2007) 139-148.

[11] J. Song, H. Kim, Y. Jang, J. Jang, Enhanced antibacterial activity of silver/polyrhodanine-composite-decorated silica nanoparticles, ACS applied materials & interfaces 5(22) (2013) 11563-11568.

[12] Z. Ma, H. Ji, D. Tan, Y. Teng, G. Dong, J. Zhou, J. Qiu, M. Zhang, Silver nanoparticles decorated, flexible SiO 2 nanofibers with long-term antibacterial effect as reusable wound cover, Colloids and Surfaces A: Physicochemical and Engineering Aspects 387(1) (2011) 57-64.

[13] J. Song, H. Song, H. Kong, J.-Y. Hong, J. Jang, Fabrication of silica/polyrhodanine core/shell nanoparticles and their antibacterial properties, Journal of Materials Chemistry 21(48) (2011) 19317-19323.

[14] Y. Tian, J. Qi, W. Zhang, Q. Cai, X. Jiang, Facile, one-pot synthesis, and antibacterial activity of mesoporous silica nanoparticles decorated with well-dispersed silver nanoparticles, ACS applied materials & interfaces 6(15) (2014) 12038-12045.

[15] J. Jegal, K.H. Lee, Nanofiltration membranes based on poly (vinyl alcohol) and ionic polymers, Journal of applied polymer science 72(13) (1999) 1755-1762.

[16] X.H. Qin, S.Y. Wang, Electrospun nanofibers from crosslinked poly (vinyl alcohol) and its filtration efficiency, Journal of applied polymer science 109(2) (2008) 951-956.
[17] R. Rudra, V. Kumar, P.P. Kundu, Acid catalysed cross-linking of poly vinyl alcohol (PVA) by glutaraldehyde: effect of crosslink density on the characteristics of PVA membranes used in single chambered microbial fuel cells, RSC Advances 5(101) (2015) 83436-83447.
[18] J.S. Kim, E. Kuk, K.N. Yu, J.-H. Kim, S.J. Park, H.J. Lee, S.H. Kim, Y.K. Park, Y.H. Park, C.-Y. Hwang, Antimicrobial effects of silver nanoparticles, Nanomedicine: Nanotechnology, Biology and Medicine 3(1) (2007) 95-101.
[19] K. Kawahara, K. Tsuruda, M. Morishita, M. Uchida, Antibacterial effect of silver-zeolite on oral bacteria under anaerobic conditions, dental materials 16(6) (2000) 452-455.

CHAPTER 8

Cellulose Acetate/ZnO/AgNP Composite Nanofibers

8.1 Introduction

This chapter reports electrospun CA/ZnO/AgNP composite nanofibers for biologically safer and sustained antibacterial applications. The ZnO/AgNP nanoparticles were synthesized using dopamine hydrochloride (Dopa) as reducing agent and adhesive agent to immobilize AgNPs on ZnO nanoparticles. A simple solution-mixing procedure effectively generated AgNPs on ZnO nanoparticles. Synthesis of the ZnO/AgNP nanoparticles, fabrication of CA/ZnO/AgNP composite nanofibers and their characterization for antibacterial properties are reported and discussed in detail.

8.2 Synthesis of ZnO/AgNP nanoparticles

The zinc oxide/silver nanoparticle (ZnO/AgNP) composite nanoparticles were synthesized by an environmentally green process using dopamine hydrochloride (Dopa) as adhesive and reducing agent. The Dopa can polymerize to form a poly-dopamine coating on varying substances at pH 8.5 which can reduce the metal ions into respective nanoparticles. To synthesize the ZnO/AgNP composite nanoparticles, the ZnO nanoparticles were first coated with Dopa film which upon treatment with silver nitrate solution generated silver nanoparticles (AgNPs) on surface of the ZnO nanoparticles. In the typical process, 300mg of Dopa were dissolved in 150mL of 1M Tris HCl buffer. Then 1gram ZnO nanoparticles were added into the solution. The mixture was rigorously mixed for eighteen hours on a magnetic stirrer. The Dopa coated ZnO nanoparticles were obtained by centrifugation for twenty minutes at 5000rpm. The nanoparticles were multiple times washed with de-ionized water and centrifuged. A 200mM silver nitrate solution was prepared and the Dopa coated ZnO nanoparticles were added into 300mL of the solution. The mixture was then stirred for eighteen hours on a magnetic stirrer at very high rpm. In the end the ZnO/AgNP nanoparticles were collected by centrifuging at 5000rpm for twenty minutes and dried at 50^0C for 24h in a drying oven.

8.3 Fabrication of CA/ZnO and CA/ZnO/AgNP nanofibers

For preparation of CA/ZnO/AgNP composite nanofibers two concentrations of ZnO/AgNP nanoparticles, 5wt% (CA/ZnO/AgNP1) and 10wt% (CA/ZnO/AgNP2) were chosen. The CA/ZnO composite nanofibers were prepared using 10wt% of ZnO nanoparticles. The CA (17 wt %) was first dissolved in DMF/acetone (1:2, wt/wt) solvent system. After complete dissolution of CA the nanoparticles were added into the solution and kept under strong stirring for 3h. The solutions were sonicated for 1h. Detail of electrospinning apparatus and procedure has already been reported in previous chapters. Distance between the needle tip and the metallic cylinder was kept 15 cm and uniform nanofiber mats were prepared at 18kV electric voltage. To control the solution flow rate 0.06mm/min feed speed was used in preparation of all the samples.

8.4 Results and discussions

8.4.1 Synthesis of ZnO/AgNP nanoparticles

Synthesis of ZnO/AgNP composite nanoparticles by Dopa was studied using XRD analysis, XPS and TEM observations. XRD patterns of ZnO (Figure 8.1a) and ZnO/AgNP (Figure 8.1b) exhibited their respective patterns. The ZnO nanoparticles showed diffraction angles (2θ) at 31.68^0, 34.32^0, 36.2^0, 47.42^0, 56.52^0, 62.79^0, 67.91^0 and 69.04^0 which belong to (100), (002), (101), (102), (110), (103), (200) and (112) crystal planes of ZnO nanoparticles. The ZnO/AgNP patterns depicted all the patterns of ZnO nanoparticles. Additionally X-ray diffractions (2θ) at 38.12^0, 44.2^0, 64.4^0 and 77.4^0 were also observed which correspond to (111), (200), (220) and (311) planes of spherical AgNPs having face centered cubic (FCC) structure which confirms crystallinity and purity of the AgNPs [1]. No additional X-ray diffraction pattern was seen in the ZnO/AgNP pattern which demonstrated that the composite nanoparticles were free of impurities. Thus FCC structure of AgNPs and no additional X-ray diffraction pattern illustrates that the Dopa was highly effective in generation of AgNPs on ZnO nanoparticles. Average crystallite sizes of ZnO and AgNPs in ZnO/AgNP composite nanoparticles were calculated to be 17.85nm and 11.68nm respectively.

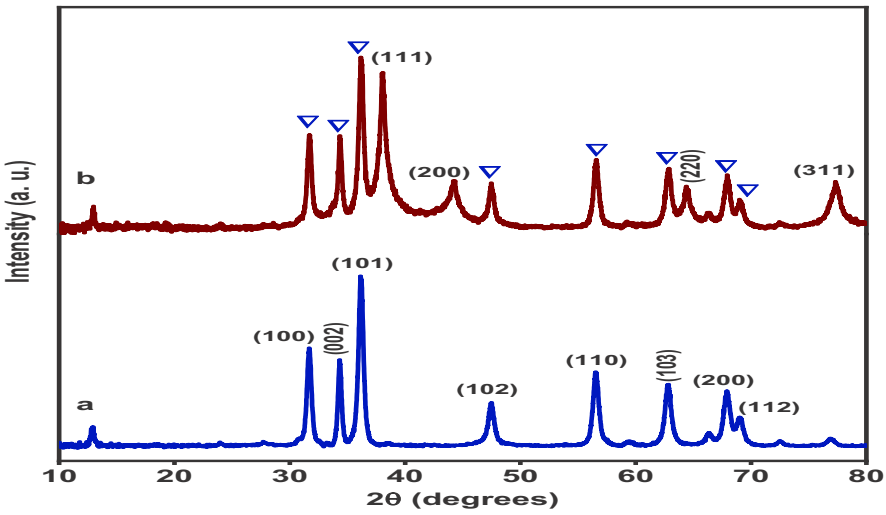

Figure 8.1 XRD patterns of the nanoparticles (a) ZnO (b) ZnO/AgNP

The synthesized ZnO/AgNP composite nanoparticles wwer further studied using XPS studies. The XPS results (Figure 8.2) showed formation of polydopamine coating and generation of AgNPs on ZnO nanoparticle surfaces. The dopamine hydrochloride forms strong adhesive coating at alkaline pH (pH: 8.5). The polydopamine contains catechol groups which oxidize into quinone and donate their electrons to silver ions thus convert them into metallic nanoparticles. The peaks at binding energies (B.E.) 265.5eV, 399.67eV and 530.65eV represent C 1s, N 1s and O 1s which belong to the polydopamine coating. The Zn 2p and Ag 3d peaks in wide scan XPS spectrum correspond to ZnO and AgNP nanoparticles. The narrow scan spectrum of Zn 2p and Ag 3d were obtained to further study the nanoparticles. The Zn 2p narrow scan shows two peaks at B.E. 1043.65eV and 1020.65eV corresponding to Zn $2p_{3/2}$ and Zn $2p_{1/2}$ respectively [2]. The de-convoluted narrow scan spectrum of Ag 3d showed two peaks at B.E. 373.3eV and 367.3eV corresponding to Ag $3d_{3/2}$ and Ag $3d_{5/2}$

respectively. These two peaks had a doublet slitting of 6.0eV which suggests that the generated AgNPs were metallic[3].

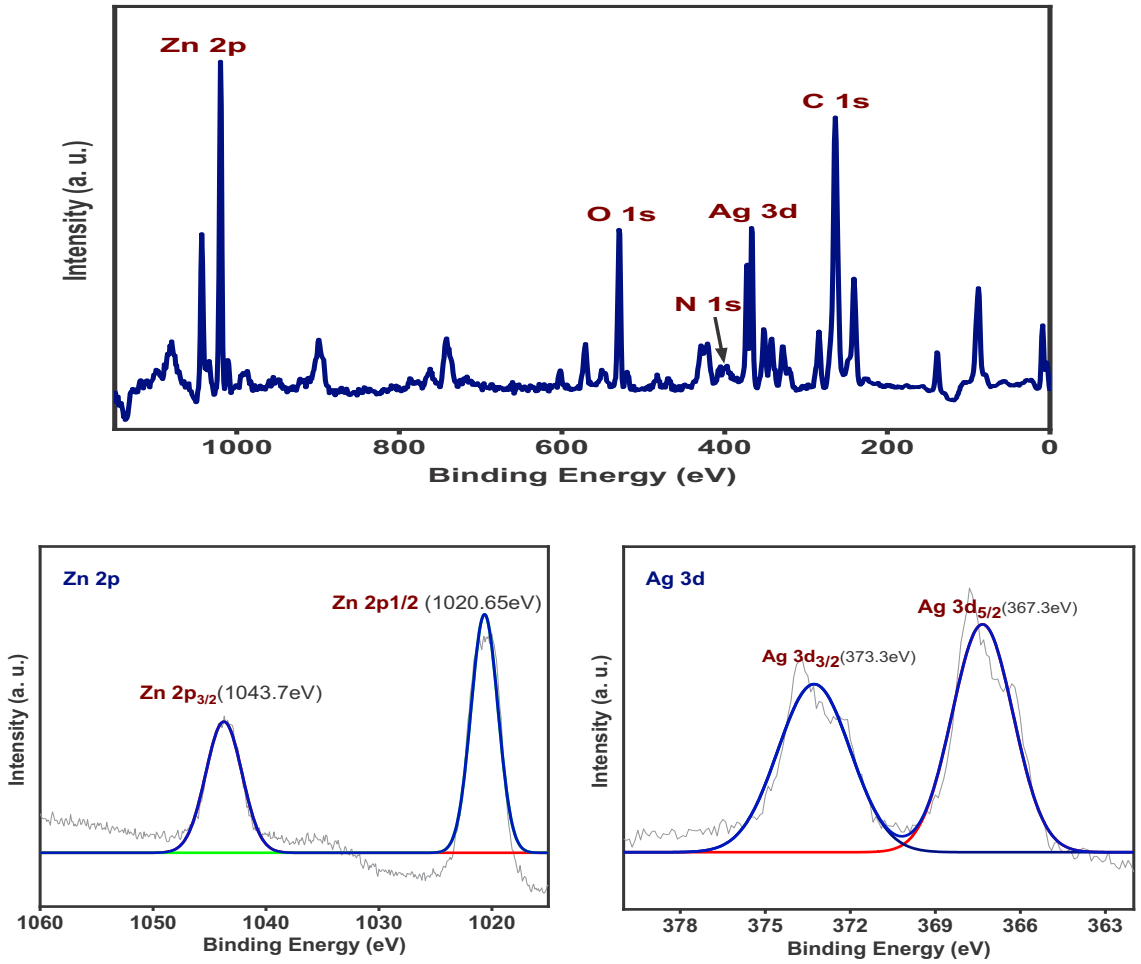

Figure 8.2 XPS results of the ZnO/AgNP composite nanoparticles

The morphology and crystallinity of the ZnO/AgNP composite nanoparticles were investigated using TEM analysis. The TEM images (Figure 8.3) showed AgNPs anchored on the surface of ZnO nanoparticles. Both the ZnO and AgNPs were spherical shaped. The HRTEM image demonstrated crystalline ZnO and AgNP nanoparticles. The ZnO nanoparticles showed 0.52nm inter planar distance which corresponds to their (001) crystal planes [4]. While the AgNPs depicted inter planar distance of 0.241nm which represents (111) planes of the AgNPs [5]. The TEM images confirm that the AgNPs successfully grown on the ZnO nanoparticle surfaces suggesting effectiveness of the Dopa mediated process in synthesis of ZnO/AgNP composite nanoparticles.

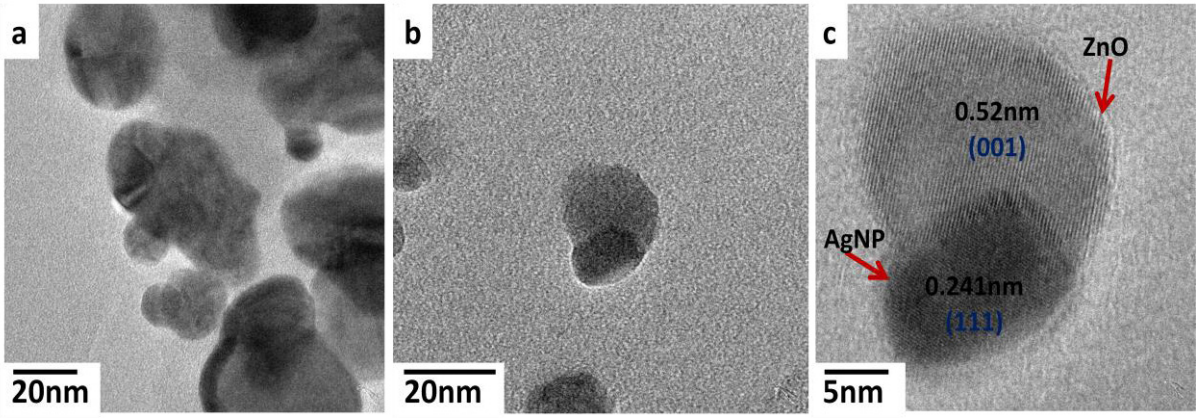

Figure8.3 (a, b) TEM images (c) HRTEM image of ZnO/AgNP nanoparticles

8.4.2 Fabrication of the composite nanofibers

Incorporation of the nanoparticles into the CA nanofibers was investigated using XRD analysis. For comparison purpose CA/ZnO composite nanofibers were also fabricated. The CA/ZnO nanocomposite exhibited all the corresponding diffraction patterns of ZnO nanoparticles. While the CA/ZnO/AgNP1 and CA/ZnO/AgNP2 depicted diffraction patterns of both the ZnO and AgNPs (Figure 8.4).

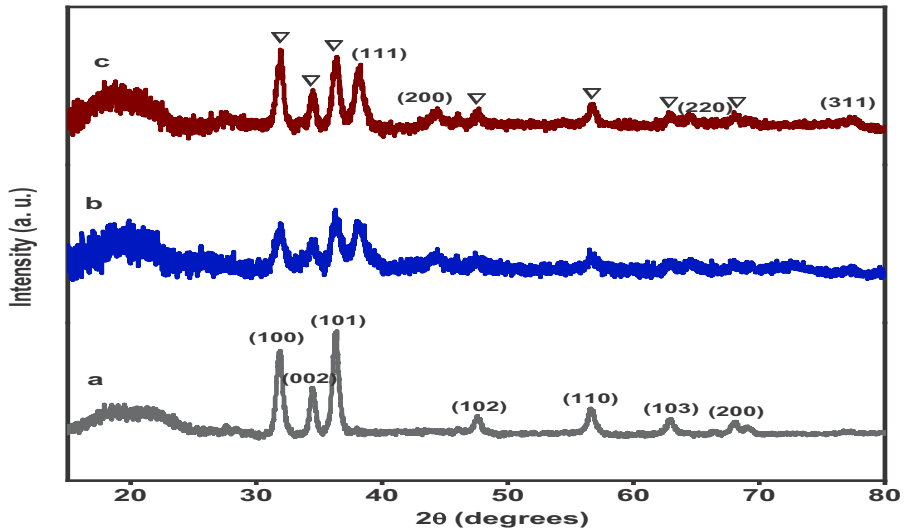

Figure 8.4 XRD patterns of composite nanofibers (a) CA/ZnO (b) CA/ZnO/AgNP1 (c) CA/ZnO/AgNP2

TEM observations were conducted to analyze loading and distribution of the ZnO and ZnO/AgNP nanoparticles in CA/ZnO and CA/ZnO/AgNP composite nanofibers respectively. All the sample depicted CA nanofibers incorporated with respective nanoparticles (Figure 8.5). The ZnO nanoparticles in CA/ZnO nanocomposite were densely located in the CA nanofibers. Comparing CA/ZnO/AgNP1 with CA/ZnO/AgNP2 composite nanofibers, the latter demonstrated comparatively higher contents, dense distribution and some larger aggregation of the ZnO/AgNP nanoparticles owing to higher concentration of the nanoparticles used in their fabrication (10wt. %).

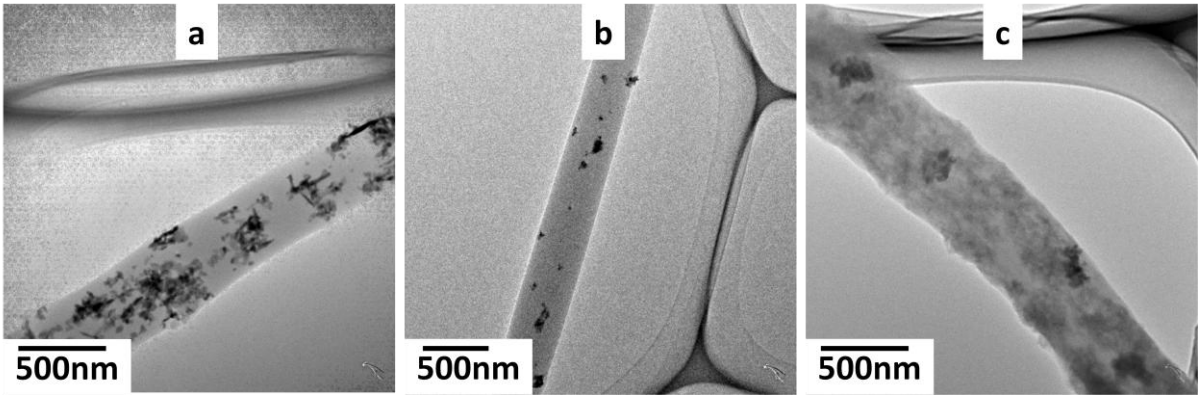

Figure 8.5 TEM images of the composite nanofibers (a) CA/ZnO (b) CA/ZnO/AgNP1 (c) CA/ZnO/AgNP2

Morphologies of CA, CA/ZnO and CA/ZnO/AgNP nanofibers were observed using scanning electron microscopy (SEM). All the samples depicted regular and bead free nanofibers (Figure 8.6). Due to improvement of solution properties with addition of nanoparticles (i.e. conductivity) the diameters of CA/ZnO and ZA/ZnO/AgNP nanocomposites were observed to decrease. Since the AgNPs are metallic having higher conductivities than pure ZnO nanoparticles, incorporation of composite nanoparticles greatly improved solution properties which in turn largely decreased diameters of the CA/ZnO/AgNP nanofibers. Furthermore, owing to higher contents of the nanoparticles, the CA/ZnO and CA/ZnO/AgNP nanocomposites showed intermittent thick places which may be respective nanoparticle aggregates.

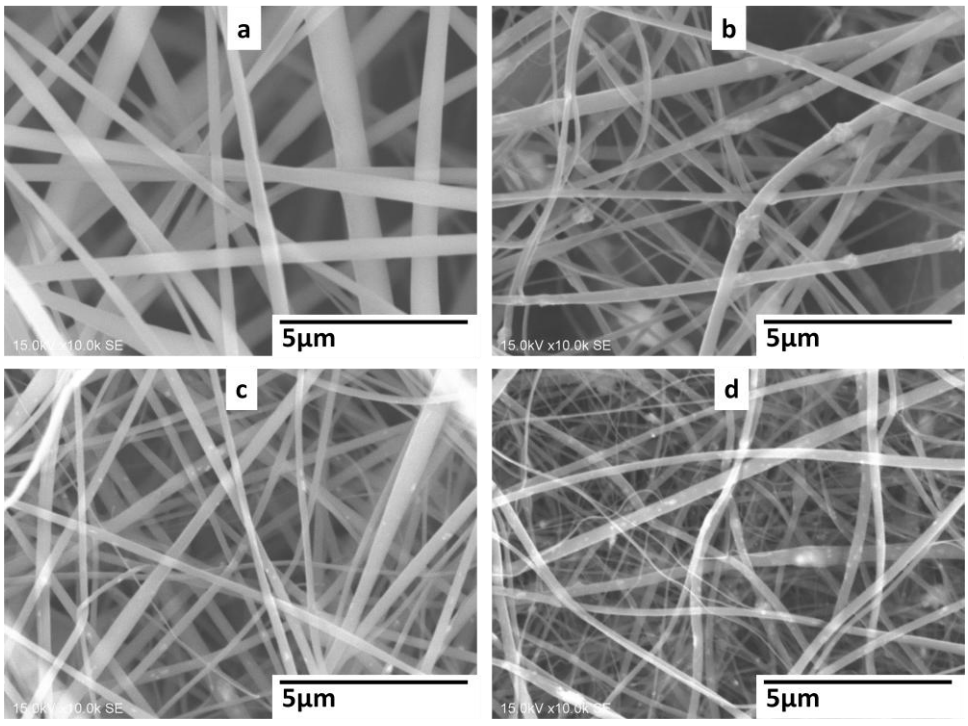

Figure 8.6 SEM images of (a) CA (b) CA/ZnO (c) CA/ZnO/AgNP1 (d) CA/ZnO/AgNP2

The Fourier transform infra-red spectroscopy analysis was carried out to investigate possible effect of incorporation of the nanoparticles on chemical structures of the CA nanofibers. All the samples exhibited respective peaks of cellulose acetate (Figure 8.7). Incorporation of ZnO and ZnO/AgNP nanoparticles did not show any significant effect on chemical structures of the nanofibers. A peak at 1740cm^{-1} was assigned to stretching vibrations of C=O (carbonyl functional groups). The peaks at 1365cm^{-1} was assigned to bending vibration in CH_3 groups. The peaks at 1235cm^{-1}, 1042 cm^{-1} were assigned to stretching vibrations of C-O-C groups[6]. The reported peaks in FTIR spectrum are representative of CA structure.

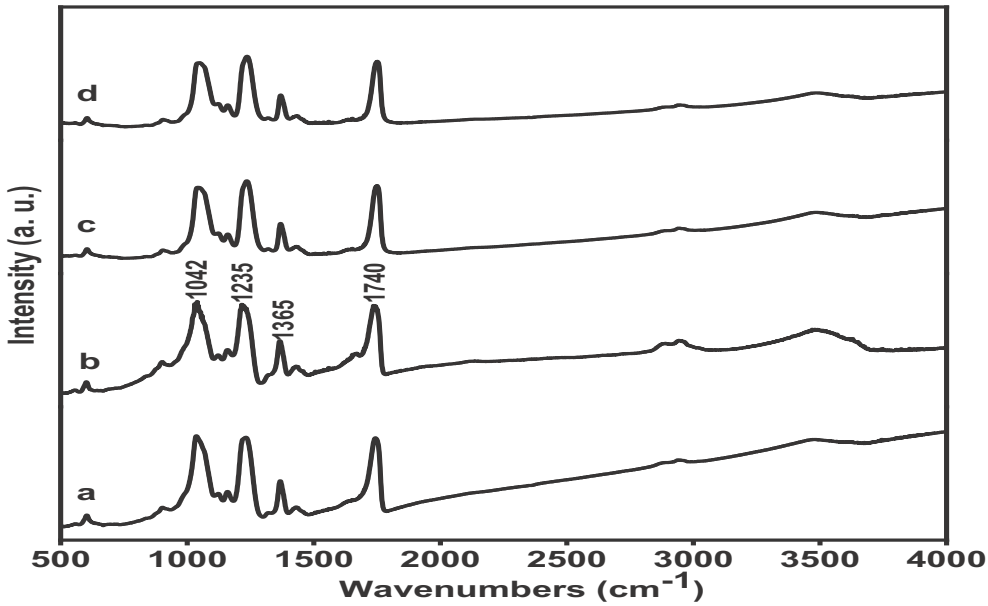

Figure 8.7 FTIR spectrum of the nanofibers (a) CA (b) CA/ZnO (c) CA/ZnO/AgNP1 (d) CA/ZnO/AgNP2

8.4.3 Antibacterial tests of CA/ZnO/AgNP

The antibacterial activities of the CA/ZnO and CA/ZnO/AgNP composite nanofibers were studied in detail by investigating growth inhibition performance on agar plates and in liquid medium. The quantitative bactericidal properties were also investigated by relative cell viability (%) assay. All the antibacterial tests were conducted against *E. coli* (Gram-negative bacteria) and *S. aureus* (Gram-positive bacteria).

The agar plate disc diffusion test results reported in Table 8.1 and Figure 8.8A show effective growth inhibition of both the strains by CA/ZO/AgNP samples. The mean halo width (mm) values by CA/ZnO/AgNP1 against *E. coli* and *S. aureus* were 0.66mm and 0.69mm respectively. While the CA/ZnO/AgNP2 demonstrated 1.27mm and 1.32mm halo widths against *E. coli* and *S. aureus* strains respectively. Larger halo widths formed by CA/ZnO/AgNP2 were due to higher contents of ZnO/AgNP nanoparticles. Although, both CA and CA/ZnO nanofibers did not show any halo widths, however, bacterial colonization on CA samples were observed while the CA/ZnO inhibited such bacterial colonisations. It was also observed that the CA/ZnO/AgNP composite nanofibers demonstrated slightly higher antibacterial activities against *E. coli* than *S. aureus* bacteria.

The quantitative bactericidal test results given in Figure 8.8B revealed 100% bactericidal properties (0% viable cells) of the CA/ZnO/AgNP2 samples against both the test strains. The CA/ZnO/AgNP1

showed 1.6% and 2.8% relative cell viabilities with *E. coli* and *S. aureus* strains. These results suggest CA/ZnO/AgNP2 as an effective antibacterial CA/ZnO/AgNP nanocomposite.

Growth curves of the *E. coli* and *S. aureus* strains incubated with samples were obtained to observe growth inhibition properties of the samples in liquid medium. The results given in Figure 8.8C revealed CA/ZnO/AgNP samples effectively inhibited growth of both the strains up to 108h (tested time). Extended time antibacterial activities of the proposed composite nanofibers may be due to several factors. Primarily the AgNPs are anchored on ZnO nanoparticles. The composite nanoparticles are embedded inside the CA polymer matrix. Another important factor is the Dopa chemistry used in the synthesis of AgNPs. Apart from being an effective reducing agent, Dopa is strong adhesive agent. It has been reported that the Dopa mediated AgNP generation effects silver leaching due to strongly adhered AgNPs on the used substrates [7-8]. Thus anchored AgNPs, embedding inside nanofibers and Dopa mediated bonding ensures long term and sustained antibacterial properties. Contradictory to disc diffusion test method, the CA/ZnO nanocomposite depicted a degree of antibacterial properties in the liquid medium test. However, the bacteriostatic activities were lower than the CA/ZnO/AgNP nanofibers and their effectiveness decreased with incubation time which may be due to release of zinc ions. On the other hand the CA/ZnO/AgNP composite nanofibers demonstrated excellent growth inhibition properties. It is suggested that the antibacterial properties of these novel nanofiber composites would be based on generation of reactive oxygen species (ROS) such as peroxides, oxygen radicals and hydroxyl radicals.

Table 8.1 Antibacterial activity test results (halo width, mm)

	Halo Width (mm)			
	CA	CA/ZnO	CA/ZnO/AgNP1	CA/ZnO/AgNP2
E. coli	-----	-----	0.66	1.27
S. aureus	-----	-----	0.69	1.32

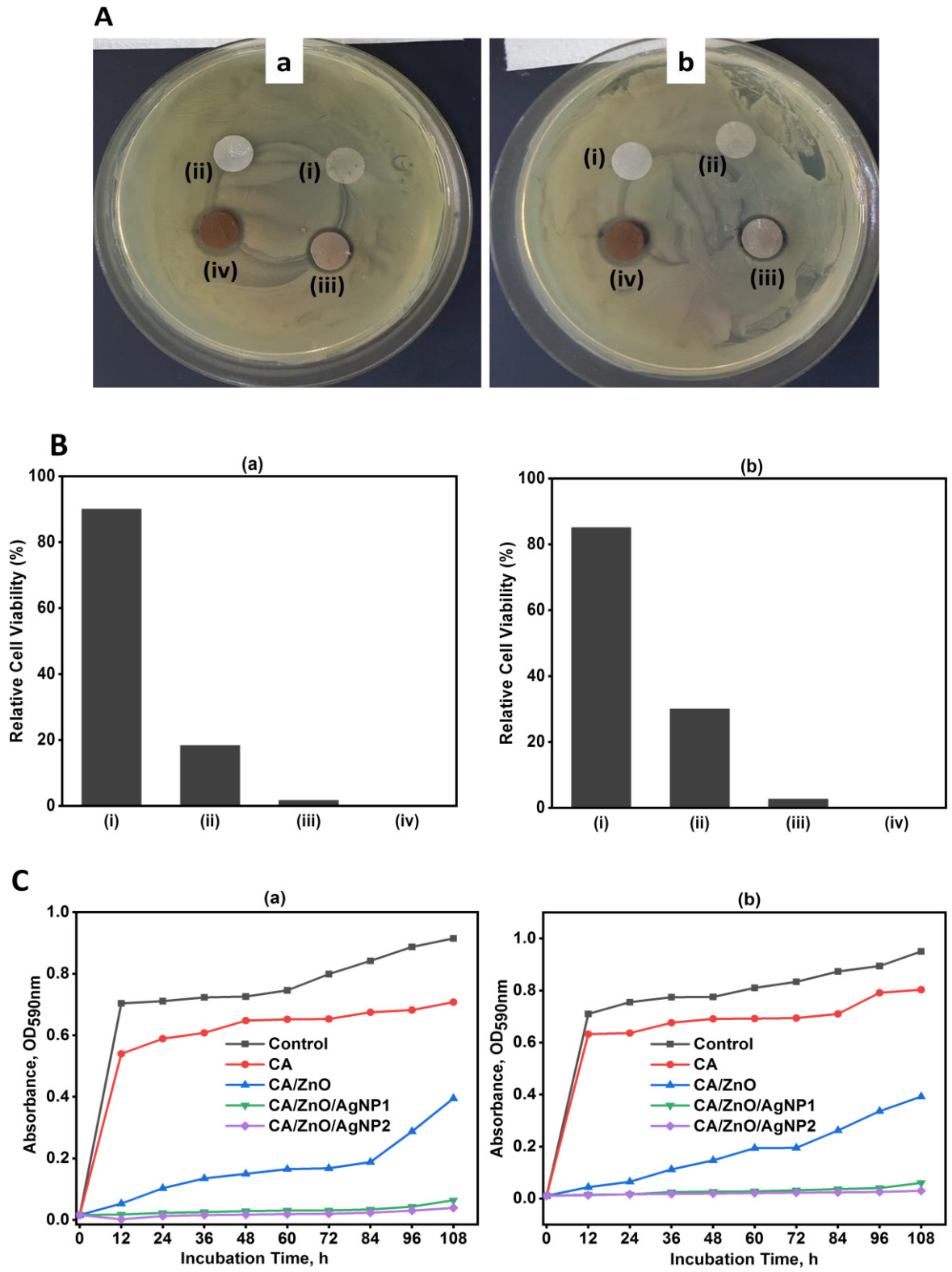

Figure 8.8 Antibacterial activity results (A) photographic images of disk diffusion test (B) bactericidal assay (relative cell viability, %) (C) liquid medium bacteria growth inhibition of the samples (i) CA (ii) CA/ZnO (iii) CA/ZnO/AgNP1 (iv) CA/ZnO/AgNP2 against (a) *E. coli* (b) *S. aureus* strains

8.5 Conclusions

The research successfully concluded synthesis of CA/ZnO/AgNP nanofibers for sustained and prolonged antibacterial applications. The ZnO/AgNP were synthesized by an environmentally green procedure and used to prepare CA/ZnO/AgNP nanofiber webs by electrospinning technique. All the characterization techniques used, confirmed synthesis of metallic ZnO/AgNP nanoparticles and their localization into CA nanofibers. The antibacterial test results evidenced excellent bacteriostatic and bactericidal properties of the CA/ZnO/AgNP nanofibers. The CA/ZnO/AgNP nanofibers were effective in inhibiting growth of the *E. coli* and *S. aureus* bacteria on agar plates and yielded 0% viable bacteria cells in relative cell viability tests. The time dependent antibacterial tests confirmed CA/ZnO/AgNP's effectiveness in growth inhibition of the bacterial strains for up to 108h (tested time).

References

[1] S.S. Patil, M.G. Mali, M.S. Tamboli, D.R. Patil, M.V. Kulkarni, H. Yoon, H. Kim, S.S. Al-Deyab, S.S. Yoon, S.S. Kolekar, Green approach for hierarchical nanostructured Ag-ZnO and their photocatalytic performance under sunlight, Catalysis Today 260 (2016) 126-134.
[2] J. Liqiang, W. Baiqi, X. Baifu, L. Shudan, S. Keying, C. Weimin, F. Honggang, Investigations on the surface modification of ZnO nanoparticle photocatalyst by depositing Pd, Journal of Solid State Chemistry 177(11) (2004) 4221-4227.
[3] M. Gopiraman, D. Deng, S. Saravanamoorthy, I.-M. Chung, I.S. Kim, Gold, silver and nickel nanoparticle anchored cellulose nanofiber composites as highly active catalysts for the rapid and selective reduction of nitrophenols in water, RSC Advances 8(6) (2018) 3014-3023.
[4] X. Zou, H. Fan, Y. Tian, S. Yan, Synthesis of Cu 2 O/ZnO hetero-nanorod arrays with enhanced visible light-driven photocatalytic activity, CrystEngComm 16(6) (2014) 1149-1156.
[5] A.W. Jatoi, I.S. Kim, Q.-Q. Ni, Cellulose acetate nanofibers embedded with AgNPs anchored TiO2 nanoparticles for long term excellent antibacterial applications, Carbohydrate Polymers (2018).
[6] M. Gopiraman, A.W. Jatoi, S. Hiromichi, K. Yamaguchi, H.-Y. Jeon, I.-M. Chung, K.I. Soo, Silver coated anionic cellulose nanofiber composites for an efficient antimicrobial activity, Carbohydrate Polymers 149 (2016) 51-59.
[7] C. Luo, Z. Zou, B. Luo, W. Wen, H. Li, M. Liu, C. Zhou, Enhanced mechanical properties and cytocompatibility of electrospun poly (l-lactide) composite fiber membranes assisted by polydopamine-coated halloysite nanotubes, Applied Surface Science 369 (2016) 82-91.
[8] X. Gao, J. Song, P. Ji, X. Zhang, X. Li, X. Xu, M. Wang, S. Zhang, Y. Deng, F. Deng, Polydopamine-templated hydroxyapatite reinforced polycaprolactone composite nanofibers with enhanced cytocompatibility and osteogenesis for bone tissue engineering, ACS applied materials & interfaces 8(5) (2016) 3499-3515.

CHAPTER 9

Ultrasonic dyeing of Polyurethane Nanofibers

9.1 Introduction

This chapter presents research on ultrasonic dyeing of polyurethane (PU) nanofibers. The PU nanofibers were fabricated by electrospinning process and were subsequently dyed following exhaust method using sonication. The two disperse dyes selected were a low energy disperse dye (CI Disperse Blue 56) and a high energy disperse dye (CI Disperse Red 167:1). The ultrasonic energy have been used in order to achieve higher color build-up on PU nanofibers. The temperature/time (T/T) diagram of the proposed dyeing process has also been suggested. The dyeing time and dyeing temperature were optimized. Color build-up properties (measured in terms of K/S values), dye fixation (%) and color fastness properties have been studied in detail.

9.2 Research background

Polyurethane (PU) is an important polymer and covers huge proportion in conventional textiles and specialty clothing. Due to its self-healing characteristics it is also known as spandex. The self-healing properties of PU are governed by its segmented structures with repeated soft segment and hard segment (Scheme 9.1a). Properties of PU can be tuned by length of these soft segments and hard segments [1-2]. PU has been widely used in apparel and specialty clothing such as in shirts, trousers, hosiery, stretchable and wrinkle free garments, sportswear, swimsuits, undergarments, tights, corsets, bodices and other shape recovery garments. Apart from conventional textiles, uses of PU in technical textiles, smart and functional materials are enormous and rapidly growing [3-4].

Substantial work has already been done on electrospinning of PU into nanofibers using electrospinning technique. Owing to nano fibrous structure and characteristic properties of PU, the dyed PU nanofibers are highly desirable candidate for apparel and specialty clothing.

There are numerous research articles available on the dyeing of nanofibers with varying dye classes [5-8]. However, dyeing of PU nanofibers by exhaust method has not yet been reported. The researchers reported low color yield as a barrier in dyeability of nanofibers and their subsequent uses in apparel [8-9]. In general, dye uptake by a textile substrate depends on its chemical and physical structures. The functional groups, proportion of amorphous to crystalline regions define dye uptake by the substrate and final color build-up [10-12]. Another considerable aspect is glass transition temperature, Tg, of the polymers which is related to structure and chemical bonding in the polymer. The degree of crystallinity, inter and intra molecular bonding, chemical interaction

between polymer chains, alignment of polymer chains and fiber orientation along its axis affects dye molecule's interaction and mobility in the textile substrate.

PU has segmented structure named as hard segment and soft segment linked together by urethane linkages [13]. The hard segment is a rigid point composed of closed ring cyclic hydrocarbons and acts as a memory point to recover after an external stimulus while the soft segments consists of open chain hydrocarbons and controls its stretchability [14]. Related to the dyeing, functional groups present in the urethane linkage promote diffusion of disperse dyes from surface to inside the polymer structure while the amorphous soft segment provides dye sites for the dyes. Based on the glass transition temperature, Tg, PU produced by SMP (Shape Memory Polymer) Technologies is available as 9020, 7520, 6520, 5520, 4520, 3520 and 2520. In the research 9020 was chosen owing to its higher Tg in the group; 90^0C.

Dyeing mechanism of almost all dye classes follow three main steps such as diffusion of dye molecules from dye liquor onto the substrate's surface, dye sorption on the surface and dye diffusion from surface into the polymer structure. The dyeing of a textile can be accomplished by continuous method, semi-continuous method and exhaust method [15].

Sonication in general produces ultrasonic cavitations in the bulk media, transient cavitations near the substrate surface and mobilizes the molecules on and within the substrates. Related to dyeing, in our opinion ultrasonic cavitations break dye aggregates in the bulk media and promote diffusion of disperse dye molecules towards the PU nanofiber surface. The transient cavitations enhance dye sorption on the PU nanofiber surface. Furthermore, sonication swell the soft segment of PU [16] producing sufficient space for disperse dye molecules to diffuse inside polymer chains.

In the present work we first time carried out our study on dyeability of PU nanofibers with disperse dyes by exhaust method. The ultrasonic energy was used to enhance dye uptake of the PU nanofibers. Two disperse dyes belonging to different dye classes, such as CI Disperse Blue 56 (a low energy level anthraquinone dye) and CI Disperse Red 167:1 (a high energy level azoic dye), were chosen. Conventional exhaust dyeing of PU is carried out at 100 ^{0}C for about one hour[3, 17-18]. Successful dyeing of PU nanofibers with high color yield, in reduced time and at temperature lower than its Tg, suggested US dyeing as an efficient and economically viable strategy to decide its suitability in apparel and surgical clothing.

9.3 Fabrication and dyeing of PU nanofibers

The polyurethane (PU) nanofibers were fabricated using DMF as solvent. For this purpose, a 28% (wt.%) solution of PU was prepared and continuously stirred for 12 hours at room temperature using magnetic stirrer. Electrospinning was carried out as reported in experimental section except that the electric voltage and TCD for PU nanofibers were 18kV and 15cm respectively.

Dyeing of PU nanofibers was carried out in a sonication bath using two disperse dyes namely CI Disperse Red 167:1 (CIR) and CI Disperse Blue 56 (CIB). Chemical structures of the dyes are presented in Scheme 9.1. A 1:100 fiber to dye liquor ratio was used. In order to optimize the dyeing time, PU samples were dyed for 10, 20, 30, 40, 50, 60, 70 and 80 minutes. To optimize the dyeing temperature, the experiments were performed at 30, 40, 50, 60, 70, 80 and 90^{0}C. The research was further extended to evaluate effect of dye concentrations on the color build-up properties of PU. For this purpose, six varying dye concentrations (1%, 2%, 3%, 4%, 5% and 6%) were used. The ultrasonic dyeing was carried out at 60Hz and 55 watts. Input energy given to the dye bath was 0.302 W/cm^2. To remove unfixed dye from the nanofibers, the samples were repeatedly washed with warm water (60^{0}C) and cold water (30^{0}C) until no further color bleeding was observed. Dye solution was sonicated for five (5) minutes at 25^{0}C prior to addition of PU nanofibers into the dye bath. The suggested temperature/time (T/T) diagram for the dyeing process is given in scheme 9.2.

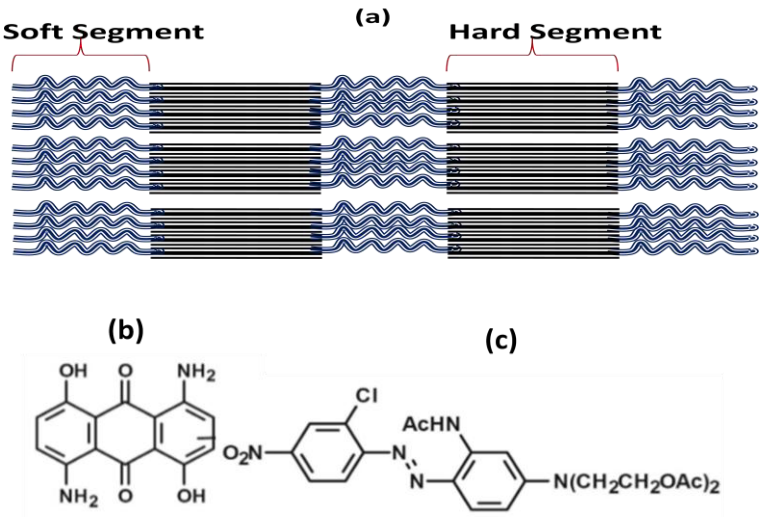

Scheme 9.1 (a) Illustration of segmented structure of PU and chemical structures of the used dyes (b) CI Disperse Blue 56 (c) CI Disperse Red 167:1

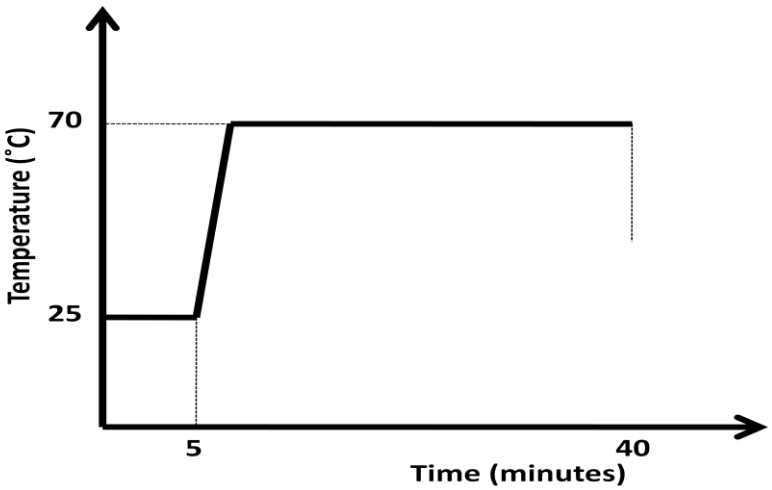

Scheme 9.2 Temperature/Time (T/T) diagram for exhaust dyeing of PU nanofibers using ultrasonic energy

9.4 Results and discussions

9.4.1 Optimization of dyeing temperature

To optimize the dyeing temperature, PU nanofiber mats were dyed with sonication using 1% dye concentration and one hour dyeing process time. The results given in Figure 9.1 demonstrated K/S values increasing with increasing temperature such that higher K/S values were obtained at 70 ^{0}C for both dyes. At this temperature K/S values for CIB and CIR were 2.7 and 6.9 respectively. The higher K/S values by CIR dye may be attributed to its high energy level [4]. These findings are in agreement with our previous research results. Glass transition temperature of a polymer has important role in deciding dyeing temperature in exhaust dyeing method. Tg of PU used in the research was 90^{0}C. Generally, dyeing of PU is carried out from 90-100^{0}C. Our research results show insignificant improvement in the dye uptake over 70^{0}C, thus, it was taken as optimum dyeing temperature and used for further experimentations. This optimized temperature is lower than Tg of PU used in this research. This optimum dyeing temperature lower than Tg of PU may be due to ultrasonic energy. The ultrasonic energy improves dye diffusion from dye liquor to PU nanofibers, swells the PU polymer chains allowing higher dye uptake at temperature lower than its Tg.

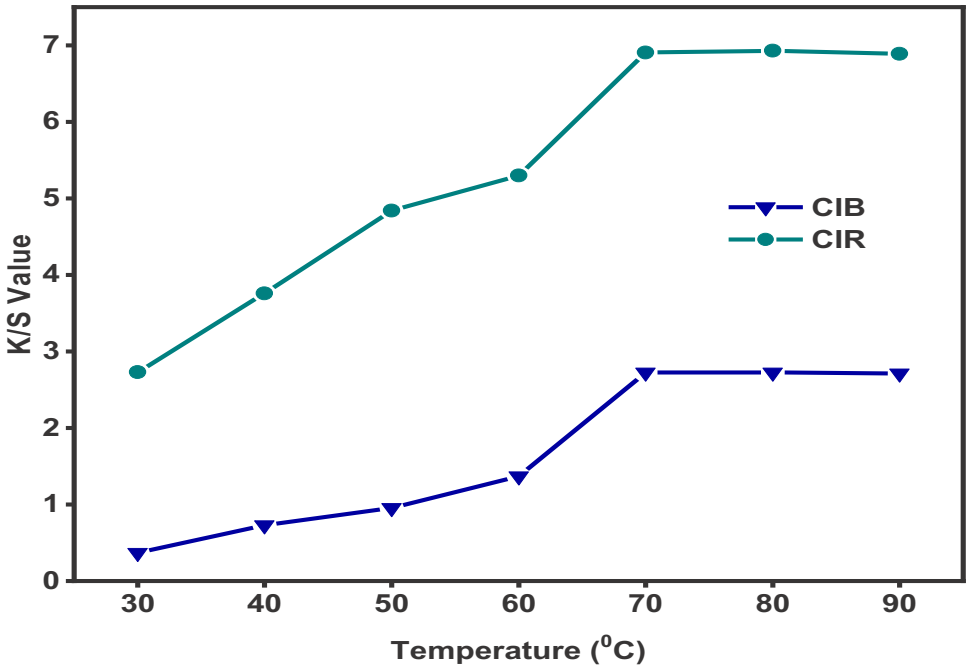

Figure 9.1 Optimization of dyeing temperature for ultrasonic dyeing of PU nanofibers

9.4.2 Optimization of dyeing time

Using the optimized temperature (70^0C) and 1% dye solution, the research was further extended to optimize the time for ultrasonic assisted dyeing. The results shown in Figure 9.2 reveal K/S values increasing with the dyeing time such that higher K/S values were achieved in 40 minutes. For dyeing time of 40 minutes, the K/S values of the samples dyed with CIB and CIR were 2.0 and 6.8 respectively. Proceeding the dyeing time over 40 minutes did not show significant improvement in color build-up of the PU nanofiber. Thus it was decided as optimum dyeing time for ultrasonic dyeing of PU nanofibers. Exhaust dyeing processes of PU are generally carried out at 100 ^{0}C for about one hour. The decrease in dyeing process time from one hour to 40 minutes may once again be due to the effect of sonication. The ultrasonic energy renders higher dye exhaustion and improves diffusion of disperse dyes inside the PU polymer chains by swelling its soft segment.

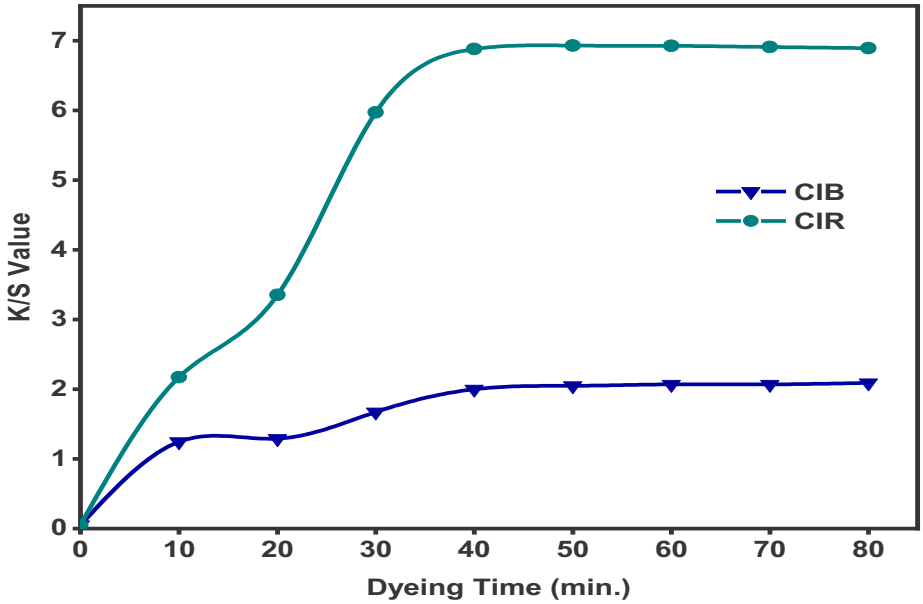

Figure 9.2 Optimization of dyeing time for ultrasonic dyeing of PU nanofibers

9.4.3 Effect of dye concentrations

The results for the effect of dye concentrations on color build-up properties of PU nanofibers are reported in Figure 9.3. The results exhibited increase of K/S values with enhancing dye concentration in the solution. The higher dye concentration means more number of dye molecules available in the dye liquor which in turn ensure increased dye transfer from the dye liquor to nanofiber surface. Furthermore, ultrasonic cavitations break-up the dye aggregates and further promote diffusion of dye molecules. Increase in the K/S values were more pronounced for CIR than CIB which may be attributed to CI Disperse Red 167:1 being high energy level dye. For 6% dye concentration, highest K/S values obtained with CIB and CIR were 9.53 and 16.55 respectively.

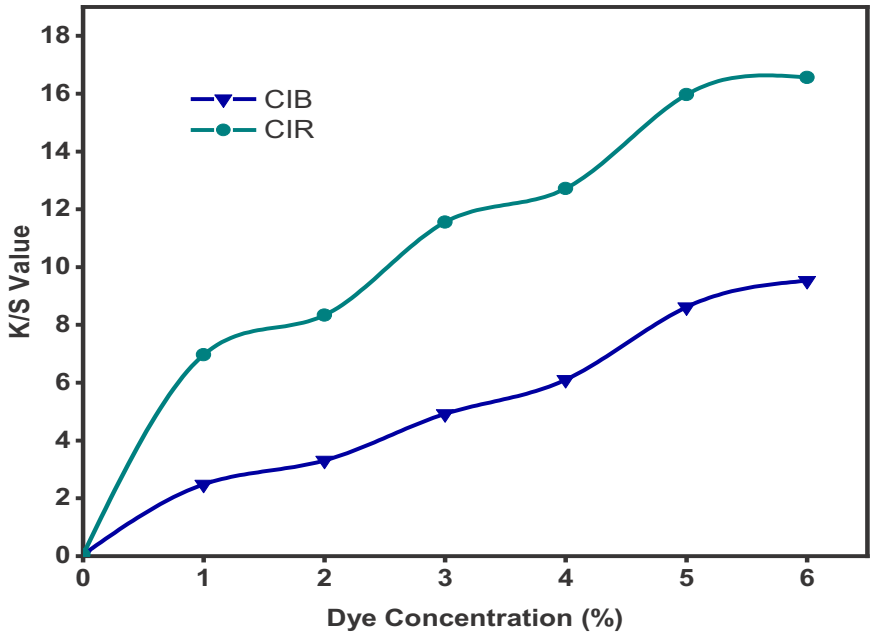

Figure 9.3 Effect of dye concentrations on color build-up of PU nanofibers

9.4.4 Dye fixation

Dye fixation (%F) is a measure of proportion of the dye molecules fixed on a substrate's dye sites to the dye molecules adsorbed on the substrate. It provides an estimate of economic viability of the process and better user satisfaction. The %F of the two disperse dyes were calculated at varying dye concentrations and results are reported in Figure 9.4. It is evident from the results that dye fixation percentages decreased with increasing dye concentration of disperse dyes. For example for 1% dye concentration, %F value for CIB and CIR were 83.48% and 85.18% respectively. However for 6% dye concentration dye fixation (%) values were 73.35% and 75.34% for CIB and CIR respectively. These results are in agreement with our previous findings. It is further observed that the CIR has higher dye fixation than the CIB. Lower dye fixation at higher dye concentrations illustrates higher diffusion of disperse dye molecules from dye liquor to fiber surfaces while only a certain proportion is diffused into the dye sites. The remaining disperse dye molecules were washed away during washing-off processes.

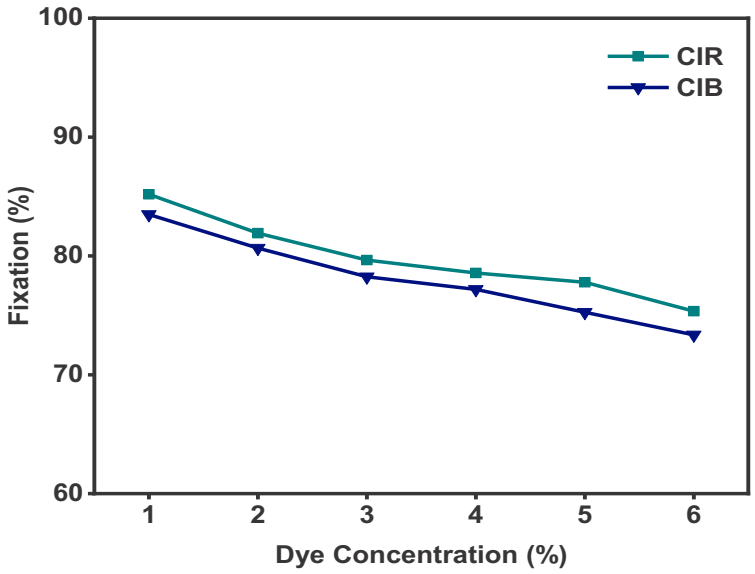

Figure 9.4 Effect of dye concentrations on dye fixation (%) of CIB and CIR

9.4.5 Colorfastness properties

Color fastness of the CIB and CIR samples against light, washing and hot pressing were conducted to observe color bleeding resistance against each stimulus. As shown in Table 9.1 both the CIB and CIR were rated 8 for light fastness which demonstrated their excellent light fastness properties. The washing fastness results reveal very good color bleeding resistance (shade change) and good to very good resistance to staining on the multi-fibers. Both the CIB and CIR were given 4/5 rating for shade change. The hot pressing fastness test results exhibit good (staining: 3/4 for CIB and 4 for CIR) to very good (shade change: 4/5 for both CIB and CIR) color bleeding resistance of the dyed nanofibers against heat.

Table 9.1 Color fastness to light, washing and hot pressing of CIB and CIR nanofiber samples

Sample	Light Fastness	Washing Fastness							Hot pressing Fastness	
		Shade Change	Staining on Multifibers[1]						Shade Change	Staining
			CT	COT	PA	PE	PAC	W		
CIB	8	4/5	4/5	4/5	4	3/4	3/4	4	4/5	3/4
CIR	8	4/5	4/5	4/5	4	4	3/4	4/5	4/5	4

[1]CT: cellulose triacetate; COT: cotton; PA: polyamide; PE: polyester; PAC: polyacrylic; W: wool.

9.4.6 Morphologies of PU nanofibers

The scanning electron microscopy images of control (undyed and without ultrasonic treatment), CIB, CIR and Blank US (sonicated without dye at optimum conditions) depicted in Figure 9.5 demonstrate

regular and smooth nanofiber structure without beads. The sonication does not produce any significant effect on the morphology of the nanofibers except for a little increase in their diameters which may be the result of ultrasonic cavitations. The average diameter of the control sample was 340nm while that of sonicated samples was calculated to be about 430nm. Furthermore, the diameters of CIB, CIR and blank US samples were approximately same which suggests that the increase in diameter was solely due to the effect of sonication. For physical observations photographic images of the control, CIB and CIR samples are given in Figure 9.6.

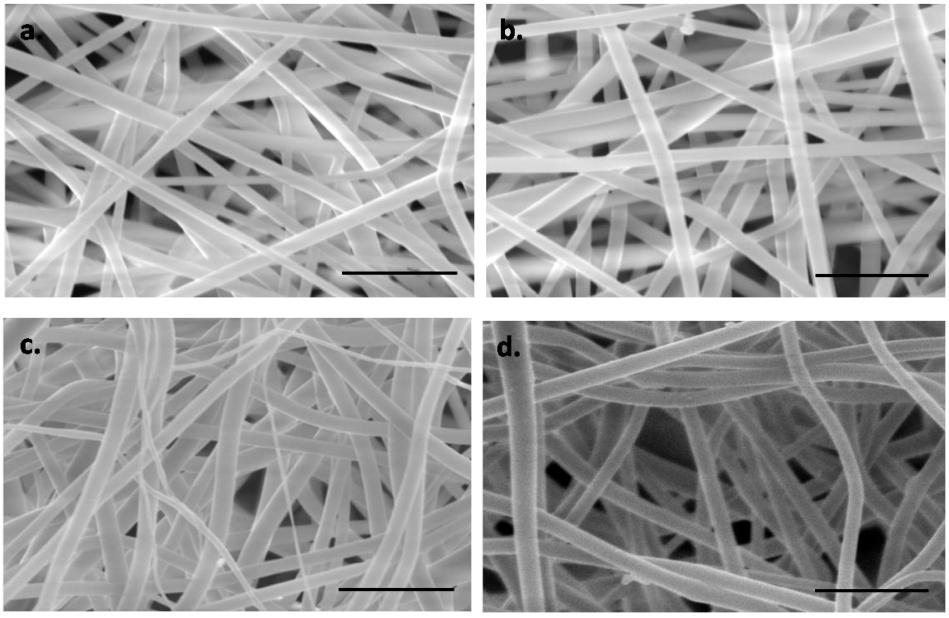

Figure 9.5 Scanning electron microscopy (SEM) images of PU nanofibers (a) control (b) CIB (c) CIR (d) Blank US (scale bar 3µm)

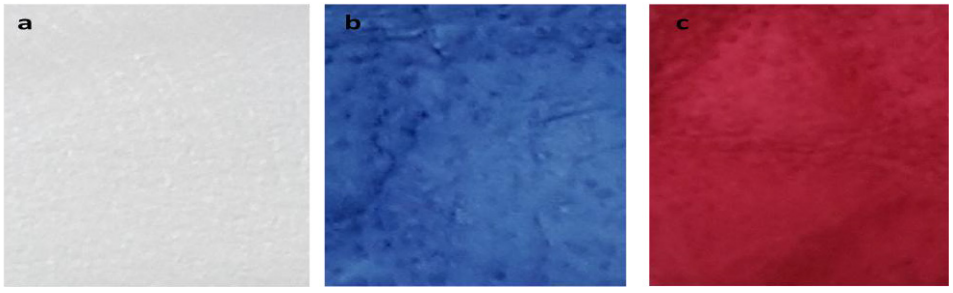

Figure 9.6 Photographic images of (a) control (b) CIB (c) CIR

9.4.7 FTIR results

It is evident from the FTIR spectrum given in Figure 9.7 that neither sonication nor the dyeing process has any effect on inter and/or intra molecular chemical bonding in PU nanofibers. The dominant polyurethane peaks [19] can be clearly seen in FTIR spectrum of all the samples. Such as a

peaks at 1715 cm^{-1} assigned to stretching vibrations of C=O, 1600 cm^{-1} to stretching vibrations of N-H groups, 1510 cm^{-1} to bending vibrations of amide II, 1214 cm^{-1} to O-C stretching vibrations, 1160 cm^{-1} to C-O-C stretching vibrations and 2925 $cm^{-1}$to C-H stretching vibrations. Due to very small proportion of the dye into the nanofibers, characteristics peaks of the dyes were not be observed in the FTIR spectrum.

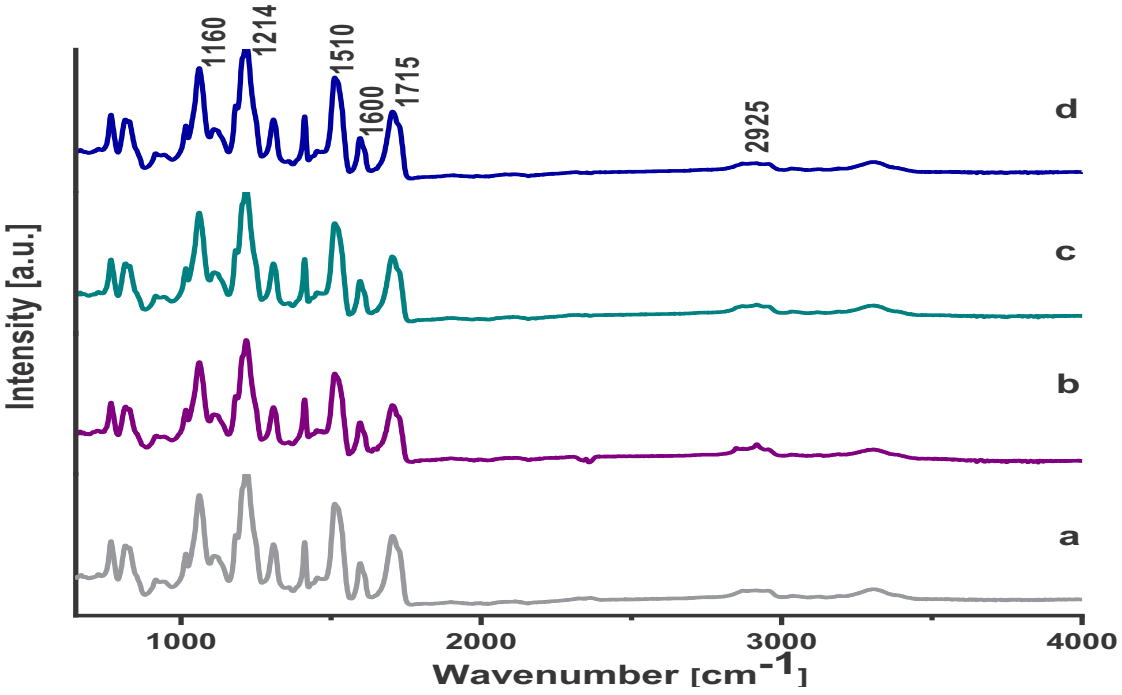

Figure 9.7 FTIR spectrum of PU nanofibers (a) control (b) CIB (c) CIR (d) Blank US

9.4.8 XRD patterns of PU nanofibers

X-ray diffraction studies were conducted to investigate effect of ultrasonic dyeing on the crystallographic structure of PU nanofibers. The results reported in Figure 9.8 demonstrate that ultrasonic dyeing does not alter crystallographic structure of the PU nanofibers. All the samples depicted diffraction angles (2θ) of the amorphous polyurethane at 20.14^0 [20].

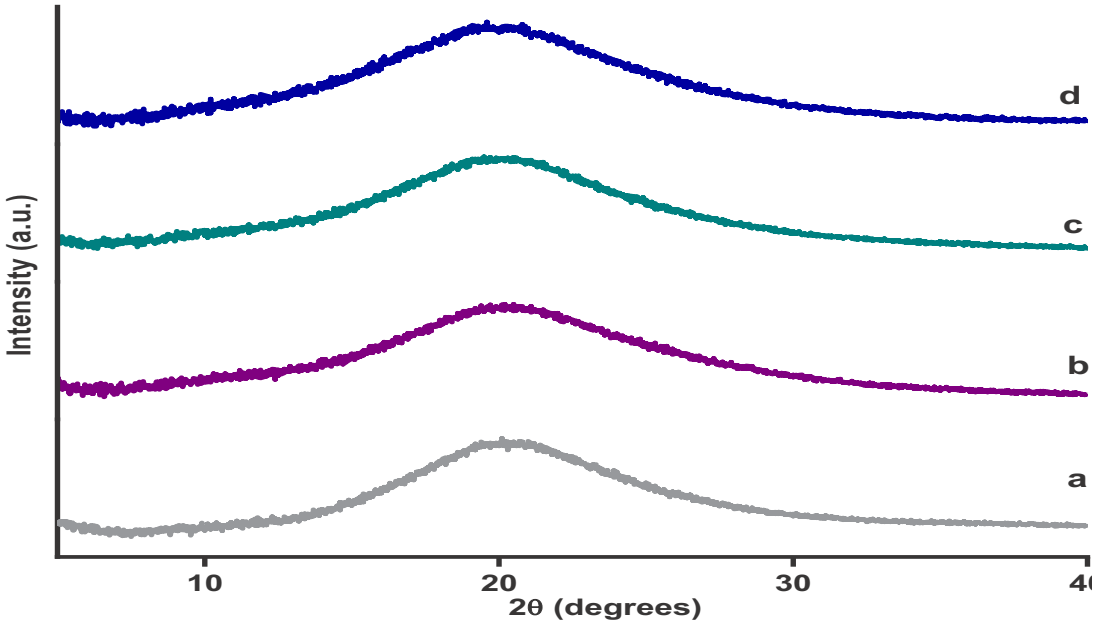

Figure 9.8 XRD patterns of the PU nanofibers (a) control (b) CIB (c) CIR (d) Blank US

9.4.9 Mechanical properties of the nanofibers

In addition to satisfying higher color build-up, it is important that textile structures should possess sufficient mechanical strength so that it can withstand the forces during use. Thus, tensile strength (MPa) of the PU samples was measured following standard test method ASTM D-638 and results are given in Figure 9.9. It is evident that tensile strength of the nanofiber mats was substantially improved after ultrasonic dyeing. The tensile strength of the samples increased from 2.8MPa for control sample to 4.29MPa for the ultrasonically dyed samples. The increase in tensile strength may be due to ultrasonic cavitations which imparts stiffness [21] to the samples resulting in increase of its strength. By comparing the tensile strength results of CIB and CIR with blank US samples, it is evident that the dyes are not responsible for increase in the strength rather it is the sonication which improves tensile strength of PU nanofibers.

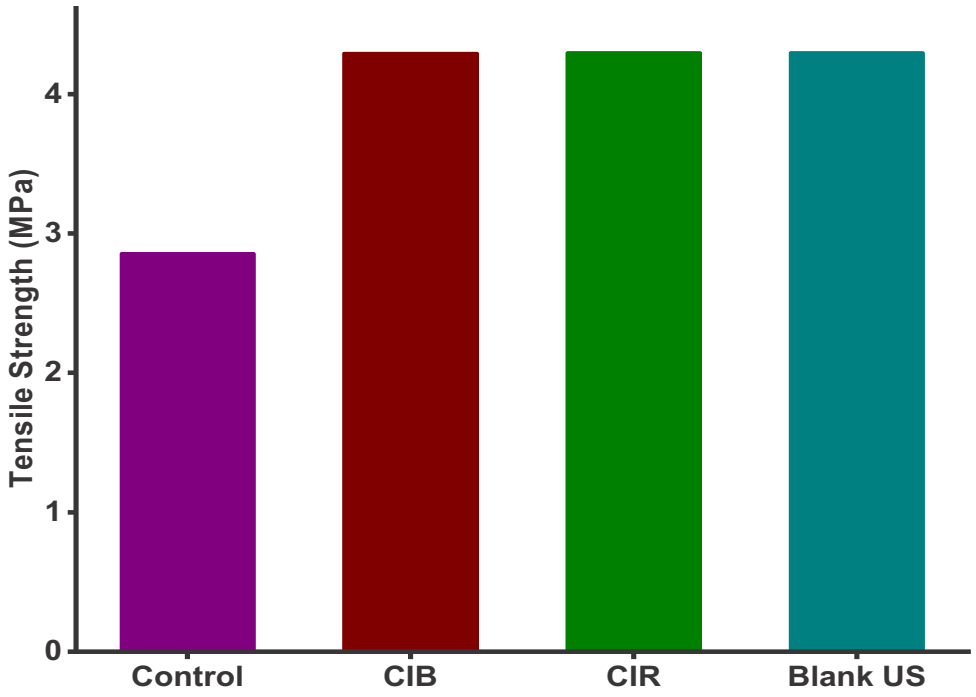

Figure 9.9 Tensile strength (MPa) of the control, CIB, CIR and Blank US nanofiber samples

9.5 Conclusions

Exhaust dyeing of PU nanofibers with disperse dyes using sonication for higher color build-up has been successfully completed. Ultrasonic cavitations increase diffusion of the dye molecules from dye liquor to the PU nanofiber surface and increases mobility of disperse dye molecules into the polymer chains by swelling its soft segment yielding higher K/S values. Based on the obtained higher K/S values (color build-up), 70^0C and 40 minutes were observed as optimum dyeing conditions for ultrasonic dyeing of PU nanofibers. The PU nanofibers were successfully dyed at temperature lower than its glass transition temperature (Tg) and in lesser time. SEM, FTIR and XRD results show that ultrasonic assisted dyeing does not significantly affect morphology and structures of PU nanofibers. Excellent light fastness and good to very good washing fastness results were obtained from the color fastness tests of ultrasonically dyed PU nanofibers. Furthermore, ultrasonic dyeing is observed to improve tensile strength of PU nanofibers.

References

[1] H. Zhuo, J. Hu, S. Chen, L. Yeung, Preparation of polyurethane nanofibers by electrospinning, Journal of Applied Polymer Science 109(1) (2008) 406-411.

[2] H.J. Yoo, S.S. Mahapatra, J.W. Cho, High-speed actuation and mechanical properties of graphene-incorporated shape memory polyurethane nanofibers, The Journal of Physical Chemistry C 118(19) (2014) 10408-10415.

[3] D. Randall, S. Lee, The Polyurethane Book, 2000, Ed., John Wilely & Sons Press.
[4] A. Khatri, S. Ali, A.K. Jhatial, S.H. Kim, Dyeability of polyurethane nanofibres with disperse dyes, Coloration Technology 131(5) (2015) 374-378.
[5] D. Fantini, L. Costa, Dye, fluorophores and pigment coloration of nanofibers produced by electrospinning, Polymers for Advanced Technologies 20(2) (2009) 111-121.
[6] Z. Khatri, R.A. Arain, A.W. Jatoi, G. Mayakrishnan, K. Wei, I.-S. Kim, Dyeing and characterization of cellulose nanofibers to improve color yields by dual padding method, Cellulose 20(3) (2013) 1469-1476.
[7] A. Almasian, G. Chizari Fard, M. Parvinzadeh Gashti, M. Mirjalili, Z. Mokhtari Shourijeh, Surface modification of electrospun PAN nanofibers by amine compounds for adsorption of anionic dyes, Desalination and Water Treatment 57(22) (2016) 10333-10348.
[8] M. Park, M.M. Rabbani, H.K. Shin, S.-J. Park, H.Y. Kim, Dyeing of electrospun nylon 6 nanofibers with reactive dyes using electron beam irradiation, Journal of Industrial and Engineering Chemistry 39 (2016) 16-20.
[9] M. Khatri, F. Ahmed, A.W. Jatoi, R.B. Mahar, Z. Khatri, I.S. Kim, Ultrasonic dyeing of cellulose nanofibers, Ultrasonics sonochemistry 31 (2016) 350-354.
[10] H. Jiang, L. Zhang, J. Cai, J. Ren, Z. Cui, W. Chen, Quinoidal bithiophene as disperse dye: Substituent effect on dyeing performance, Dyes and Pigments (2018).
[11] S.M. Burkinshaw, G. Salihu, The role of auxiliaries in the immersion dyeing of textile fibres: Part 11 residual inorganic electrolyte levels present during the wash-off of commercial grade reactive dyes, Dyes and Pigments (2017).
[12] K. Wojciechowski, Halochromic effects of azophthalimide dyes and their prediction by PPP method, Dyes and Pigments 32(4) (1996) 199-208.
[13] T.-K. Chen, Y.-I. Tien, K.-H. Wei, Synthesis and characterization of novel segmented polyurethane/clay nanocomposites, Polymer 41(4) (2000) 1345-1353.
[14] A.R. Horrocks, S.C. Anand, Handbook of technical textiles, Elsevier2000.
[15] J. Shore, Cellulosics dyeing, Society of Dyers and Colourists1995.
[16] S. Lee, B. Kim, High solid and high stability waterborne polyurethanes via ionic groups in soft segments and chain termini, Journal of colloid and interface science 336(1) (2009) 208-214.
[17] H.H. Wang, K.V. Chen, A novel synthesis of reactive nano-clay polyurethane and its physical and dyeing properties, Journal of Applied Polymer Science 105(3) (2007) 1581-1590.
[18] S.L. D Randall, The polyurethane book, (2002).

[19] A.R. Unnithan, G. Gnanasekaran, Y. Sathishkumar, Y.S. Lee, C.S. Kim, Electrospun antibacterial polyurethane–cellulose acetate–zein composite mats for wound dressing, Carbohydrate polymers 102 (2014) 884-892.
[20] R. Nirmala, D. Kalpana, R. Navamathavan, Y.S. Lee, H.Y. Kim, Preparation and characterizations of silver incorporated polyurethane composite nanofibers via electrospinning for biomedical applications, Journal of nanoscience and nanotechnology 13(7) (2013) 4686-4693.
[21] A.W. Jatoi, F. Ahmed, M. Khatri, A. Tanwari, Z. Khatri, H. Lee, I.S. Kim, Ultrasonic-assisted dyeing of Nylon-6 nanofibers, Ultrasonics sonochemistry 39 (2017) 34-38.

CHAPTER 10

Ultrasonic Dyeing of Polyacrylonitrile (PAN) Nanofibers

10.1 Introduction

This chapter reports ultrasonic dyeing of polyacrylonitrile (PAN) nanofibers. A systematic study on dyeability of PAN nanofibers will extend its use in textile apparel industry. Dyeing process parameters such as dyeing time, temperatures and concentrations of dyes have been optimized. Comparison of ultrasonic dyeing and conventional dyeing methods of PAN nanofibers have also been given. Effects of ultrasonic dyeing on the morphology, chemical state, crystallographic structure and mechanical strength of PAN nanofibers have been discussed.

10.2 Research backgrounds

Polyacrylonitrile (PAN) is an important polymer used in numerous applications due to its superior properties. The PAN posses better processing ability, chemical stability, flame resistance and resistance to oxidative degradation, sunlight and weather. These properties along with better mechanical characteristics, good thermal and chemical stability endow PAN applications in clothing textiles, sportswear, knitted garments, blankets, rugs, upholstery, awnings, socks, sweaters and children garments.

Electrospinning of PAN into nanofiber webs reduces fiber diameters to several hundred nanometers and the webs posses all the properties inherent to nanofiber structures. PAN nanofibers have so far been successfully used in air filtration [1], as carbon fiber precursor [2], heavy metal removal from contaminated water [3], antimicrobial applications, batteries, electrical energy storage and in supercapacitors [4].

Although dyeability of several nanofibers has been reported, however, to the best of our knowledge dyeability of PAN nanofibers has not yet been reported. Coloration of polyacrylonitrile or acrylics in general is difficult because of its compact structure. The acrylics are generally dyed with basic dyes and the dyeing process is carried out at boiling temperature which is completed in about two hours. The nanofiberous structure of PAN nanofibers further make it difficult to produce colored PAN nanofibers because nanofibers scatter higher proportion of light from their surface.

Thus we carried out our study on coloration of PAN nanofibers with disperse dyes using ultrasonic energy to promote dyeability of PAN nanofibers and achieve higher color up-take.

The dyeing procedure was carried out at mildly acidic conditions. Dyeing process parameters such as coloration temperature, coloration time, concentrations of dyes were optimized. The dyeing

completed in one hour and at 80^{0}C. A comparison of ultrasonic dyeing with conventional (without sonication) dyeing of PAN nanofibers has also been reported.

10.3 Fabrication and dyeing of PAN nanofibers

PAN nanofibers were fabricated using DMF as solvent. Typically, 10% (wt.%) of PAN was dissolved in DMF and stirred continuously for 24 hours using magnetic stirrer. Electrospinning was carried out as reported in experimental section except that electric voltage and TCD used were 15kV and 15cm.

The PAN nanofibers were dyed in an ultrasonic bath using disperse dyes following exhaust dyeing method. The two dyes used for PAN dyeing were CI Disperse Blue 56 (CIB) and CI Disperse Red 167:1 (CIR). Dyeing temperature and dyeing time were first optimized. For optimization of dyeing temperature, PAN nanofiber samples, were dyed at 30^{0}C, 40^{0}C, 50^{0}C, 60^{0}C, 70^{0}C, 80^{0}C, 90^{0}C for 1hour using 1% (w/v) solution of each dye. In the second step dyeing experiments were performed for 20min., 30min, 40min., 50min., 60min., 70min. and 80min., using optimized temperature and 1% dye solution. The research was further extended to investigate affect of dye concentrations (1%, 2%, 3%, 4%, 5% and 6%) on coloration of PAN nanofibers. All the ultrasonic dyeing experiments were performed in an ultrasonic bath with 60Hz frequency, 55 watts and input energy of 0.302 W/cm^2. A 1:100 fiber to liquor ratio was used in the dyeing experiments. The dyeing experiments were conducted using test tubes containing dye solutions and the samples with a fixed fiber to liquor ration. The test tubes were placed in the ultrasonic bath using a stand such that bottom of the tubes was 1.5 cm above the bottom surface of the ultrasonic equipment. After the dyeing process, the samples were washed with DI water until no color bleeding was observed. For comparison of ultrasonic energy supported (US) dyeing and conventional dyeing (without sonication), 1% and 4% dye concentrations were selected. For comparisons, the dyeing procedure was carried out for 1hour at 80^{0}C. The washing-off process was performed using warm water (50^{0}C), hot water (80^{0}C) and normal water (25^{0}C) respectively. Chemical structures of the dyes used and polyacrylonitrile polymer are depicted in Figure 10.1. The PAN nanofiber samples dyed with CIB are denoted as USB and those dyed with CIR are represented as USR.

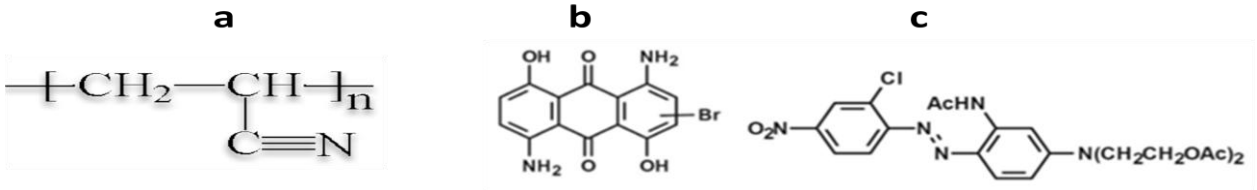

Figure 10.1 Chemical structures of (a) PAN (b) CI Disperse Blue 56 dye and (c) CI Disperse Red 167:1

10.4 Results and discussions

10.4.1 Optimization of dyeing temperature

Effect of dyeing temperature on ultrasonic assisted dyeing of PAN nanofibers has been reported in Figure 10.2. The results show a linear relationship between dyeing temperature and K/S values until maximum K/S values are achieved at 80^0C. Both the disperse dyes exhibit similar relationship with temperature, however, the CIR show comparatively higher color build-up (K/S values) on the PAN nanofibers. For both dyes, the maximum K/S values were obtained at 80^0C. At this temperature, the K/S values obtained for CIB and CIR were 0.142 and 0.196 respectively. Further extending the temperature could not show any improvement in the K/S values. Thus 80^0C was taken as optimal dyeing temperature for ultrasonic dyeing of PAN nanofibers. The CIB is a low energy level disperse dye while CIR belongs to high energy level disperse dyes. The effect of higher K/S values by USR samples may be attributed to its high energy level. Other reason for higher K/S values by the CIR may be due to chemical structure of the two dyes. The CIB dye molecules are comparatively more linear than the CIR dye molecules. During dyeing process, due to the affect of ultrasonic cavitations and high temperature, the PAN polymer chains open-up to allow more space for the dye molecules to penetrate. However, during washing-off processes the CIB dye molecules are more prone to bleed thus producing comparatively lower final K/S values.

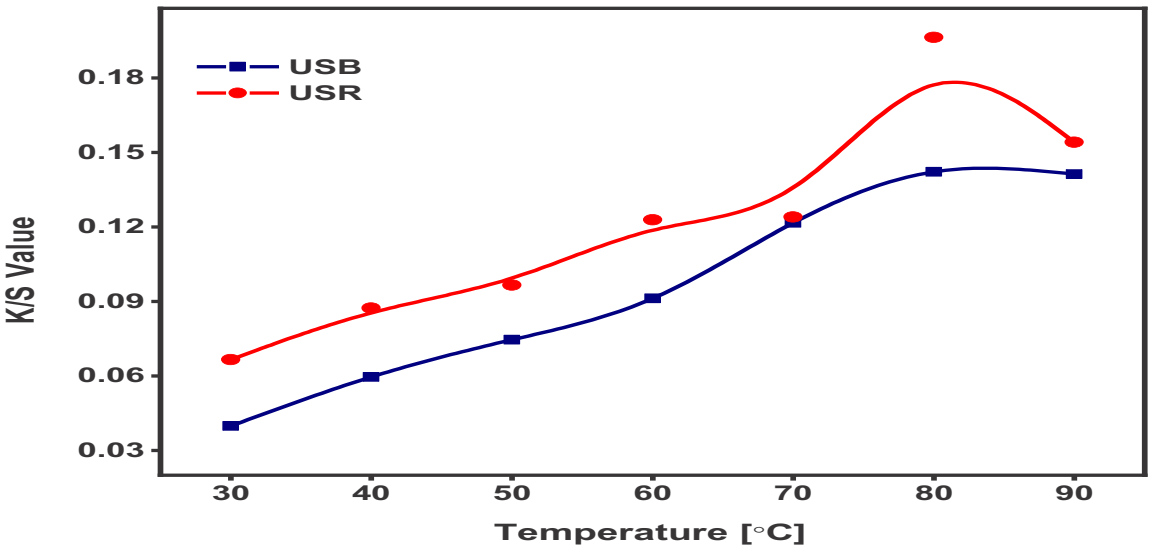

Figure 10.2 Effect of dyeing temperature on color build-up (K/S values) of PAN nanofibers

10.4.2 Optimization of dyeing time

In the next step for ultrasonic dyeing of PAN nanofibers, the research was extended to study influence of dyeing process time on color build-up of PAN nanofibers. The results shown in Figure

10.3 demonstrated higher K/S values in 60minutes; 0.14216 and 0.2056 for USB and USR respectively. Thus 1hour dyeing time was decided as optimum time for ultrasonic dyeing of PAN nanofibers using the disperse dyes. The USR samples exhibited similar trend producing higher color build-up in comparison to USB samples. The effect may once again be due to the chemical structure of the dyes and the CR being high energy level dye.

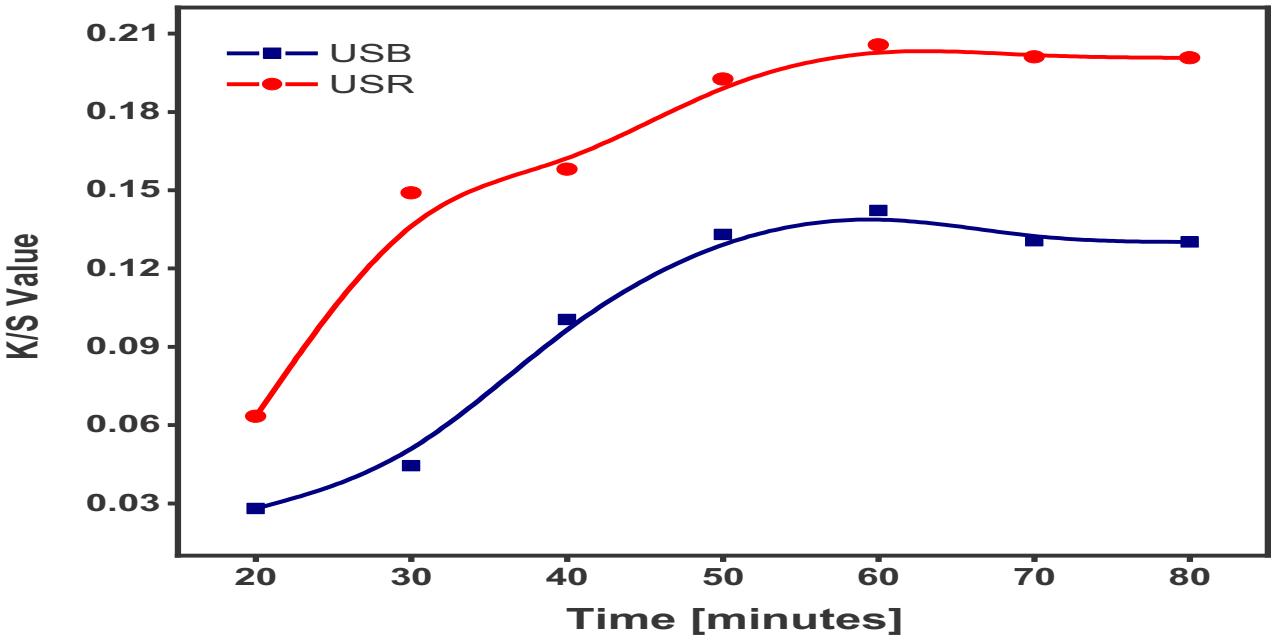

Figure 10.3 Effect of dyeing time on K/S values of PAN nanofibers

10.4.3 Optimization of dye concentrations

Using the optimized dyeing temperature and time in the previous sections, dyeing of PAN nanofibers was carried out using different dye concentrations and results are reported in Figure 8.4. The results demonstrate increase in K/S values with increasing dye concentrations. For example, for 1% dye concentration, the K/S values of USB and USR were 0.142 and 0.2056 respectively which increased to 0.302 and 0.51 respectively for 6% dye concentrations. The USB and USR samples exhibited similar trend such that the USR produce higher K/S values.

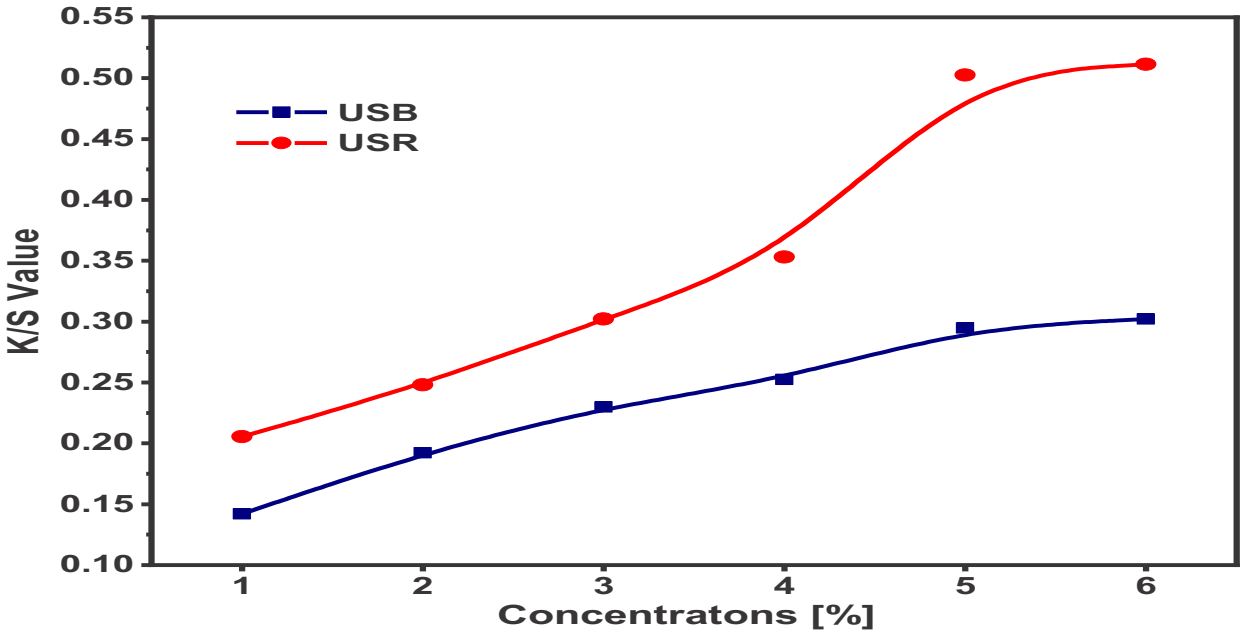

Figure 10.4 Effect of dye concentrations on K/S values of PAN nanofibers

10.4.4 Dye fixation (%F)

Fixation of the CIB and CIR dyes on PAN nanofibers (%F) were calculated using the previously described equation 9 (section 2.13.2). The results given in Figure 10.5 show comparative dye fixation of CIB and CIR dyes on PAN nanofibers; USB and USR respectively. It can be observed that percentile fixation of both the dyes on PAN nanofibers decreased with increasing concentration of the dyes in the solution. The USR samples show moderately higher dye fixation than the USB samples. For PAN nanofiber samples with 1% dye concentration, the %F values were 82.65% and 82.9% on USB and USR respectively which reduced to 76.7% and 74.13% respectively in the samples dyed using 5% dye concentration. It is a common experience in coloration procedures that the dye fixation (%) reduces with increasing concentration of dyes. Furthermore, the CIR exhibited comparatively higher dye fixation than the CIB dyes which demonstrated its lower color bleeding effect. This effect may be due to the chemical structure of the dyes. The CIB dye molecule is comparatively more linear than the CIR dye molecule. Due to combined effect of ultrasonic cavitations and temperature during dyeing process, the PAN polymer chains open and create more space for diffusion of the dye molecules. It is expected that during washing-off process the more linear CIB dye molecule may more easily be washed-off in comparison to the comparatively less linear CIR dye molecules which may be trapped after the PAN nanofibers are relaxed (after dyeing).

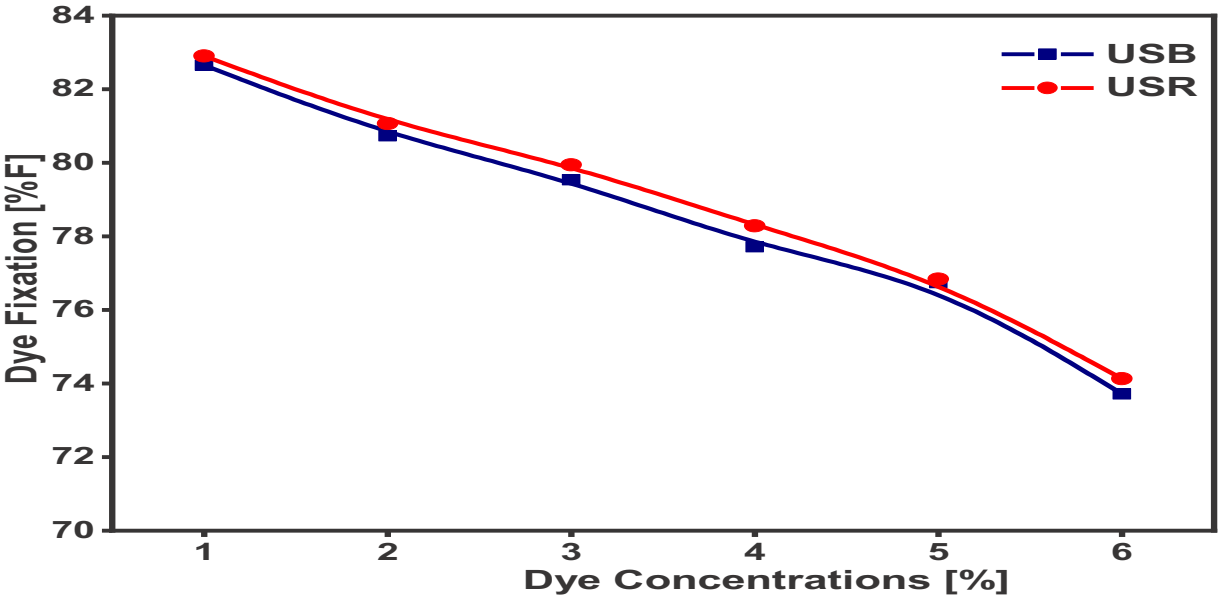

Figure 10.5 Dye fixations (%F) of the dyes on PAN nanofibers at different dye concentrations

10.4.5 Comparison of US and conventional dyeing methods

The results given in Figure 10.6 present a comparison of US dyeing and conventional dyeing of PAN nanofibers using 1% and 4% concentrations of the two dyes. The results are reported as percentile increase in K/S values when using US dyeing method. In US dyeing method, the ultrasonic cavitations break the dye aggregation, enhance dye exhaustion and improve dye diffusion on and inside the nanofiber structure. At the sufficiently higher temperature, the ultrasonic energy opens the PAN polymer chains, creating more space thus making it easier for the direct dye molecules to penetrate. Thus may produce higher color build-up on the PAN nanofibers. As shown, the results demonstrated 48.37% and 55.09% increase in K/S values with US dyeing for 1% and 4% dye concentrations respectively using CIB dye. While an increase of 51.2% (1% dye concentration) and 66.33% (4% dye concentrations) in K/S values was observed with CIR dyes. In the conventional dyeing method only the temperature mobilizes the dye molecules and opens the polymer chains (keeping the other factors constant) while in the US dyeing method ultrasonic cavitations in the bulk media and transient cavitations near the substrate yield improvements in color build-up on PAN nanofibers.

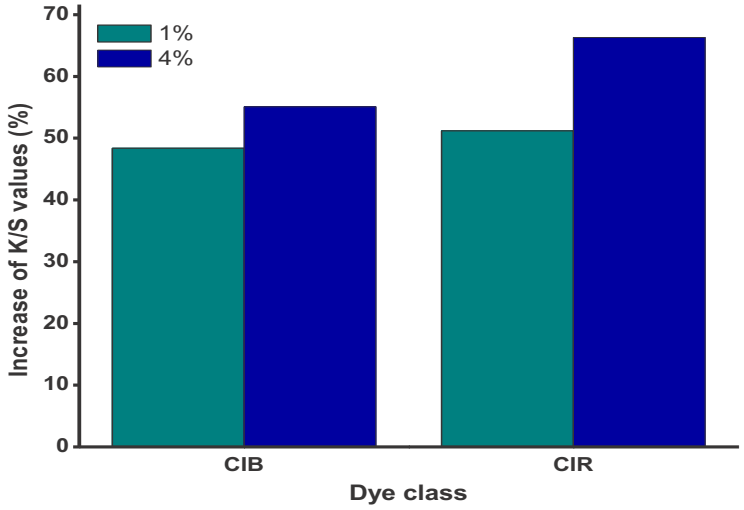

Figure 10.6 Comparison of ultrasonic dyeing method with conventional dyeing method

10.4.6 Colorfastness test results

Color fastness tests provide insight into potential of a colored textile to resist color bleeding/deterioration when exposed to the respective agents/stimuli. For apparel and surgical clothing applications it is more common practice to conduct washing fastness, light fastness and hot pressing fastness test of the dyed goods in order to determine color bleeding resistance of a dyed product against washing, light and heat respectively. From the results given in Table 10.1, it is evident that the PAN nanofibers dyed with CIB and CIR dyes posses excellent, very good and good color fastness to washing, light and hot pressing respectively. These color fastness test results demonstrated sufficiently higher color bleeding resistance which confirms suitability of the PAN nanofibers dyed with disperse dyes in clothing applications.

Table 10.1 Color fastness test results of USB and USR nanofiber samples

Sample	Light Fastness	Washing Fastness							Hot pressing Fastness	
		Shade change	Staining on Multifibers[1]							
			CT	CTN	PM	PS	PA	WL	Shade Change	Staining
USB	8	4/5	4/5	5	4	4	3/4	4/5	4/5	3/4
USR	8	4/5	5	5	4/5	4/5	4/5	5	4/5	4

[1]CT: cellulose triacetate; CTN: cotton; PM: polyamide; PS: polyester; PA: polyacrylic; WL: wool.

10.4.7 Morphologies of PAN nanofibers

Effect of ultrasonic dyeing on morphology of the PAN nanofibers was studied by SEM analysis and the results are given in Figure 10.7. The PAN nanofibers with regular and smooth morphology can be seen in Figure 10.7a. Comparing the undyed sample (UD) with USB and USR it is clear that sonication has no significant affect on the morphology of PAN nanofibers except a moderate increase in their diameters. Average diameters of the UD nanofiber samples were calculated to be 282nm which increased to 317nm and 318nm in USB and USR samples which suggests some residual strain in the nanofibers after completions of the US dyeing. This effect may be due to ultrasonic cavitations. The observed effect of ultrasonic dyeing on the PAN nanofibers is in agreement with our previous findings.

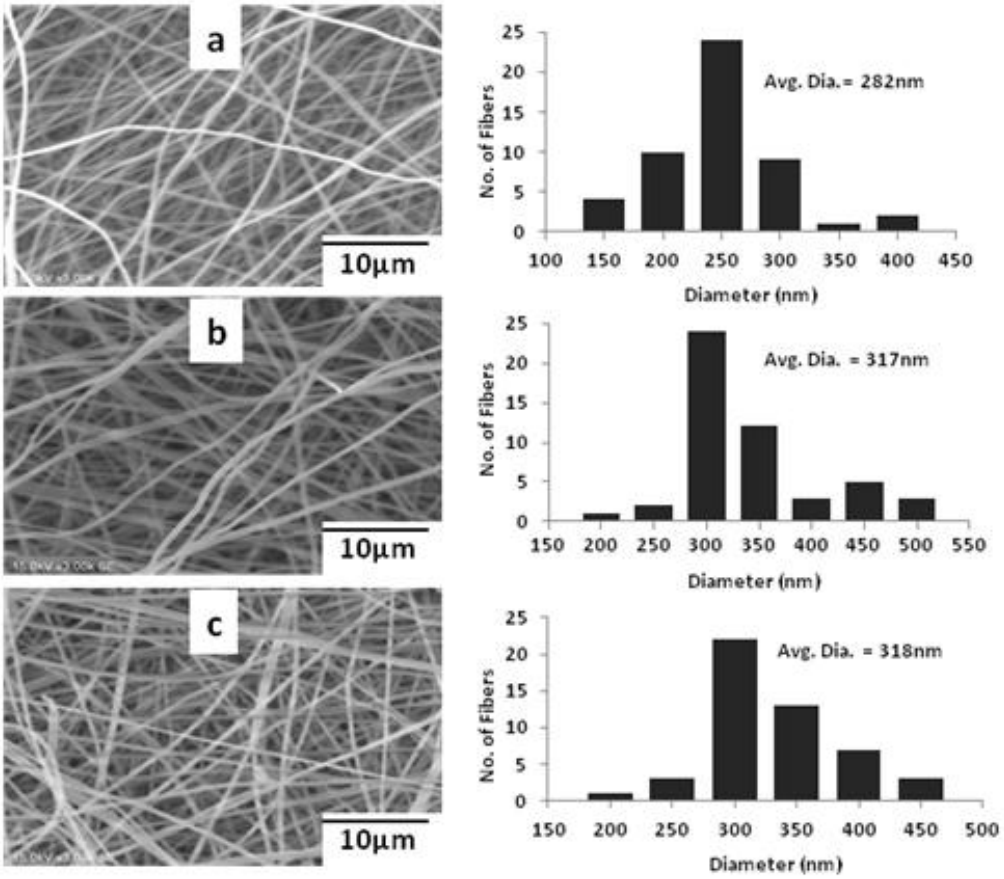

Figure 10.7 SEM images and average diameter distribution of PAN nanofibers (a) UD (b) USB (c) USR

10.4.8 FTIR analysis of PAN nanofibers

Influence of ultrasonic dyeing on chemical structure of PAN nanofibers was studied by FTIR analysis and the results are given in Figure 10.8. All the samples show characteristic peak of nitrile (C≡N) group at 2245 cm^{-1}. The peak at 1450 cm^{-1} is assigned to CH_2 deformations and at 2930 cm^{-1} to CH_2 stretching vibrations [5-6]. The results didn't show any new peak or any peak shift in the FTIR

spectrum of USB and USR when compared to UD sample which illustrates that ultrasonic dyeing of PAN nanofibers does not affect on its chemical structure or intermolecular interactions.

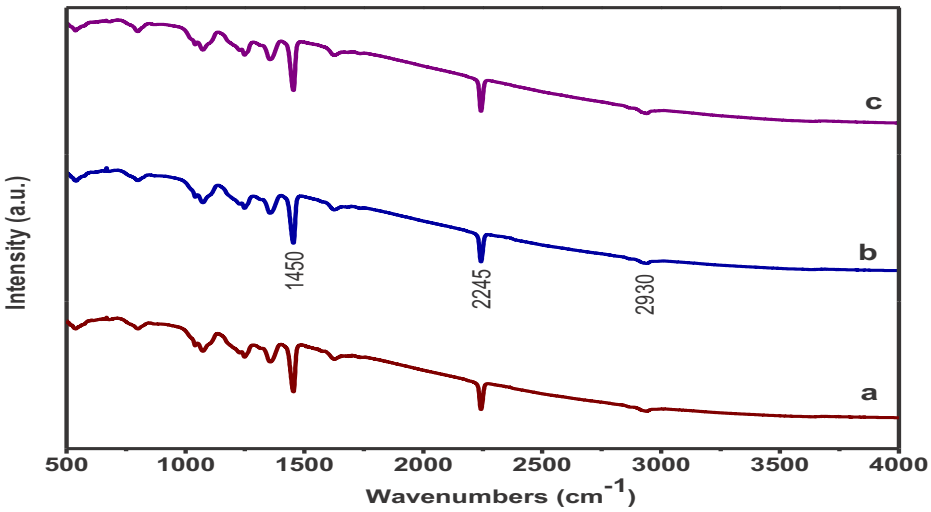

Figure 10.8 FTIR spectrum of PAN nanofibers (a) UD (b) USB (c) USR

10.4.9 X-ray diffraction analysis of PAN nanofibers

The XRD spectrum of the UD, USB and USR is presented in Figure 10.9. The PAN shows a strong diffraction angle (2θ) at 16.9^0 which correspond to 5.3Å d-spacing and a weak diffraction angle 2θ at 29.73^0 for 3.03Å d-spacing. The diffraction angle 2θ at 16.9^0 represents (10$\bar{1}$0) reflections while 29.73^0 diffraction angle (2θ) is from (1120) reflections [7]. XRD patterns of all the samples show both the diffraction angles and without any alteration in crystallographic structures.

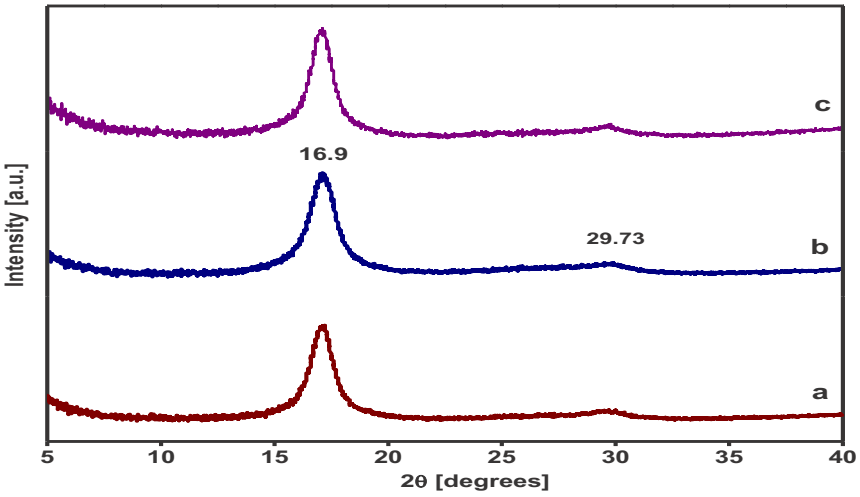

Figure 10.9 XRD results of PAN nanofibers (a) UD (b) USB (c) USR

10.4.10 Mechanical strength of PAN nanofibers

Tensile strength (MPa) results of UD and ultrasonically dyed PAN nanofibers (USB and USR) are reported in Figure 10.10. The results show ultrasonic dyeing process increase the tensile strength of PAN nanofibers. Tensile strength of UD samples was 8.27MPa which increased to 17.2MPa in the ultrasonically dyed PAN nanofibers. Increase in tensile strength of PAN nanofibers during ultrasonic dyeing is in agreement with our previous research results and may be attributed to stiffening of the nanofibers due to ultrasonic cavitations.

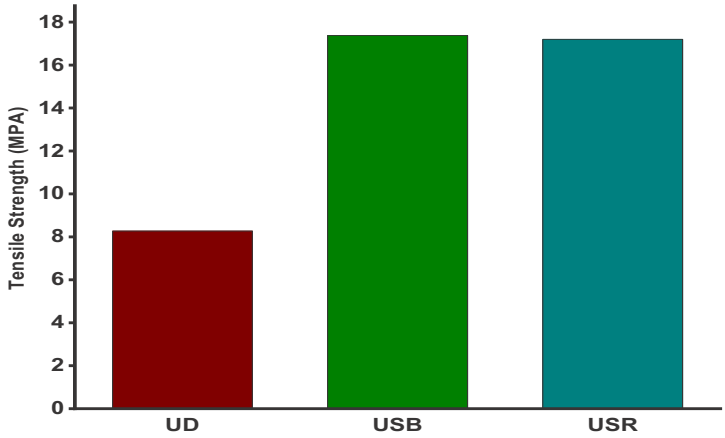

Figure 10.10 Tensile strength (MPA) results of undyed (UD) and dyed PAN nanofibers (USB and USR)

10.5 Conclusions

The PAN nanofibers were successfully dyed with disperse dyes using ultrasonic energy assisted batch dyeing method. Dyeing temperature, dyeing times and concentration of dyes were optimized. The results demonstrated 80^0C and one hour as optimal dyeing temperature and dyeing time respectively for sonication assisted coloration of PAN nanofibers. Comparison of the US dyeing with conventional dyeing method exhibited around 50% (CIB dye, 1% concentration) and more than 50% increase in K/S values when using US dyeing method. The dyed PAN nanofibers exhibited excellent light fastness, very good washing fastness and good to very good hot pressing fastness.

References

[1] N. Wang, Y. Si, N. Wang, G. Sun, M. El-Newehy, S.S. Al-Deyab, B. Ding, Multilevel structured polyacrylonitrile/silica nanofibrous membranes for high-performance air filtration, Separation and Purification Technology 126 (2014) 44-51.

[2] S. Gu, J. Ren, G. Vancso, Process optimization and empirical modeling for electrospun polyacrylonitrile (PAN) nanofiber precursor of carbon nanofibers, European polymer journal 41(11) (2005) 2559-2568.
[3] H. Malik, U.A. Qureshi, M. Muqeet, R.B. Mahar, F. Ahmed, Z. Khatri, Removal of lead from aqueous solution using polyacrylonitrile/magnetite nanofibers, Environmental Science and Pollution Research 25(4) (2018) 3557-3564.
[4] C. Ma, J. Chen, Q. Fan, J. Guo, W. Liu, E. Cao, J. Shi, Y. Song, Preparation and one-step activation of nanoporous ultrafine carbon fibers derived from polyacrylonitrile/cellulose blend for used as supercapacitor electrode, Journal of Materials Science 53(6) (2018) 4527-4539.
[5] P. Kampalanonwat, P. Supaphol, Preparation and adsorption behavior of aminated electrospun polyacrylonitrile nanofiber mats for heavy metal ion removal, ACS applied materials & interfaces 2(12) (2010) 3619-3627.
[6] P.K. Neghlani, M. Rafizadeh, F.A. Taromi, Preparation of aminated-polyacrylonitrile nanofiber membranes for the adsorption of metal ions: comparison with microfibers, Journal of hazardous materials 186(1) (2011) 182-189.
[7] S.F. Fennessey, R.J. Farris, Fabrication of aligned and molecularly oriented electrospun polyacrylonitrile nanofibers and the mechanical behavior of their twisted yarns, Polymer 45(12) (2004) 4217-4225.

CHAPTER 11

Ultrasonic Energy Assisted Dyeing of Nylon-6 Nanofibers

11.1 Introduction

This chapter reports sonication assisted dyeing of the Nylon 6 nanofibers with two disperse dyes. The Nylon 6 nanofibers were fabricated by electrospinning technique and dyed with and without sonication following batch dyeing method. Likewise the PU and PAN dyeing, process parameters were optimized and compared with conventional dyeing (without sonication).

11.2 Research background

Related to functional applications of nanofibers, high surface to volume ratio, nano-scale diameter of fibers and porosity are considerably important features of nanofibers. However, this high surface to volume ratio of the nanofibers is also the main reason of low color yield in coloration of the nanofibers [1]. High surface to volume ratio results in higher scattering of the light rendering lower color yield in comparison to conventional fibers [2]. Although researchers previously reported dyeing of polymeric nanofibers [3], however, improvement of color yield still remains a challenge. In the dyeing of nanofibers, ultrasonic energy has been used to improve color yield and achieve higher dye uptake. In our opinion, the lower color yield problem in coloration of nanofibers could be resolved by higher dye mass transfer from the dye liquor to the nanofibers. Ultrasonic energy in this case may help possibly due to three phenomenon happening in dye liquor, on/near fiber surface and within the substrates. The ultrasonic energy breaks dye aggregates due to ultrasonic cavitations, transient cavitations near fiber surface improve dye sorption and sonication influence mass transfer within and between fibers/yarns in the substrate [4] thus may result in higher color yields.

In the present work, we report ultrasonic dyeing of a polyamide nanofiber (Nylon-6) with disperse dyes. The glass transition temperature (Tg) of nylon nanofibers is less than 100 ^{0}C that make it very easy to dye at atmospheric conditions using ultrasonic energy. CI Disperse Blue 56 and CI Disperse Red 167:1 dyes were used in this research and dyeing experiments were conducted with and without sonication following batch dyeing method.

11.3 Fabrication and coloration of Nylon-6 nanofibers

The Nylon-6 nanofibers were electrospun using 22 wt% of Nylon-6 in formic acid as solvent. The solution was mixed using magnetic stirrer for 12 h at room temperature. Nanofiber webs of about 85 µm ± 5µm thickness were fabricated using electrospinning apparatus installed with high voltage supply (Har-100*12, Matsusada Co., Tokyo, Japan). Distance between the tip and metallic rotating collector was 15 cm and a 15 kV electric voltage was used.

The Nylon-6 nanofibers were dyed with and without sonication following batch-wise dyeing method. The mass of nanofiber webs used were 30 g/m^2± 5g. Five dye concentrations of the above described two dyes (0.2%, 0.5%, 1%, 3%, 5% out mass of web) and nanofiber mass to dye liquor ratio of 1:100 were used in the experiments. The dyeing of nanofibers was carried out at six different temperatures 40 to 90 °C (40, 50, 60, 70, 80 and 90 °C) and for six varying dyeing times ranging from 10 to 60 min (10, 20, 30, 40, 50 and 60 min.) for optimization of dyeing time and dyeing temperature. Acetic acid was used to adjust bath pH at 6.0. Ultrasonic assisted dyeing was carried out at output power of 180 W and at 38 kHz frequency. A 0.9 W/cm^2 input energy to the dye bath was used. In order to remove unfixed dye, the samples were rinsed with cold then warm water followed by hot rinsing at 80 °C.

11.4 Results and discussions

11.4.1 Dyeing temperatures of US dyeing and conventional dyeing

For optimization of dyeing temperature, Nylon-6 nanofiber samples were dyed with CI Disperse Blue 56 for 60min. using 0.5% dye concentration. The dyeing was carried out with and without sonication and the results calculated in terms of K/S values (equation 8, section 2.13.1) are reported in Figure 11.1. The results demonstrate increase in color yield of the nanofibers with increasing temperature. The color yield for ultrasonic assisted dyeing rapidly increased from 50 °C and reached at maximum K/S values of 0.6 at 80 °C, whereas, for conventional dyeing (without sonication) the K/S values moderately increased and reached highest value of 0.55 at 90 °C. The nanofibers dyed with sonication showed a slight decrease in color yield value at 90 °C. This may be attributed to dye hydrolysis due combined effect of higher temperature and sonication. Generally higher dyeing temperatures are prone to accelerate hydrolysis of the dyes and reduce dye uptake [5]. Since, the dye uptake reached maximum value at 80 °C in ultrasonic assisted dyeing method, further increasing the temperature may promote dye migration from dye sites in nanofibers to the dye liquor leading to decrease in color yield. Based on these results 80 °C for ultrasonic assisted dyeing and 90 °C for conventional dyeing were decided as optimum dyeing temperatures.

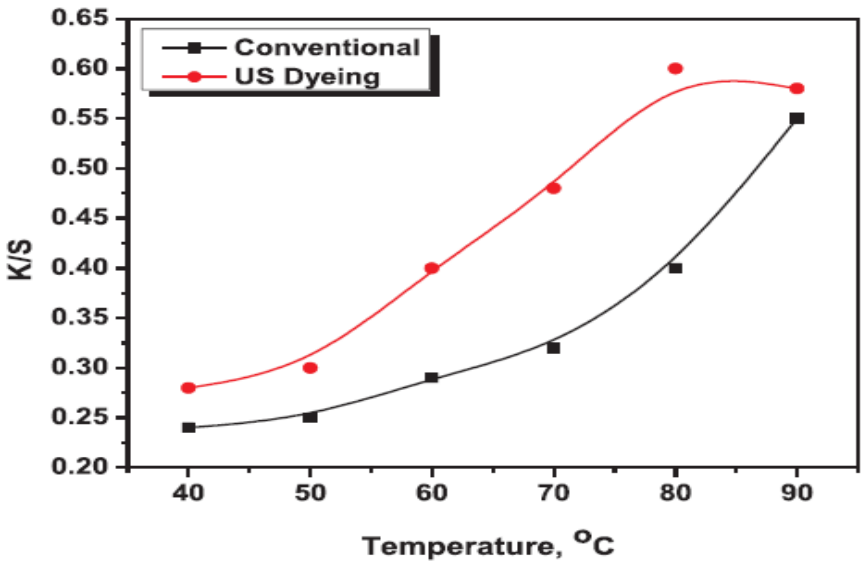

Figure 11.1 Effect of dyeing temperature on dye build-up property in conventional dyeing and ultrasonic assisted dyeing of Nylon-6 nanofibers.

11.4.2 Dyeing time of US dyeing and conventional dyeing

The dyeing temperature optimized in section 11.4.1 was used for optimization of dyeing times and results are given in Figure 11.2. The results show higher dye uptake in ultrasonic assisted dyeing in comparison to conventional dyeing. For ultrasonic assisted dyeing, a rapid increase in color yield is observed from 10 min to 20 min rendering maximum color yield of 0.6 at 30 minutes dyeing time. Whereas in conventional dyeing the dye uptake increased moderately with increasing dyeing time and reached highest K/S values of 0.55 in 60 minutes. Rapid increase in dye uptake and higher color yield in ultrasonic assisted dyeing can be attributed to ultrasonic cavitations which break the aggregated dye and increase color yield [2]. It is suggested that sonication influences the mass transfer within the substrates and the transient cavitations near fiber surface are responsible for improved results [6]. Based on the results 30 minutes and 60 minutes were decided as optimum dyeing times in ultrasonic assisted and conventional dyeing respectively.

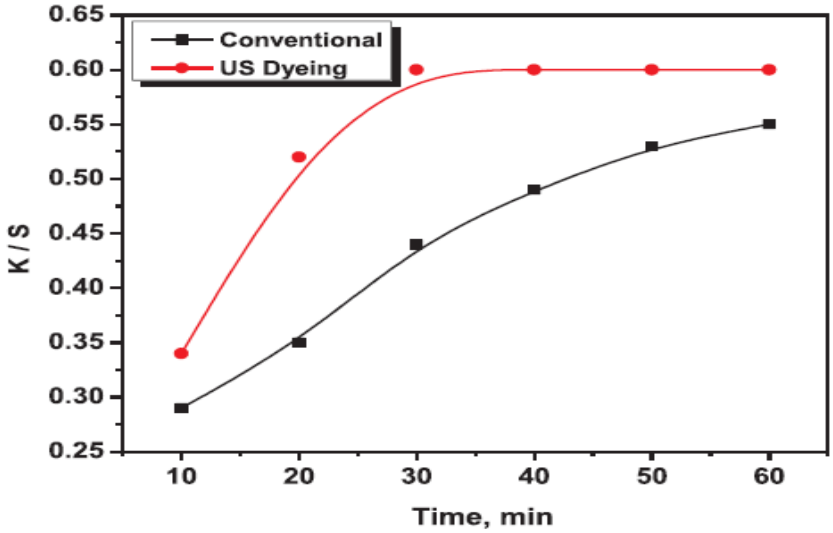

Figure 11.2 Effect of dyeing time on color build-up property in conventional dyeing and ultrasonic assisted dyeing of Nylon-6 nanofibers.

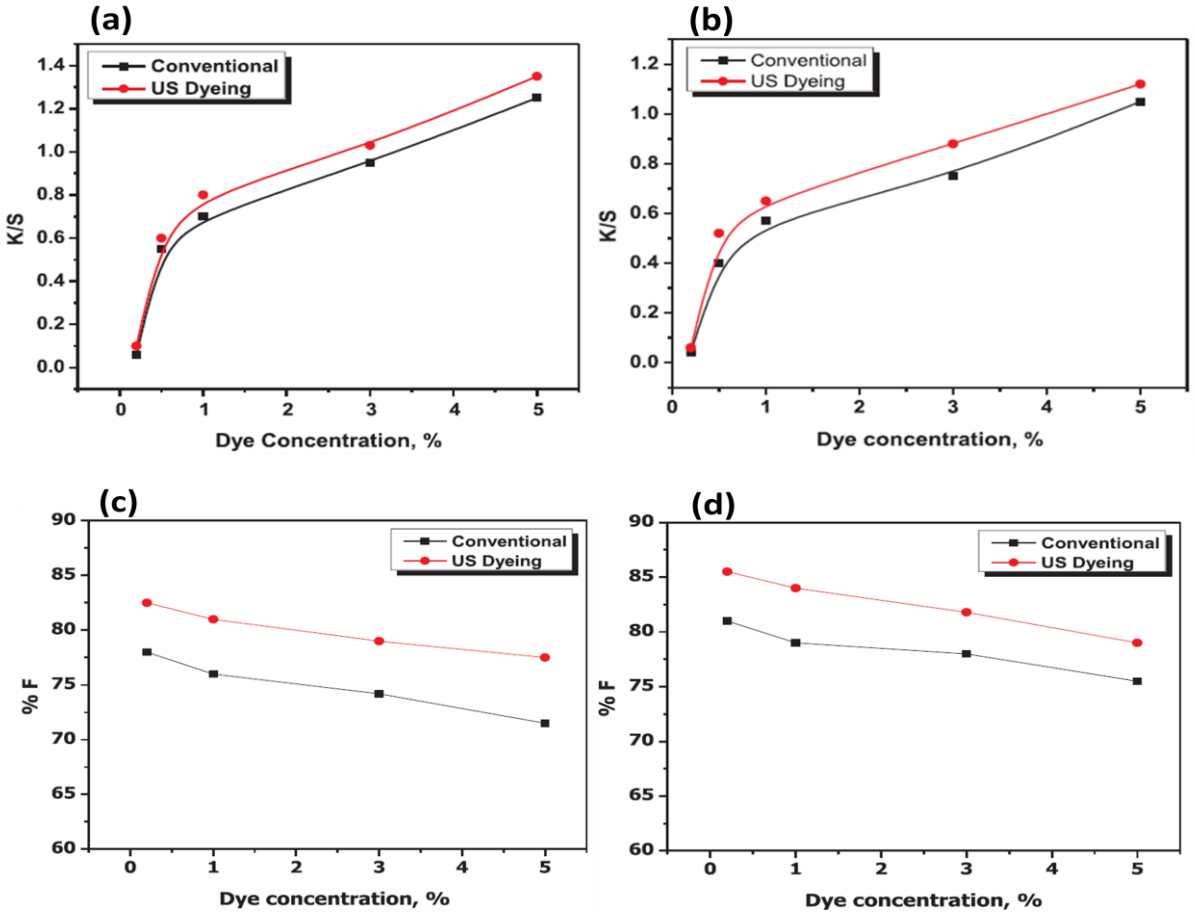

Figure 11.3 Effect of Blue 56 dye concentration on (a) color build-up and (c) dye fixation and Effect of Red 167:1 dye concentration on (b) color build-up and (d) dye fixation.

11.4.3 Optimization of dye concentration

Effect of dye concentrations on color build-up properties of CI Disperse Blue 56 and CI Disperse Red 167:1 were investigated using previously optimized conditions. Five different dye concentrations (0.2%, 0.5%, 1%, 3% and 5%) of each dye were used and the color build up properties were measured in terms of K/S values. The results reported in Figure 11.3 demonstrated increase in color yield with increasing dye concentrations for both dyes. The K/S values for ultrasonic assisted dyeing were higher in comparison to conventional dyeing such that the ultrasonic assisted dyeing with CI Disperse Blue 56 produced 17.33% higher color yield than conventional dyeing (3% dye concentration). Similarly for CI Disperse Red 167:1 dye, increase in color yield was 8.4% higher with sonication than without sonication (3% dye concentration). This increase in color yield with sonication may once again be attributed to the ultrasonic cavitations. Comparing Figure 11.3a with Figure 11.3b, it is evident that K/S values of CI Disperse Blue 56 (Figure 11.3a) are higher in comparison to those for CI Disperse Red 167:1 (Figure 11.3b). This difference is due to the dye fiber interaction parameters such as molar extinction coefficient and affinity of the dyes etc. The CI Disperse 56 dye is anthraquinone dye while the CI Disperse 167:1 is azoic dye. The effect of dye concentrations on dye fixation (%F) has been shown in Figure 11.3c and 11.3d. Irrespective to the class of dye, the US dyeing showed a significant increase in %F in comparison to conventional dyeing, however, the %F decreased as the dye concentration increased from 0.2% to 5%. Red 167:1 in Figure 3d showed relatively higher %F than the Blue 56 dye (Figure 11.3c) in both the US dyeing as well as conventional dyeing. For instance, dye fixation (%F) at 0.2% concentration of Blue 56 in US dyeing showed %F of 82.5%, whereas, Red 167:1 exhibited 86.0%. The conventional dyeing method, at 0.2% concentration of Blue 56 produced 72% and Red 167:1 produced 81.0%, dye fixation (%F). Higher values of dye fixation by US dyeing method can be due to the effect of cavitations during US dyeing process.

11.4.4 Color fastness results

An important aspect of dyed materials is resistant to color bleeding against various agents such as washing and light. Color fastness to washing (shade change and staining) and light fastness tests of the nanofibers dyed with both the dyes (CI Disperse Blue 56 and CI Disperse Red 167:1) were performed with samples dyed with 1% dye concentration. The results given in Table 11.1 demonstrated good (shade change) to very good (staining on multifibers) for both dyes. Color fastness to washing of the nanofibers dyed with CI Disperse Red 167:1 was comparatively better than the samples dyed with CI Disperse Blue 56. The light fastness test results showed average rating for both dyes in both the conventional and US dyeing method. Color fastness to hot pressing was

also determined for samples dyed with both the disperse dyes. For shade change and staining, the ratings obtained with CI disperse 167:1 were 4/5 and with CI Disperse Blue 56 obtained rating was 4. Since the CI Disperse Red 167:1 is high energy level dye, it showed better fastness (hot pressing) results than the CI Disperse Blue 56. The ultrasonic dyeing method and conventional dyeing method did not show a significant effect on color fastness properties of Nylon-6 nanofibers.

Table 11.1 Color fastness to light, color fastness to washing and hot pressing fastness

Dyes and dyeing method	Hot pressing fastness		Light fastness (24 h)	Washing fastness (Sh.Ch)	[3]Washing fastness (staining on multifibers)				
	Sh.Ch	St			CT	CO	PA	PES	PAC
[1]US-CI Disperse Blue 56	4	4	2	3/4	4	4	3/4	4/5	4/5
[2]CI Disperse Blue 56	4	4	3	3/4	4	4	3/4	4/5	4/5
[1]US-CI Disperse Red 167:1	4/5	4/5	2	3/4	4/5	4/5	4/5	4/5	5
[2]CI Disperse Red 167:1	4/5	4/5	2	3/4	4/5	4/5	4/5	4/5	5

Sh.Ch= Shade Change; St.= Staining.

[1]Ultrasonic (US) dyeing conditions: temperature: 80°C; time: 30min; dye concentration: 1%.

[2]Conventional dyeing conditions: temperature: 90°C; time: 60min; dye concentration: 1%.

[3]CT: cellulose triacetate; CO: cotton; PA: polyamide; PES: polyester; PAC: polyacrylic; WO: wool.

11.4.5 Morphologies of Nylon-6 nanofibers

Morphologies of the undyed and dyed nanofibers were observed using SEM analysis and results are given in Figure 11.4a–e. The undyed nylon-6 nanofibers show smooth and regular morphology (Figure 11.4a). The Nylon-6 nanofibers dyed with CI Disperse Blue 56 and CI Disperse Red 167:1 show a moderate increase in nanofiber diameters in comparison to undyed samples. The US dyeing method exhibited some insignificant surface irregularities.

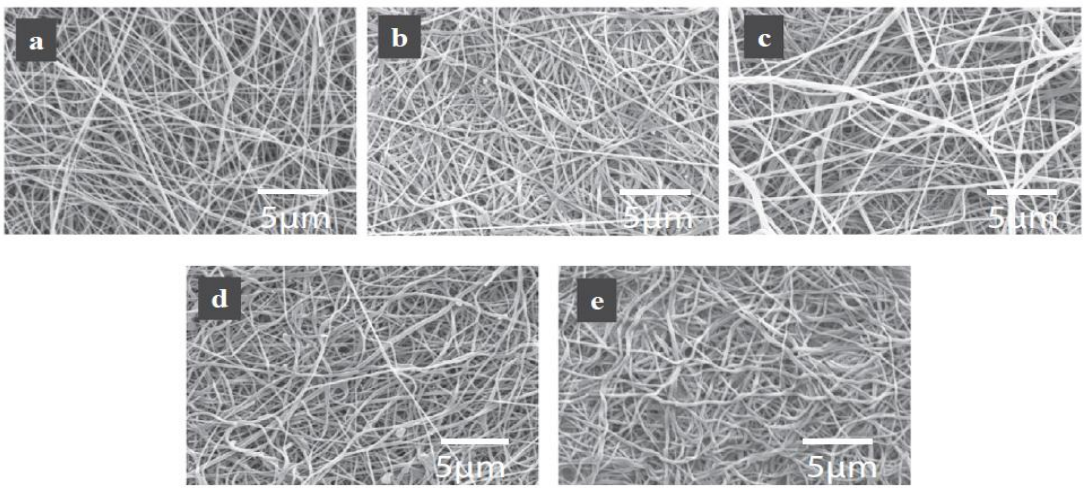

Figure 11.4 SEM images of (a) undyed Nylon 6 nanofibers (b) Conventionally dyed with Red 167:1 (c) US dyed with Red 167:1 (d) Conventionally dyed with Blue 56 (e) US dyed with Blue 56.

11.4.6 Mechanical properties of Nylon-6 nanofibers

Figure 11.5 shows comparison of tensile strength between US dyed nanofibers and conventionally dyed nanofibers. The nanofibers dyed with US dyeing method showed a significant increase of tensile strength in comparison to those dyed with conventional dyeing method. This can be attributed to the cavitations during ultrasonic dyeing that imparted stiffness to the nanofibers. For comparison, blank dyeing with and without US was also carried out. The results revealed that the dye class in particular, has no significant effect on imparting strength after dyeing. The tensile strength values of Nylon-6 nanofibers dyed with US dyeing method were between 3.0 to 3.5N, which suggests its usage as surgical apparel.

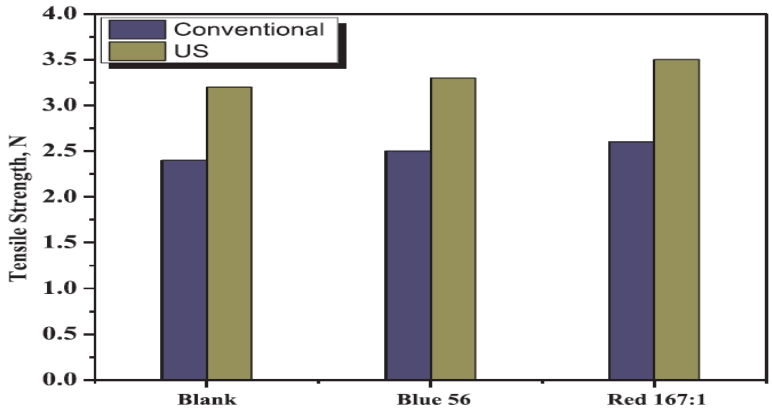

Figure 11.5 Tensile strength of US dyed and conventionally dyed Nylon-6 nanofibers

11.5 Conclusions

A comparative investigation on US dyeing and conventional dyeing of Nylon-6 nanofibers with disperse dyes has been successfully completed. We conclude that Nylon 6 nanofibers can be dyed with two disperse dyes CI Disperse Blue 56 and CI Disperse Red 167:1 with and without sonication by batch dyeing method. US dyeing method produced better color yield than conventional dyeing. US dyeing completed in 30 minutes while conventional dyeing in one hour. Irrespective to the dye class used, the US dyeing showed a significant increase in %F in comparison to conventional dyeing. However, the %F decreased with increase of dye concentrations. The nanofibers dyed with US dyeing method showed a significant increase in tensile strength in comparison to conventional dyeing method.

References

[1] Z. Khatri, G. Mayakrishnan, Y. Hirata, K. Wei, I.-S. Kim, Cationic-cellulose nanofibers: preparation and dyeability with anionic reactive dyes for apparel application, Carbohydrate polymers 91(1) (2013) 434-443.
[2] M. Khatri, F. Ahmed, A.W. Jatoi, R.B. Mahar, Z. Khatri, I.S. Kim, Ultrasonic dyeing of cellulose nanofibers, Ultrasonics sonochemistry 31 (2016) 350-354.
[3] A.W. Jatoi, P.K. Gianchandani, I.S. Kim, Q.-Q. Ni, Sonication induced effective approach for coloration of compact polyacrylonitrile (PAN) nanofibers, Ultrasonics sonochemistry (2018).
[4] A.W. Jatoi, I.S. Kim, Q.-Q. Ni, Ultrasonic energy-assisted coloration of polyurethane nanofibers, Applied Nanoscience (2018) 1-10.
[5] J. Shore, Cellulosics dyeing, Society of Dyers and Colourists1995.
[6] S. Burkinshaw, D. Jeong, The clearing of poly (lactic acid) fibres dyed with disperse dyes using ultrasound. Part 1: Colorimetric analysis, Dyes and Pigments 77(1) (2008) 171-179.

CHAPTER 12

Conclusions

Research on broader aspects of electrospun nanofibers have been concluded by investigating and evaluating varying performance characteristics of the nanofiber webs. Two functionalities of the nanofibers namely antibacterial characteristics and possibility to improve coloration performance via ultrasonic method have been mainly studied.

Electrospun nanofiber structures possess highly desirable properties suitable for antibacterial applications in real infection environment. Nanofibers due to their nano-scale small diameters, higher surface area to volume ratio and porous structure bestowed with breathability and structural compatibility are substantially suitable for antibacterial applications. The two biopolymers namely cellulose acetate (CA) and polyvinyl alcohol (PVA) render added performance characteristics owing to their biocompatibility, biodegradability, hydrophilicity and moisture retaining properties. The cellulose acetate has been mainly investigated for antibacterial performances. The surface modified CA (deacetylated) was first used to prepare CA/silver nanoparticle (CA/AgNP) composite nanofibers. The AgNPs were generated on CA nanofiber surfaces by three different methods such as by dopamine hydrochloride (Dopa), heat treatment and N, N-dimethylformamide.

The Dopa due to catechol chemistry and amine groups formed adhesive film on deacetylated CA nanofibers which when treated with silver nitrate solution effectively adsorbed silver ions on nanofiber surfaces whereas amine groups served function of stabilizing agent to reduce/avoid aggregation of silver. The catechol groups of Dopa possess capabilities to reduce metal ions to nanoparticles. During oxidation, hydroxyl groups in catechol, lose their electron to silver ions thereby generate metallic silver nanoparticles. Thus, an environmentally green process to generate AgNPs on CA nanofibers have been developed exploiting film forming, reducing and stabilizing properties of Dopa. It was concluded that 18 hours processing in Dopa solution followed by 18 hours processing in silver nitrate solution and 2mg of Dopa per mL of Tris HCl buffer effectively generated uniformly distributed AgNPs on CA nanofiber surface. All the investigated characterization techniques confirmed preparation of CA/AgNP composite nanofibers by Dopa. The antibacterial assays exhibited excellent antibacterial activities of the CA/AgNP against Gram-negative bacteria (*E. coli*) and Gram-positive bacteria (*S. aureus*).

Thermal treatment and DMF were used as effective and efficient processes to generate uniformly distributed, small diameter (<10nm) AgNPs on CA nanofiber surfaces with higher AgNP contents. The deacetylated CA nanofiber samples after adsorption of silver ions (Ag^{+}) (150mM silver nitrate

solution for 24 hours) were heat treated at 160^{0}C for 1hour, 1.5hour and 2hours to generate AgNPs. The method successfully produced CA/AgNP composite nanofibers. Average sizes of the AgNPs produced by thermal treatment were less than 5nm. The antibacterial test (Kirby-Bauer disk diffusion test method) demonstrated excellent antibacterial activities of the CA/AgNP composite nanofibers.

The DMF induced process carried out at boiling point temperature of DMF for 45 minutes, 1hour and 1.5hours was effective and efficient in generation of AgNPs on CA nanofibers however it generated AgNPs with larger sizes in comparison to thermal treatment process (average size <10nm). The CA/AgNPs demonstrated excellent antibacterial activities however relatively small *halo width* in comparison to thermal treatment process which may be due to difference in sizes of AgNPs (larger AgNPs).

Although the CA/AgNP composite nanofibers having AgNPs decorated on nanofiber surfaces have been effective and efficient in bactericidal and bacteria growth inhibition. However, due to surface adsorption of AgNPs it is easier for the silver to leach into the external environment. This nanofiber/AgNP architecture may be efficient and effective for rapid bactericidal performances, however, literature reported several demerits of this architecture. It has been reported that excess release of silver ions and exposure to human cells may produce detrimental side-effects such as *carcinoma*, *argyria*, *argyrosis* and allergies. Similarly, rapid release of silver may be disadvantageous for long time antibacterial performances owing to earlier silver depletion. Thus to effectively tackle these problems an strategy to immobilize AgNPs on several surfaces and their incorporation in the nanofibers has been suggested. Therefore, AgNPs anchored on TiO_2nanoparticles, multiwall carbon nanotubes (CNTs), silica nanoparticles and ZnO nanoparticles were synthesized to prepare TiO_2/AgNP, CNT/AgNP, silica/AgNP and ZnO/AgNP composite nanoparticles respectively. These nanoparticles were incorporated into CA and PVA nanofibers to fabricate CA/TiO_2/AgNP, CA/CNT/AgNP, PVA/silica/AgNP and CA/ZnO/AgNP composite nanofibers for biologically safer and sustained antibacterial applications. It has been proposed that the antibacterial mechanism of these composite nanofibers would be based on generation of reactive oxygen species (ROS) such as per oxide ions, oxygen radical and hydroxyl radical which kill the bacterial strains.

The TiO_2/AgNP composite nanoparticles were synthesized by dopamine process. The TiO_2 nanoparticles (sizes<100nm) were treated with 2mg/mL of Tris HCl buffer to form adhesive coating on TiO_2 nanoparticle surface. The dopa coated TiO_2 nanoparticles were treated with 0.2M silver nitrate solution for adsorption of silver ions and subsequent generation of AgNPs. The TiO_2 nanoparticle with average size 36.12nm decorated with AgNP having average size of 5.9nm were

successfully synthesized. These composite nanoparticles were then incorporated into CA nanofibers to fabricate CA/TiO_2/AgNP composite nanofibers by electrospinning. The CA/TiO_2/AgNP composite nanofibers were highly effective in bacterial inhibition on agar plates (formed adequately large *halo width*), produced effective bacterial growth inhibition in liquid medium for tested time (72 hours) and shown 100% bactericidal properties (relative cell viability test).

The CNT/AgNP composite nanoparticles were synthesized via oxidation of CNTs by sulfuric acid and nitric acid for producing carboxylic acid and hydroxyl functional groups on CNT surfaces. The oxidized CNTs were then treated with 0.25M silver nitrate solution for Ag^+ adsorption. The AgNPs on CNT surfaces were generated by heat treatment at 210^0C for two hours. The CNT/AgNPs were then incorporated into CA nanofibers to fabricate CA/CNT/AgNP composite nanofibers by electrospinning. The CA/CNT/AgNP composite nanofibers demonstrated excellent antibacterial activities against *E. coli* and *S. aureus* strains. These composite nanofibers formed adequately large *halo width* (mm) in disk diffusion test and effectively inhibited bacteria growth in liquid medium test for the tested time (48hours). The CA/CNT/AgNP composite nanofibers with 8% (wt.%) concentration of CNT/AgNP exhibited 100% bactericidal performances (0% viable cells).

The silica/AgNP composite nanoparticles were synthesized by alcohol reduction method. The fine AgNPs having average size of 3.93nm decorated on spherical silica nanoparticles having average size of 75.14nm were obtained. The silica/AgNP composite nanoparticles were then incorporated into PVA nanofibers to fabricate PVA/silica/AgNP composite nanofibers. The PVA/silica/AgNP composite nanofibers exhibited excellent antibacterial properties against *E. coli* and *S. aureus* strains. The composite nanofibers depicted sufficiently large area of inhibition zone (mm^2), were highly effective in inhibition of *E. coli* and *S. aureus* bacteria growth in liquid medium and demonstrated excellent bactericidal performance in relative bacterial cell viability test (0% cell viability).

The ZnO/AgNP nanoparticles were synthesized by using Dopa as reducing agent. Simple solution mixing procedure effectively generated AgNPs on ZnO nanoparticles. The ZnO nanoparticles were first coated with Dopa which were then added into to silver nitrate solution for simultaneous adsorption of silver ions and their reduction into AgNPs. The ZnO/AgNP nanoparticles were then added into CA solution in two concentrations, 5 wt. % and 10 wt. % to fabricate CA/ZnO/AgNP1 and CA/ZnO/AgNP2 respectively. The CA/ZnO nanofibers were also prepared using 10 wt. % ZnO nanoparticles. The antibacterial tests conducted against *E. coli* and *S. aureus* strains confirmed effective growth inhibition on agar plates, in liquid medium and excellent bactericidal properties (relative cell viabilities, %) of the CA/ZnO/AgNP composite nanofibers. The CA/ZnO/AgNP samples were found to be excellent in growth inhibition of the bacteria up to 108h (tested time).

Second functionally of the electrospun nanofibers investigated was improvement of dye-uptake of the nanofibers. Since the nanofiber have very small diameters (upto few hundred nanometers; specifically upto 100nm) and very large surface to volume ratio which are advantageous for many applications. However, the large surface to volume ration has been referred to scatter large proportion of incident light thus has been responsible for lower color strength of the nanofibers. For this purpose, ultrasonic energy has been investigated to improve color build-up of the electrospun nanofibers. Three nanofibers namely polyurethane (PU), polyacrylonitrile (PAN) and nylon-6 were ultrasonically dyed with two disperse dyes, CI disperse blue 56 and CI disperse red 167:1, following batch-wise dyeing method. The dyeing process parameter such as dyeing process time, dyeing temperatures and dye concentrations were optimized for each nanofiber.

The optimized dyeing process time and temperature for ultrasonic dyeing of PU nanofibers were 40 minutes and 70^0C respectively. The optimized dyeing time and temperatures for ultrasonic dyeing of PAN nanofibers were 1 hour and 80^0C.

Additionally, ultrasonic dyeing did not show a significant effect on morphology, chemical and crystallographic structures, however, improved mechanical strength of the studied nanofibers.

Suggestions for Future Research

Antibacterial composite nanofibers

- In vivo characterizations of the AgNP anchored composite nanoparticles incorporated nanofibers
- Investigating the performances of the AgNP immobilized composite nanoparticles loaded nanofibers against cancer cells
- Investigating performance of these three phase nanofiber structures in other applications such as catalysis, batteries and dye sensitized solar cells (DSSCs) etc.
- Synthesis of novel state of the art composite nanoparticles and their composite nanofibers for antibacterial and other applications.

Coloration of nanofibers

- Design and development of industrial scale dyeing systems for nanofibers
- Investigating possibilities of using dyed nanofibers as apparel
- Development of ultrasonic dyeing systems for coloration of nanofibers

List of Papers

1. **Jatoi Abdul Wahab**, Yun Kee Jo, Hoik Lee, Seong-Geun Oh, Dong Soo Hwang, Zeeshan Khatri, Hyung Joon Cha, Ick Soo Kim, (2018) Antibacterial efficacy of poly(vinyl alcohol) composite nanofibers embedded with silver-anchored silica nanoparticles, **Journal of Biomedical Materials Research B: Applied Biomaterials**, 106B (3), 1121-1128
2. **Jatoi Abdul Wahab**, Ick Soo Kim, Qing-Qing Ni, (2019) Cellulose acetate nanofibers embedded with AgNP anchored TiO2 nanoparticles for long term excellent antibacterial applications, **Carbohydrate Polymers**, 207, 640-649
3. **Jatoi Abdul Wahab**, Ick Soo Kim, Qing-Qing Ni, Dopa based facile procedure to synthesize AgNP/cellulose nanofiber composite for antibacterial applications, **Applied Nanoscience** (In press)
4. **Jatoi Abdul Wahab,** Ick Soo Kim, Qing-Qing Ni, A comparative study on synthesis of AgNPs on cellulose nanofibers by thermal treatment and DMF for antibacterial activities, **Material Science and Engineering C**, 98, 1179-1195
5. **Jatoi Abdul Wahab**, Farooq Ahmed, Muzamil Khatri, Anwaruddin Tanwari, Zeeshan Khatri, Hoik Lee, Ick Soo Kim (2017) Ultrasonic-assisted dyeing of Nylon-6 nanofibers, **Ultrasonics Sonochemistry**, 39, 34-38
6. **Jatoi Abdul Wahab,** Ick Soo Kim,Qing-Qing Ni (2018) Ultrasonic energy assisted coloration of polyurethane nanofibers, **Applied Nanoscience**, 8 (6), 1505-1514
7. **Jatoi Abdul Wahab**, Pardeep Kumar Gianchandani, Ick Soo Kim, Qing-Qing Ni, Sonication induced effective approach for coloration of compact polyacrylonitrile (PAN) nanofibers, **Ultrasonics Sonochemistry,** 51, 399-405